Title
Surface Interactions of Metal-Reducing Bacteria: Attachment and Cellular Appendages

Author
Young, Thomas Dylan

Publication Date
2020

Peer reviewed|Thesis/dissertation

UNIVERSITY OF CALIFORNIA

Los Angeles

Surface Interactions of Metal-Reducing Bacteria: Attachment and Cellular Appendages

A dissertation submitted in partial satisfaction of the requirements

for the degree Doctor of Philosophy in Chemistry

by

Thomas Dylan Young

2020

ABSTRACT OF THE DISSERTATION

Surface Interactions of Metal-Reducing Bacteria: Attachment and Cellular Appendages

by

Thomas Dylan Young
Doctor of Philosophy in Chemistry
University of California, Los Angeles, 2020
Professor Paul S. Weiss, Chair

This dissertation describes investigations of the interfaces between useful micro-organisms and solid surfaces, such as electrodes. Many types of microbes are ecologically important and can be technologically useful. Electrochemically active bacteria are particularly interesting, because of their ability to couple their metabolisms with inorganic devices. For electrochemically active bacteria to engage electrodes, they must localize around the electrodes and establish electrically conductive pathways. To understand the microbial interaction with conductive materials, we investigated both the attachment characteristics of bacteria to surfaces as well as the properties of cellular appendages, which can provide extracellular electronic conductivity.

We probed the electrical and mechanical properties of bacterial appendages with atomic force microscopy methods. The adhesiveness of *Geobacter sulfurreducens* cellular appendages was determined and compared against electrical conductivity and nanoscale morphology. The electron mobility of *Geobacter sulfurreducens* pili was validated with electrostatic force microscopy as well. Design principles for correlating atomic force microscopy measurements and optical microscopy are discussed.

The attachment of *Shewanella oneidensis* to surfaces was investigated by measuring the number of adherent cells on surfaces through a combination of direct fluorescence measurement, counting colonies formed from cells removed by sonication, and microscopy of the bacteria-attached surfaces. More *S. oneidensis* cells attach to hydrophobic surfaces and mannosylated surfaces compared to bare gold.

Using mannose-decorated glycopolymers to functionalize gold surfaces, we stimulated *S. oneidensis* bacterial colonization, enriched the wild-type strain of the bacteria against Δ*mshA-D* knockout strain during co-deposition, and induced where bacteria attach on a molecular pattern. *Vibrio cholerae* was also directed to a molecular pattern. The three-dimensional multivalency of the glycopolymers enhanced the persistence of attached bacteria on the surface more than surfaces functionalized with a single glycoside per molecule. Removing the attachment enhancement required equilibration between methyl α-D-mannopyranoside competitor and the cell culture. This requirement suggests the retention of cells on glycopolymer surfaces is kinetically controlled, and not a thermodynamic result of the cluster glycoside effect. Our findings, that the surfaces we studied can induce stable initial attachment and influence the ratio of bacterial strains on the surface, may be applied to harness various useful microbial communities.

The dissertation of Thomas Dylan Young is approved.

Gerard C. L. Wong

Andrea M. Kasko

William M. Gelbart

Paul S. Weiss, Committee Chair

University of California, Los Angeles

2020

TABLE OF CONTENTS

LIST OF FIGURES, SCHEMES, AND TABLES

Figures

Schemes

Tables

LIST OF ABBREVIATIONS AND SYMBOLS

Abbreviations

AFM	atomic force microscopy
cAFM	conductive atomic force microscopy
DCM	dichloromethane
DI	deionized
DLVO	Derjaguin–Landau–Verwey–Overbeek
DP	degree of polymerization
EET	extracellular electron transport
EFM	electrostatic force microscopy
EPS	exopolysaccharide
GFP	green fluorescent protein
GPC	gel permeation chromatography
^{1}H NMR	^{1}H nuclear magnetic resonance
LB	lysogeny broth
MSH	mannose-sensitive hemagglutinin
PBS	phosphate-buffered saline
PEG	poly(ethylene glycol)

RAFT	reversible addition-fragmentation chain transfer
SECM	scanning electrochemical microscopy
SEM	standard error of the mean
SICM	scanning ion conductance microscopy
THF	tetrahydrofuran
WT	wild type
XPS	X-ray photoelectron spectroscopy

Unit Abbreviations

A	Ampere	m	meter
℃	degree Celsius	min	minute
eV	electron volt	mol	mole
g	gram	N	Newton
h	hour	rpm	revolutions per minute
Hz	Hertz	S	Siemens
J	Joule	s	second
L	liter	V	Volt
M	molar	Ω	Ohm

ACKNOWLEDGMENTS

I thank my thesis committee Prof. Gerard Wong, Prof. Andrea Kasko, Prof. William Gelbart and my advisor Prof. Paul Weiss for their mentorship and guidance. They have made it possible for me to be successful as a scientist and to think as an independent researcher.

Chapter 4 of this dissertation, as well as some of sections 3.1 and 3.2 from chapter 3 are based on the publication:

> Young, T. D.; Liau, W. T.; Lee, C. K.; Mellody, M.; Wong, G. C. L.; Kasko, A. M.; Weiss, P. S. Selective Promotion of Adhesion of *Shewanella oneidensis* on Mannose-Decorated Glycopolymer Surfaces. *ACS Applied Materials & Interfaces* **2020,** *12*, 35767–35781.

Walter Liau synthesized the glycopolymers, performed solution-phase characterization, and helped with the initial fluorescence plate reader measurements. Calvin Lee taught me how to grow and manage bacteria and was an important collaborator during our conductive biofilms project. Michael Mellody helped with data processing in this publication. Profs. Paul Weiss, Andrea Kasko, and Gerard Wong served as the principal investigators for the research reported in this publication.

I thank my undergraduate assistants for their help. The data for figures 3-2 and 3-3 from chapter 3 were produced by Xiaotong Li. The data for figure 3-4 from chapter 3 were produced by Sumana Kaluvai. I thank Michael Mellody for his separate work on our intracellular delivery project, where he worked diligently.

This work was supported by the Office of Naval Research (grant N000141410051) and the Army Research Office (grant W911NF-18-1-0254). I acknowledge the use of the California NanoSystems Institute's facilities: the Advanced Light Microscopy/Spectroscopy Laboratory and

the Integrated NanoSystems Cleanroom. I thank professor Alvaro Sagasti for the use of his lab's optical microscope and professor Kenneth Nealson for his advice and instruction.

I would also like to thank the other members of the Paul Weiss group who have given me mentorship, camaraderie, and intellectual stimulation. Similarly, I thank all of the friends I made during grad school, many across departments of chemistry, physics, and biology, for making this time enjoyable and rewarding.

I thank all the other mentors and teachers in my life who made this dissertation possible. Adam Stieg trained me on both the instrumentation and theory of atomic force microscopy. Rob Kolakowski was my first mentor in the laboratory at Seattle Genetics. He taught me how to be a chemist and inspired me to get a Ph.D. Thank you to all of my teachers, including my high school chemistry teach Jeff Reichel whose recommendation that I take AP chemistry with him set my course toward a career in chemistry in motion.

I would like to thank my family for setting the foundation for my growth as a scientist and as a person. My parents Caryn and Mike taught me great values and much more. My brother Bryan has always had an enthusiasm for the science and our education began staying up past our bedtime to read from his Big Yellow Book of Science. Finally, I thank my girlfriend Kylie for her compassionate and loving support as I completed my doctorate degree.

VITA

2012	Undergraduate researcher in the Gojko Lalic Group. I synthesized copper and ruthenium ligands, and performed tosylations of various alkynols.
2011, 2012	Chemistry intern at Seattle Genetics, Inc. I helped characterize a total synthesis route to a pyrrolobenzodiazepine monomer and create cyclodextrin based PBD drug-antibody linkers.
2013	Bachelor of Science in a double major of Chemistry (ACS certified) and Biochemistry from the University of Washington.
2015	Master of Science in Chemistry from the University of California, Los Angeles.
2016	Singapore Centre for Environmental Life Sciences Engineering summer course taken at Nanyang Technological University.
2013–2020	Graduate student researcher and teaching assistant in the Paul Weiss Group. In addition to the work described in this dissertation, I studied the delivery of DNA into human cells by mechanical poration, researched mechanisms of chemical lift-off lithography, and characterized novel materials with a multitude of spectroscopies and microscopies.

Publications

Kolakowski, R. V.; Young, T. D.; Howard, P. W.; Jeffrey, S. C.; Senter, P. D. Synthesis of a C2-aryl-pyrrolo[2,1-C][1,4]benzodiazepine monomer enabling the convergent construction of symmetrical and non-symmetrical dimeric analogs. *Tetrahedron Letters* **2015,** *56*, 4512–4515.

Biteen, J. S.; Blainey, P. C.; Cardon, Z. G.; Chun, M.; Church, G. M.; Dorrestein, P. C.; Fraser, S. E.; Gilbert, J. A.; Jansson, J. K.; Knight, R.; Miller, J. F.; Ozcan, A.; Prather, K. A.; Quake, S. R.; Ruby, E. G.; Silver, P. A.; Taha, S.; van den Engh, G.; Weiss, P. S.; Wong, G. C. L.; Wright, A. T.; Young, T. D. Tools for the microbiome: Nano and beyond. *ACS Nano* **2016,** *10*, 6–37.

Ding, M.; Shiu, H.-Y.; Li, S.-L.; Lee, C. K.; Wang, G.; Wu, H.; Weiss, N. O.; Young, T. D.; Weiss, P. S.; Wong, G. C. L.; Nealson, K. H.; Huang, Y.; Duan, X. Nanoelectronic investigation reveals the electrochemical basis of electrical conductivity in *Shewanella* and *Geobacter*. *ACS Nano* **2016,** *10*, 9919–9926.

Lee, C. K.; Kim, A. J.; Santos, G. S.; Lai, P. Y.; Lee, S. Y.; Qiao, D. F.; Anda, J. D.; Young, T. D.; Chen, Y.; Rowe, A. R.; Nealson, K. H.; Weiss, P. S.; Wong, G. C. L. Evolution of cell size homeostasis and growth rate diversity during initial surface colonization of *Shewanella oneidensis*. *ACS Nano* **2016,** *10*, 9183–9192.

Slaughter, L. S.; Cheung, K. M.; Kaappa, S.; Cao, H. H.; Yang, Q.; Young, T. D.; Serino, A. C.; Malola, S.; Olson, J. M.; Link, S.; Häkkinen, H.; Andrews, A. M.; Weiss, P. S. Patterning of supported gold monolayers via chemical lift-off lithography. *Beilstein Journal of Nanotechnology* **2017,** *8*, 2648–2661.

Nakatsuka, N.; Hasani-Sadrabadi, M. M.; Cheung, K. M.; Young, T. D.; Bahlakeh, G.; Moshaverinia, A.; Weiss, P. S.; Andrews, A. M. Polyserotonin nanoparticles as multifunctional materials for biomedical applications. *ACS Nano* **2018,** *12*, 4761–4774.

Hasani-Sadrabadi, M. M.; Sarrion, P.; Nakatsuka, N.; Young, T. D.; Taghdiri, N.; Ansari, S.; Aghaloo, T.; Li, S.; Khademhosseini, A.; Weiss, P. S.; Moshaverinia, A. Hierarchically patterned polydopamine-containing membranes for periodontal tissue engineering. *ACS Nano* **2019,** *13*, 3830–3838.

Wang, S.; Goronzy, D. P.; Young, T. D.; Wattanatorn, N.; Stewart, L.; Baše, T.; Weiss, P. S. Formation of highly ordered terminal alkyne self-assembled monolayers on the Au{111} surface through substitution of 1-decaboranethiolate. *The Journal of Physical Chemistry C* **2019,** *123*, 1348–1353.

Belling, J. N.; Heidenreich, L. K.; Tian, Z.; Mendoza, A. M.; Chiou, T.-T.; Gong, Y.; Chen, N. Y.; Young, T. D.; Wattanatorn, N.; Park, J. H.; Scarabelli, L.; Chiang, N.; Takahashi, J.; Young, S. G.; Stieg, A. Z.; De Oliveira, S.; Huang, T. J.; Weiss, P. S.; Jonas, S. J. Acoustofluidic sonoporation for gene delivery to human hematopoietic stem and progenitor cells. *Proceedings of the National Academy of Sciences* **2020,** *117*, 10976–10982.

Cheung, K. M.; Stemer, D. M.; Zhao, C.; Young, T. D.; Belling, J. N.; Andrews, A. M.; Weiss, P. S. Chemical lift-off lithography of metal and semiconductor surfaces. *ACS Materials Letters* **2020,** *2*, 76–83.

Young, T. D.; Liau, W. T.; Lee, C. K.; Mellody, M.; Wong, G. C. L.; Kasko, A. M.; Weiss, P. S. Selective promotion of adhesion of *Shewanella oneidensis* on mannose-decorated glycopolymer surfaces. *ACS Applied Materials & Interfaces* **2020,** *12*, 35767–35781.

Chapter 1. The Importance of Microbial Science and Technological Uses

1.1 THE CHEMISTRY OF LIFE

1.1.1 Biological Chemical Reactivity

Lifeforms are rich vessels of chemical reactions. In nature, the synthesis of organic compounds without the aid of a biological organism is possible, but is mostly limited to simple molecules.[1] In hydrothermal systems, methane and simple hydrocarbons are produced in the highest concentrations of the abiotic organic products.[2] Organic compounds include most of the molecular complexity known to science. Accordingly, abiotic environments can often have less chemical diversity than environments populated with biological products. Natural products continue to guide the discovery of useful chemicals.[3,4] Although isolation of natural products is challenging,[5] the relative difficulty of synthesizing libraries of chemicals compared to isolating natural products is demonstrated by virtue of the widespread use of natural products for drug discovery. Schemes to create chemicals synthetically often also cede targets with high numbers of chiral centers, large molecular size, and more rigid bond and dihedral angles.[4]

The impressive range of chemical reactions facilitated by living things is derived from the catalytic abilities of biomacromolecules. Enzymes and ribozymes, as polymers with interchangeable components, have an enormous space of possible configurations of various chemical functional groups. The permutations of enzyme constructions, sampled and selected over time, have yielded spatial control not readily available to smaller molecules or other materials.

The effectiveness of enzymes can be considered using nitrogen reduction to ammonia as an example. Industrial methods for nitrogen reduction, such as the Haber-Bosch process, have historically relied on high temperature and pressure to make the reaction of nitrogen and hydrogen gas proceed faster.[6] Heterogeneous metal catalysts have similarly required high temperature (400 °C) and pressure (50 bar) to produce turnover rates of up to 10 s^{-1}.[7] Synthetic organometallic catalysts have been developed to perform the reaction at lower temperatures, but they have not achieved the same rates as biological catalysts.[8] Direct comparison of nitrogenase and synthetic organometallic catalysts is difficult due to differences in the physical and practical aspects of each system. However, low-temperature turnover rates have been measured—in terms of ammonia equivalents—of 1.2 min^{-1} for a synthetic catalyst and 80 min^{-1} for the nitrogenase enzyme from *Klebsiella pneumoniae*.[8]

1.1.2 Varieties of Micro-organisms

The catalytic ability of enzymes is naturally packaged in cells. The cellular environment enables compartmentalization of reactants, regulation of enzyme activity and concentration, and continuous production of enzymes and cofactors to prevent loss of activity over time. These traits can make the cellular environment advantageous for industrial use of biological reactions as well. The application of biology for chemical reactions is most familiar with fermentation processes in the food industry. Wastewater treatment is another common industrial use of organisms, where cells automatically colonize the system. Using cells eliminates the need to manufacture and maintain individual enzymes and in some cases the need to control the biological processes entirely. Applying living things to industrial processes is simpler with single-cell organisms than multicellular organisms. While members of the genus *Apis* have been used to convert sugars into the fatty acid esters of beeswax, generally the use of multicellular

species is wasteful.[9] Most of the biomass of the organism is wasting energy on processes not relevant to the desired chemical reactivity.

Within the realm of the microscopic unicellular organisms, a wide variety of phenotypes exists. One of the most important divisions between different cells is whether they are a nucleus-possessing eukaryote or a part of the older domains of prokaryotes. Several fundamental aspects differ between prokaryotes, which includes the domains bacteria and archaea, and eukaryotes, which include all other known forms of life. Eukaryotes have more complex DNA handling and gene regulation machinery. This complexity is perhaps what enables eukaryotes to have orders of magnitude more genes than prokaryotes and confers the latitude to have dormant genes, rarely expressed genes, and larger amounts of non-coding sequences of DNA.[10] Having more genes enables more protein possibilities. Larger and more varied proteins are also facilitated by protein-processing features of eukaryotes such as the endoplasmic reticulum, which enables proper folding of very large proteins—antibodies. As expected, eukaryotes frequently have longer proteins over the majority of protein families.[11] Prokaryotes are smaller and have higher surface-area-to-volume ratios. The morphology and simplicity of prokaryotes is considered to contribute to their increased biomass production efficiency and greater population growth rate.[9] The increased metabolic rate per weight of prokaryotes allows bacteria to outcompete eukaryotes. The faster population growth rate, in combination with prokaryotic genomes being haploid, increases selective pressure on any given gene and facilitates more rapid adaptation to environmental conditions. Both factors have likely contributed to bacteria and archaea claiming numerous environmental niches, including extreme conditions.

Interest in microbiomes, which are categories of environmentally related ecosystems of micro-organisms, has accelerated in recent years. Bacteria have emerged as the primary focus of

research on microbiomes,[12] which may be a result of their ability to adapt to niches that require a particular chemical reaction be performed. The role of archaea in microbial communities may be less evaluated due to their relatively recent categorization in 1977.[13] Other microbes—archaea; unicellular fungi, plants, and animals; other eukaryotes—are important members of natural microbial communities in addition to bacteria. Microbes, and bacteria as a key class of micro-organism, are important components of the chemical reactivity of nature.

Several natural microbiomes crucially intersect human activity. The aforementioned nitrogenase enzymes allow microbes to reduce nitrogen in the root systems of legumes, which is necessary for soil health and agriculture.[14] The food chain of the ocean is based largely on phytoplankton—microscopic plants and photosynthetic bacteria. Humans use the marine foodstuffs and oxygen supply generated by microbial photosynthetic activity. Food science is also impacted by atmospheric microbes and other microbes that contact food, because of spoilage caused by microbes. Corrosion and surface fouling caused by microbes is destructive to materials.[15] Microbes that are commensal with humans are abundant in moist, nutrient-rich areas of the body that are not closely associated with the immune system. Health is dependent on suitable microbes functioning with the human body.[16] Microbes merit research as a key part of the biotic world, and also scientific understanding guides management of the microbiomes that affect humanity.

1.2 MICROBIAL METABOLISM, CATABOLIC AND ANABOLIC

Microbes, in addition to be scientific systems of interest, can function as chemical technology. Generally, microbes are applied as a technology by performing an oxidation or a reduction reaction. Alternatively, reactions catalyzed by a cell can be grouped as a part of catabolism or

anabolism. In the catabolic pathways of metabolism, chemical potential energy is taken from the environment and converted into energy available to the cell by breaking down large molecules into small ones that are entropically favored, such as carbon dioxide. Anabolic pathways consume small molecules to create larger biomolecules at the cost of the energetic currency of the cell.

Environmental remediation is an application of microbial metabolism where pollutants are either reduced or oxidized catabolically.[17] Organic pollutants can be oxidized and certain inorganic contaminants can be remedied by immobilizing them as a reduced state. Water treatment is another catabolic process that could be considered a type of environmental remediation. Microbes are used to oxidize carbon compounds during water treatment. Nitrogen compounds can be converted into atmospheric dinitrogen by oxidizing ammonia and reducing nitrites and nitrates. The Anammox process is a particularly useful method for reducing pollutants produced during nitrogen defixation.[18] Sulfates can also be removed from wastewater by microbial reduction to hydrogen sulfide.

Biosynthesis is a particularly powerful application of enzymatic reactions. Creation of carbon-carbon bonds abiotically is difficult. Abiotic conversion of carbon dioxide into a multiple carbon molecule requires high-energy starting materials and produces low-energy, highly oxygenated products.[19] Biologically, the synthesis of chemicals with multiple carbon atoms can be powered by the energy pool of a cell, where simple starting materials are used to produce high-energy compounds such as nucleotide triphosphates, which derive further free energy from their compartmentalized high concentrations. Several effective biochemical pathways for carbon dioxide assimilation into series of carbon-carbon bonds are known.[20,21] Catabolic biosynthetic processes have been successfully commercialized in terms of fermentation. The industrial

method of ethanol synthesis through yeast induced fermentation has remained fundamentally unchanged for over a century.[22,23] Fermentation products are metabolic byproducts of the cell and are naturally given off without the need for extraction. Reduced carbon is given off in fermentation when other, more energetically favorable, elements are not available to serve as electron acceptors.

Through anabolic biosynthesis it is possible to produce any large molecules that cells are capable of making. Anabolic processes are often coupled with catabolic pathway so they can be powered by environmental chemicals. For example, *Escherichia coli* can produce human insulin by catabolizing nutrients such as glucose, and then synthesizing the insulin protein anabolically.[24] Isolated cells from multicellular organisms are also applied anabolically. For example, monoclonal B cells are used industrially to produce antibodies. Many other biological molecules have been successfully produced from the application of cells as technology.[25] As efforts in metabolic engineering are realized, an increasing scope of products can be practically produced by biosynthesis.[26]

1.3 ELECTROACTIVE BACTERIA

Oxidation and reduction in biologically assisted chemical reactions use a wide range of redox agents to act as either a source or drain of electron. Carbohydrates and other partially oxidized carbon compounds, proteins, and water are common electron donors. Oxygen, nitrates, sulfates, and metal oxides are common electron acceptors.

Oxidation and reduction can be performed more directly, and perhaps more efficiently, with direct transfer of electrons. Integrating excited electrons directly with metabolism eliminates the molecular mass transport of chemical electron reservoirs and their waste products.

This introduction of energy can be provided through photons or with electrical current. Photosynthesis is a well-known process that integrates environmental photons with cellular metabolism. However, the efficiency of photosynthesis is not as good as solar energy capture methods like photovoltaics.[27] Photosynthetic systems also can only absorb energy from sunlight when exposed to light during the day. Providing electrical current can be scaled until limitations are encountered on power supply. A diverse group of mature technologies can produce electrical power and it is therefore a reliable source of energy.

Several examples of technologies that couple electronic devices with micro-organisms, sometimes referred to as bioelectrical systems, have been developed.[28] Microbes grown on an anode can perform catabolic reactions to generate electrical power or breakdown unwanted chemicals.[29] Anabolically, microbes can be grown on a cathode to power biosynthesis.[30] These bioelectrical systems can make use of a consortia of microbes sampled from the environment or by pure cultures. *Shewanella oneidensis* and *Geobacter sulfurreducens* are two model electroactive bacteria. *S. oneidensis* is a model species of dissimilatory metal-reducing bacteria.[31] It contains the biochemical machinery to catalyze reactions between electron donors and a wide range of oxidants, and it is therefore desirable for bioelectrical systems.[32] *S. oneidensis* has been used to produce microbial fuel cells and biosynthetic sulfurous compounds.[33,34] Likewise, *G. sulfurreducens*, as a dissimilatory metal-reducing bacteria,[35] has been used to produce electricity[36] and grow on cathodes with carbon dioxide and citrate as carbon sources, apparently converting carbon dioxide into biomass.[37]

1.4 PURE CULTURES, CO-CULTURES, AND MICROBIOMES

Microbes can perform chemical reactions as a pure culture of one species or as a mixture of many species. In many natural microbial communities, different types of microbes perform different chemical reactions and synergize to shape the chemical make-up of their ecosystem.[38] Multiple species, each specializing in a particular set of reactions, may be necessary for a particular biochemical process to occur. It makes sense that an organism would compete for a single ecological niche rather than make use of all possible nutrients, considering the energetic cost of producing enzymes to carry out each pathway of chemical reactions. Sediment profiles have layers of microbes according to the niche they are competing for.[39] Aerobes compete for the most powerful electron acceptor present—oxygen. Once oxygen is consumed iron and manganese are used as electron acceptors by specialist microbes. Deeper into sediment nitrate-reducing bacteria become abundant, followed by sulfur-reducing bacteria using less powerful electron acceptors after the previous ones are depleted. Each electron acceptor is a nutrient that produces an ecological niche where their concentrations are high. The most competitive organism in a niche begins to displace others. Similarly to the niches formed in depths of sediment, other ecological niches can be competed over based on the metabolic reactions necessary to extract energy from the environment.

Interest in applied consortia of microbes or co-cultures of a few select strains follows from the observations of the natural specialization of individual microbes. However, the functionality of a community of microbes is a matter of the enzymes that are expressed, not the species present.[40] A distribution of species is a projection of a distribution of genes. Rather than in a mixture of species, a set of functional genes can be constructed in a single cell—until the number of genes exceeds the limit of genome size for a particular cell type.

Microbial engineering under a single-species paradigm has several advantages. Mass transport is not required between cells. As a reductionist approach, less needs to be understood about the system. Unforeseen interactions between species are not possible. Fewer variables exist to produce rare events by chance. On the other hand, engineering of microbe consortia, *i.e.*, microbiomes, enables modularity, the possibility of introducing unlimited genes, and the dependability of operating close to the natural state of micro-organisms.

Influential chemistry and promising biological technologies are possible by implementing the correct set of genes, regardless of whether these genes are separated by cell membranes or not. Whether it results from microbial consortia, single species, or individual enzymes, the chemistry of biology remains one of the great frontiers of science.

1.5 REFERENCES

1. Reeves, E. P.; Fiebig, J. Abiotic synthesis of methane and organic compounds in earth's lithosphere. *Elements* **2020,** *16*, 25–31.

2. McCollom, T. M.; Seewald, J. S. Abiotic synthesis of organic compounds in deep-sea hydrothermal environments. *Chemical Reviews* **2007,** *107*, 382–401.

3. Lamberth, C.; Jeanmart, S.; Luksch, T.; Plant, A. Current challenges and trends in the discovery of agrochemicals. *Science* **2013,** *341*, 742–746.

4. Atanasov, A. G.; Waltenberger, B.; Pferschy-Wenzig, E.-M.; Linder, T.; Wawrosch, C.; Uhrin, P.; Temml, V.; Wang, L.; Schwaiger, S.; Heiss, E. H.; Rollinger, J. M.; Schuster, D.; Breuss, J. M.; Bochkov, V.; Mihovilovic, M. D.; Kopp, B.; Bauer, R.; Dirsch, V. M.; Stuppner, H. Discovery and resupply of pharmacologically active plant-derived natural products: A review. *Biotechnology Advances* **2015,** *33*, 1582–1614.

5. Bucar, F.; Wube, A.; Schmid, M. Natural product isolation – how to get from biological material to pure compounds. *Natural Product Reports* **2013,** *30*, 525–545.

6. Foster, S. L.; Bakovic, S. I. P.; Duda, R. D.; Maheshwari, S.; Milton, R. D.; Minteer, S. D.; Janik, M. J.; Renner, J. N.; Greenlee, L. F. Catalysts for nitrogen reduction to ammonia. *Nature Catalysis* **2018,** *1*, 490–500.

7. Jacobsen, C. J. H.; Dahl, S.; Clausen, B. S.; Bahn, S.; Logadottir, A.; Nørskov, J. K. Catalyst Design by Interpolation in the Periodic Table: Bimetallic ammonia synthesis catalysts. *Journal of the American Chemical Society* **2001,** *123*, 8404–8405.

8. Del Castillo, T. J.; Thompson, N. B.; Peters, J. C. A synthetic single-site Fe nitrogenase: high turnover, freeze-quench ^{57}Fe Mössbauer data, and a hydride resting state. *Journal of the American Chemical Society* **2016,** *138*, 5341–5350.

9. DeLong, J. P.; Okie, J. G.; Moses, M. E.; Sibly, R. M.; Brown, J. H. Shifts in metabolic scaling, production, and efficiency across major evolutionary transitions of life. *Proceedings of the National Academy of Sciences* **2010,** *107*, 12941–12945.

10. Gregory, T. R. Synergy between sequence and size in large-scale genomics. *Nature Reviews Genetics* **2005,** *6*, 699–708.

11. Brocchieri, L.; Karlin, S. Protein length in eukaryotic and prokaryotic proteomes. *Nucleic Acids Research* **2005,** *33*, 3390–3400.

12. Hooks, K. B.; O'Malley, M. A. Contrasting strategies: Human eukaryotic versus bacterial microbiome research. *Journal of Eukaryotic Microbiology* **2020,** *67*, 279–295.

13. Woese, C. R.; Fox, G. E. Phylogenetic structure of the prokaryotic domain: The primary kingdoms. *Proceedings of the National Academy of Sciences* **1977,** *74*, 5088–5090.

14. Chaparro, J. M.; Sheflin, A. M.; Manter, D. K.; Vivanco, J. M. Manipulating the soil microbiome to increase soil health and plant fertility. *Biology and Fertility of Soils* **2012,** *48*, 489–499.

15. Videla, H.; Herrera, L. Microbiologically influenced corrosion: Looking to the future. *International Microbiology: The Official Journal of the Spanish Society for Microbiology* **2005,** *8 3*, 169–80.

16. Huttenhower, C.; Gevers, D.; Knight, R.; Abubucker, S.; Badger, J. H.; Chinwalla, A. T.; Creasy, H. H.; Earl, A. M.; FitzGerald, M. G.; Fulton, R. S.; Giglio, M. G.; Hallsworth-Pepin, K.; Lobos, E. A.; Madupu, R.; Magrini, V.; Martin, J. C.; Mitreva, M.; Muzny, D. M.; Sodergren, E. J.; Versalovic, J.; Wollam, A. M.; Worley, K. C.; Wortman, J. R.; Young, S. K.; Zeng, Q.; ... ; Birren, B. W.; Gibbs, R. A.; Highlander, S. K.; Methé, B. A.; Nelson, K. E.; Petrosino, J. F.; Weinstock, G. M.; Wilson, R. K.; White, O.; The human microbiome project, C. structure, function and diversity of the healthy human microbiome. *Nature* **2012,** *486*, 207–214.

17. Gadd, G. M. Metals, minerals and microbes: Geomicrobiology and bioremediation. *Microbiology* **2010,** *156*, 609–643.

18. Jin, R.-C.; Yang, G.-F.; Yu, J.-J.; Zheng, P. The inhibition of the anammox process: A review. *Chemical Engineering Journal* **2012,** *197*, 67–79.

19. Peters, M.; Köhler, B.; Kuckshinrichs, W.; Leitner, W.; Markewitz, P.; Müller, T. E. Chemical technologies for exploiting and recycling carbon dioxide into the value chain. *ChemSusChem* **2011,** *4*, 1216–1240.

20. Berg, I. A. Ecological aspects of the distribution of different autotrophic CO_2 fixation pathways. *Applied and Environmental Microbiology* **2011,** *77*, 1925–1936.

21. Claassens, N. J.; Cotton, C. A. R.; Kopljar, D.; Bar-Even, A. Making quantitative sense of electromicrobial production. *Nature Catalysis* **2019,** *2*, 437–447.

22. Hansen, E. C., *Undersøgelser over Alkoholgjaersvampenes Fysiologi Og Morfologi*. Comité du laboratoire: Carlsberg, 1883.

23. Mohd Azhar, S. H.; Abdulla, R.; Jambo, S. A.; Marbawi, H.; Gansau, J. A.; Mohd Faik, A. A.; Rodrigues, K. F. Yeasts in sustainable bioethanol production: A review. *Biochemistry and Biophysics Reports* **2017,** *10*, 52–61.

24. Riggs, A. D. Bacterial production of human insulin. *Diabetes Care* **1981,** *4*, 64–68.

25. Pham, J. V.; Yilma, M. A.; Feliz, A.; Majid, M. T.; Maffetone, N.; Walker, J. R.; Kim, E.; Cho, H. J.; Reynolds, J. M.; Song, M. C.; Park, S. R.; Yoon, Y. J. A review of the microbial production of bioactive natural products and biologics. *Frontiers in Microbiology* **2019,** *10*, 1404.

26. Lee, J. W.; Na, D.; Park, J. M.; Lee, J.; Choi, S.; Lee, S. Y. Systems metabolic engineering of microorganisms for natural and non-natural chemicals. *Nature Chemical Biology* **2012,** *8*, 536–546.

27. Blankenship, R. E.; Tiede, D. M.; Barber, J.; Brudvig, G. W.; Fleming, G.; Ghirardi, M.; Gunner, M. R.; Junge, W.; Kramer, D. M.; Melis, A.; Moore, T. A.; Moser, C. C.; Nocera, D. G.; Nozik, A. J.; Ort, D. R.; Parson, W. W.; Prince, R. C.; Sayre, R. T. Comparing photosynthetic and photovoltaic efficiencies and recognizing the potential for improvement. *Science* **2011,** *332*, 805–809.

28. Bajracharya, S.; Sharma, M.; Mohanakrishna, G.; Dominguez Benneton, X.; Strik, D. P. B. T. B.; Sarma, P. M.; Pant, D. An overview on emerging bioelectrochemical systems (BESS): Technology for sustainable electricity, waste remediation, resource recovery, chemical production and beyond. *Renewable Energy* **2016,** *98*, 153–170.

29. Logan, B. E.; Rabaey, K. Conversion of wastes into bioelectricity and chemicals by using microbial electrochemical technologies. *Science* **2012,** *337*, 686–690.

30. Lovley, D. R.; Nevin, K. P. Electrobiocommodities: Powering microbial production of fuels and commodity chemicals from carbon dioxide with electricity. *Current Opinion in Biotechnology* **2013,** *24*, 385–390.

31. Venkateswaran, K.; Moser, D. P.; Dollhopf, M. E.; Lies, D. P.; Saffarini, D. A.; MacGregor, B. J.; Ringelberg, D. B.; White, D. C.; Nishijima, M.; Sano, H.; Burghardt, J.; Stackebrandt, E.; Nealson, K. H. Polyphasic taxonomy of the genus *Shewanella* and description of *Shewanella oneidensis* sp. nov. *International Journal of Systematic and Evolutionary Microbiology* **1999,** *49*, 705–724.

32. Fredrickson, J. K.; Romine, M. F.; Beliaev, A. S.; Auchtung, J. M.; Driscoll, M. E.; Gardner, T. S.; Nealson, K. H.; Osterman, A. L.; Pinchuk, G.; Reed, J. L.; Rodionov, D. A.; Rodrigues, J. L. M.; Saffarini, D. A.; Serres, M. H.; Spormann, A. M.; Zhulin, I. B.; Tiedje, J. M. Towards environmental systems biology of *Shewanella*. *Nature Reviews Microbiology* **2008,** *6*, 592–603.

33. Ringeisen, B. R.; Henderson, E.; Wu, P. K.; Pietron, J.; Ray, R.; Little, B.; Biffinger, J. C.; Jones-Meehan, J. M. High power density from a miniature microbial fuel cell using *Shewanella oneidensis* DSP10. *Environmental Science & Technology* **2006,** *40*, 2629–2634.

34. Xiao, X.; Ma, X.-B.; Yuan, H.; Liu, P.-C.; Lei, Y.-B.; Xu, H.; Du, D.-L.; Sun, J.-F.; Feng, Y.-J. Photocatalytic properties of zinc sulfide nanocrystals biofabricated by metal-reducing bacterium *Shewanella oneidensis* MR-1. *Journal of Hazardous Materials* **2015,** *288*, 134–139.

35. Holmes, D. E.; Finneran, K. T.; O'Neil, R. A.; Lovley, D. R. Enrichment of members of the family *Geobacteraceae* associated with stimulation of dissimilatory metal reduction in uranium-contaminated aquifer sediments. *Applied and Environmental Microbiology* **2002,** *68*, 2300–2306.

36. Bond, D. R.; Lovley, D. R. Electricity production by *Geobacter sulfurreducens* attached to electrodes. *Applied and Environmental Microbiology* **2003,** *69*, 1548–1555.

37. Ueki, T.; Nevin, K. P.; Woodard, T. L.; Aklujkar, M. A.; Holmes, D. E.; Lovley, D. R. Construction of a *Geobacter* strain with exceptional growth on cathodes. *Frontiers in Microbiology* **2018,** *9*, 1512.

38. Bauer, M. A.; Kainz, K.; Carmona-Gutierrez, D.; Madeo, F. Microbial wars: Competition in ecological niches and within the microbiome. *Microbial Cell* **2018,** *5*, 215–219.

39. Jones, J. G.; Berner, R. A.; Meadows, P. S.; Durand, B.; Eglinton, G. Microbes and microbial processes in sediments [and discussion]. *Philosophical Transactions of the Royal Society of London. Series A, Mathematical and Physical Sciences* **1985,** *315*, 3–17.

40. Morgan, X. C.; Segata, N.; Huttenhower, C. Biodiversity and functional genomics in the human microbiome. *Trends in Genetics* **2013,** *29*, 51–58.

Chapter 2. Electron Transport in Biological Nanoscopic Filaments

2.1 INTRODUCTION

2.1.1 Extracellular Electron Transport in Bacteria

Interactions of internal microbial processes and the extracellular environment require transport of particles or energy between the inside and outside of a cell. This transport can be mediated through direct contact with the outer cell membrane, random transmission into extracellular media, or use of cellular appendages. Appendages are important in circumstances where matter must be transported at a distance and directed at a particular target. Transfer of momentum by flagella, transfer of DNA by conjugative pili, and electron transport by conductive appendages are examples where bacteria utilize appendages.

In the case of electrochemically active bacteria, mass transport between the inside and the outside of a cell also includes electron transport. These bacteria are able to couple the energetics of a cell to its surroundings by extracellular transportation of electrons. As electron sources or drains may be localized on metals or mineral oxides, the extracellular transfer of electrons can be critical to the metabolism and life of electroactive bacteria. In applications where electrical power is produced by or supplied to biological cells through electrodes, the method of extracellular electron transport (EET) is important for the overall efficiency of the system. Extracellular electron transport has been observed in several species, notably in delta- and gamma-proteobacteria and the genuses *Geobacter* and *Shewanella*.[1] Even the well-studied organisms *Escherichia coli* and *Pseudomonas aeruginosa* are capable of extracellular electrochemical activity.[2] Direct contact of a cell's outer membrane to electron reservoirs is one

way that electrons can be transported beyond the cell. Extracellular electron transport through soluble electron mediators or electrically conductive cellular appendages has also been observed.[3]

The simplest mechanism for EET is direct contact with the outer membrane, which requires no structures beyond the proteins bound to the outer membrane. Direct contact EET has been observed in microbes such as methanotrophs, that transfer electrons to other microbes within their consortia to create syntrophic relationships.[4] Electron transport has been observed along cells. Cable bacteria are fused cells that share an outer membrane and periplasmic space. Electrons are transported several centimeters along the cell bodies of cable bacteria.[5-7]

Soluble electron mediators provide EET without direct contact of the outer membrane to an electron reservoir. Redox active molecules can be excreted into extracellular space and transfer electrons by drifting between cells and electron reservoirs.[8] Soluble electron shuttles act by diffusion, which may limit transfer rate and require production of new redox molecules as they are lost to the surroundings. As such, electrons shuttles are less effective over long distances and more effective between cells within a biofilm,[9] a biofilm being a group of microbes and secreted material that forms on surfaces.

Extracellular electron transport through cell appendages, termed nanowires, is the most recently discovered route.[10] Appendages enable electrons to be directed through space by virtue of the physical localization of appendages as condensed matter. Whereas, the anisotropic nature of secreted electron mediators is a fundamental limitation when an electron reservoir is located in a particular direction from the bacterium. Electrical conduction through cellular appendages is

worth investigating to understand the different features, and potential advantages, it possesses compared to the other methods of EET.

2.1.2 Types and Function of Bacterial Appendages

Before discussing the electrical properties of bacterial nanowires further, we will first consider what possibilities exist for the material composition of biological appendages. What can an appendage of a bacterium be made of? Various types of biomolecules can be extended from the bacterial cell as an appendage. Let us consider the major classes of biological macromolecules: proteins, saccharides, lipids, and nucleic acids. We will consider examples of gram-negative bacteria as our species of interest are all proteobacteria.

Perhaps the best understood type of appendages is protein fibers. Extracellular protein fibers on bacteria include flagella and pili. Flagella are protein filaments, generally composed of the protein flagellin, that propel bacteria by rotating. Pili are a broad class of hair-like protein fibers that are can serve various roles. Flagella can be distinguished from pili by their generally larger size. Pili have diameters ranging from 4 to 12 nm.[11] The diameter of polar flagella may be 30–40 nm and peritrichous flagella elsewhere on the cell body may have a diameter of around 15 nm for some species.[12]

Pili have been categorized into types previously, however these nomenclatures have not been readily adopted by the scientific community.[13] Two types that are recognized in pili categorization are type I pili—also known as chaperone-usher pili—and type IV pili. Confusingly, some pili are components of secretion systems that are also numbered by type. Six secretion systems are known in gram-negative bacteria, with the type 3, 4, and 6 secretion systems containing pili that extend beyond the outer membrane.[14] These pili typically are used to

exchange cellular material with other cells and are widely used in pathogens to secrete such things as virulence factors into host cells. Nucleic acid exchange is another major function, the type 4 secretion system evolved from ancestral bacterial conjugation machinery and includes the canonical conjugative pili.[14,15] Some of the other proteinaceous appendages have homology with the gram-negative secretion systems. The type 3 secretion system is derived from the protein system used to produce flagella. Similarly, the type 2 secretion system, which does not produce pili, is structurally related to the molecular components of type IV pili production.[16]

The three types of pili that are not components of secretion systems (chaperone-usher pili, type IV pili, and curli) have roles in attachment and motility and have different mechanisms of formation.[11] Chaperone-usher pili are constructed by transferring the major pili proteins across the periplasm with the aid of chaperone proteins. Curli proteins are excreted from the cell and form fibers by amyloid aggregation on targets on the outside of the bacterial outer membrane. Type IV pili form by polymerization from a pool of the pilin proteins stored on the inner membrane. The reversal of the polymerization of type IV pili provides the special ability among the classes of pili to retract.[16] The ability for type IV pili to rapidly grow and retract enables functions such as twitching motility, DNA uptake, and surface sensing.[16]

The simplest way for lipids to compose bacterial appendages is as extensions of the cell membrane. Several different membrane extensions have been reported. Prosthecae are extensions of the cell proper, which contain an outer membrane, inner membrane, and peptidoglycan layer. *Caulobacter crescentus* is a well-known prosthecate bacterium that produces membrane extensions approximately 100 nm in diameter with the function of facilitating nutrient uptake in diffusion-limited, oligotrophic environments.[17] Membrane tubules that attach *Salmonella enterica* to other bacteria and host eukaryotes have been reported with average diameters ranging

from 60–90 nm.[18] Bacterial membranes can also be extended from the cell body as a series of outer membrane vesicles. In *Myxococcus xanthus*, fused outer membrane vesicles with a width of 30–60 nm were observed, often connecting neighboring cells. The outer membrane vesicle chains show a single membrane and appear as either a series of discrete vesicles (meaning the vesicle chains appeared as a series of connected spheres) or with a continuous lumen, presumably after a fusion event.[19] Outer membrane extensions, in the form of tubes, fused vesicle chains, and flagellar sheaths, have been observed as early at 1971 in *Beneckea* species.[12]

Extracellular DNA is produced by bacteria and is a key structural component of bacterial biofilms.[20] DNA can form microfilaments between bacterial cells[21] and has been observed as a component of 10–100 nm thick filaments from *Enterococcus faecalis*.[22] The importance of Holliday junctions to the stability of extracellular DNA networks[20] may indicate the widespread presence of individual DNA duplexes, rather than bundles of cation-aggregated DNA strands. Filaments composed of single duplexes of DNA molecules would have a diameter of about 2 nm. The mechanism for secretion of extracellular DNA is unknown in many species, but the usage of the type 4 secretion system and vesicle trafficking has been observed in some cases.[23]

Polysaccharides are also a critical component of bacterial biofilms and extracellular space.[24,25] As one of the key components bacteria produce extracellularly, polysaccharides were first indicated to be the adhesive tethers for bacterial interaction with solids. The structural matrix of biofilms is referred to by the initialism EPS, originally meaning exopolysaccharides before being expanded to include nucleic acids and proteins as extracellular polymeric substances.[26] Polysaccharides are both secreted in a dissociated state and produced with cell association, for example by covalent bonding to membrane lipids.[25] Polysaccharides and nucleic acids—as far as their roles of extending beyond the cell of a bacterium while maintaining

interactions with the secreting cell—appear similar to curli, in that the polymers are secreted into an anisotropic network. The functionality of proteins and membranes to produce channels to transmit material at a distance, and of type IV pili to form and retract rapidly for transient surface interaction, does not appear prevalent with saccharides or nucleic acids.

Besides the main classes of macromolecules described above, other metabolic polymers, such as humic acids or polyhydroxyalkanoates, could produce extracellular structures if conditions occured that caused association of such polymers.[27]

2.1.3 Bacterial Nanowires: Electrically Conductive Appendages for Extracellular Electron Transport

Electrically conductive appendages from *Geobacter sulfurreducens* were first reported by Derek Lovley and co-workers in 2005.[10] The diameter of the nanowires that were attached to the cell body and measured by transmission electron microscopy was roughly 5 nm. Pili sheared off of the cells and measured by conductive atomic force microscopy (cAFM) had a diameter of roughly 15 nm. The electrical conductance of fibers isolated from cell culture was also measured by cAFM and was about 8 millisiemens (mS) across the width of the fibers to a graphite surface. The knockout of the protein PilA, which has the conserved amino acids of type IV pili, appeared to prevent the formation of cellular appendages and to prevent growth on iron III oxide. Fibers isolated from the cell culture of *Shewanella oneidensis* and *Pseudomonas aeruginosa* did not show conductivity in this report.

Gorby *et al.* in 2006 demonstrated the electrical conductivity of appendages from *S. oneidensis*, as well as *Synechocystis* PCC6803 and *Pelotomaculum thermopropionicum*.[28] These results, provided by scanning tunneling microscopy, suggested the nanowires were a

bundle of fibers. Furthermore, staining with a protein-specific dye—NanoOrange—suggested the nanowires contained protein. The bacterial appendages were not conductive in *S. oneidensis* strains that had the MtrC and outer membrane cytochrome OmcA proteins knocked out, nor in mutants where the GspD protein of the type II secretion system was disrupted.

Why did the original measurements by Lovley and co-workers not show conductivity in appendages of *S. oneidensis*? It may have been due to measurement errors, such as material build up on the cAFM probe producing high contact resistance and preventing appreciable conductance. It may be that the nature of the nanowires allows their conductivity to change, which would not likely be the case if the conductivity is an intrinsic property of the structural elements of the appendages. Finally, the objects measured may not have been the same material measured by Gorby *et al.*

When appendages are classified by one assay per sample, as they seem to have been in the two studies above, only size and shape can be used to determine if the appendages are the same objects in each measurement. This analysis of size and shape may suffice for a single researcher using well-controlled conditions, but becomes more liable to error when reproduction by other laboratories or different experimental conditions is attempted—especially when not accompanied with statistical analyses and a precise, quantitative definition. The method of depositing matter from cell culture creates the possibility of filaments found on the surface being different types of pili, different cellular appendages—like flagella, or debris that was not an appendage on a bacterial cell. It has been suggested that the appearance of bacterial appendages may be artifacts of extracellular matter condensing into filaments upon sample dessication.[29] Without precise characterization, a given fiber from a cell culture may mistakenly be referred to as a nanowire. The *S. oneidensis* appendage analyzed in Lovley and co-worker's 2005 report has

a diameter of approximately 30 nm consistent with flagella, whereas the diameter of the *S. oneidensis* nanowires reported by Gorby *et al.* in 2006 were 50–150 nm in diameter. The rich LB medium and unspecified oxygen conditions used by Lovley and co-workers could have prevented the metabolic state necessary for nanowire formation.

The unpredictability of cell culture behavior[30] and the dependence of nanowire formation on specific metabolic conditions with sufficient electron acceptor limitation[31] calls for careful analysis regarding the identity of material extracted from cell culture, which is a complex mixture of biological products. With thorough characterization that can unambiguously identify bacterial appendages, we sought to resolve inconsistencies in previously reported findings of bacterial nanowires and to use complementary techniques to better understand bacterial nanowires. Without further corroboration of the published literature, the importance, the characteristics of, and even the existence of nanowires within a bacterial biofilm are putative.

Elucidating the nanowire composition would be instructive to determine the mechanism of electrical conductivity through the nanowires. The mechanism of electron transport through bacterial nanowires is fundamental to understanding them. *S. oneidensis* and *G. sulfurreducens* emerged as model systems for understanding electron transport through bacterial nanowires. A different mechanism has been proposed for the electron transport through each of these model systems.[32]

The nanowires of *G. sulfurreducens* were postulated to have coherent metal-like conductivity through the PilA protein.[33] "Metal-like" refers to having higher conductivity at lower temperature rather than the overall magnitude of conductivity, which is semiconductive. When aromatic amino acid residues in the PilA protein were replaced with alanine residues, the

resulting appendages were not conductive, suggesting electrons propagate through interactions with the aromatic side chains.[34] A 3.2 Å periodic spacing, observed by X-ray diffraction, appears to be associated with the aromatic groups in the PilA protein.[35] For the conductive protein model to apply to a given nanowire, that nanowire will necessarily be composed of protein. As a type IV pilus, protein would comprise the structural element and the conductive component of such a nanowire.

As described above, electron transport through the nanowires of *S. oneidensis* is associated with outer membrane cytochromes—proteins that contain redox-active iron sites. Incoherent electron hopping is theorized to occur between the iron atoms where the electrons can localize.[36] Outer membrane cytochromes are found embedded in the outer membrane of *S. oneidensis,* but could also exist as part of a protein superstructure. Outer membrane cytochromes were observed along *G. sulfurreducens* appendages, which were considered to be conductive pili based on morphological comparisons to earlier measurements.[37] Besides the protein for the cytochromes themselves, a nanowire deriving conductivity from electron hopping between iron-containing heme units may contain other biological material to connect the cytochromes; polymerization of cytochromes is also possible.[38] For sufficient electron transport rates, the electron localizations of the cytochromes need to be less than a nanometer apart, therefore the proteins would be closely positioned to each other.[39]

Light was shed on the mysterious nature of the chemical composition of *S. oneidensis* nanowires in 2014 when membrane-associating fluorescent stain was applied to cell cultures by El-Naggar and co-workers.[40] Using other fluorescent markers specific to various cellular areas and materials, they concluded that appendages of *S. oneidensis* are extensions of the outer membrane that contained proteins—including the electron transport proteins OmcA and MtrC—

and periplasm. Atomic force microscopy (AFM) was used to match the information from fluorescence with nanoscale features. The diameter of the appendages was reported as 10 nm, while the published AFM images show an approximately 40 nm diameter. The morphology of the appendages matched that of previously reported membrane extensions and fused vesicle chains. Electrical measurements were not taken of the membrane extensions in the 2014 report however. Relation to the previously observed *S. oneidensis* appendages was limited to size, shape, and a correlation of the growth of the fluorescently-labeled appendages with respiration rate and electron acceptor availability.

Identification of nanowires based on size and shape is limited however. The morphology of reported *S. oneidensis* nanowires has varied from fiber bundles,[28] to homogenous linear strands,[41] to homogenous and wavy,[42] to series of fused orbs. The diameter of the appendages was reported smaller in El-Naggar and co-workers' 2014 paper than previous reports of *S. oneidensis* nanowires. While meaningful for excluding small pili as possible identities, the size of *S. oneidensis* appendages does not appear to be precise. It seems that neither size nor shape provide a rigorous definition of what a bacterial nanowire is. The evidence from the fluorescent staining experiments indicated membrane extensions are perhaps the most likely basis of the conductive nanowires observed in *S. oneidensis*, but does not go far enough to eliminate doubts that other appendages could be the conductive nanowires instead of, or in addition to, the fluorescently labeled membrane extensions. The EET mechanism of bacterial nanowires has remained elusive and was heavily contentious at the time of the research described in this chapter despite years of research on the key model systems.[43] Robust characterization of cellular appendages is needed to determine unambiguously the composition of the appendages and therefore the possible electron transport mechanisms. Both electrical information, to validate

function as a nanowire, and complementary chemical or mechanical information, to determine composition and structure, are needed from any given appendage to form conclusions on the properties of bacterial nanowires. By understanding the material composition of bacterial nanowires, the nature of nanowires is elucidated and with them a major component of EET. Understanding this fundamental interaction of microbial metabolism with the environment is a major part of understanding microbes and the possibilities for harnessing them.

My goal was to resolve discrepancies in the literature, corroborate evidence to increase confidence in the respective theory, and to devise methods for the conclusive analysis of cellular appendages. Single-appendage electrical measurements are important to exclude the properties of other material from the cell culture and effects of contact resistance. Scanning probe microscopies, such as AFM, can resolve sub-cellular components and provide electrical and mechanical information.

Combining the electrical and mechanical information of AFM with the chemical information provided by optical microscopy with fluorescent probes enables the desired characterization. To rigorously determine what a bacterial nanowire is, I sought to use a combination of conductive atomic force microscopy and fluorescence imaging.

2.2 MEASUREMENTS OF *SHEWANELLA ONEIDENSIS* AND *GEOBACTER SULFURREDUCENS* NANOWIRES

2.2.1 Induction of Microbial Nanowires Generation

The first experimental difficulty in studying bacterial nanowires is producing nanowires reliably. Nanowires are known to grow in response to oxygen limitation, where electron acceptors must

be provided at a low enough concentration to limit bacterial growth in order for nanowire growth to appear.[28] Here we used a method of sudden oxygen limitation that does not require the use of a chemostat.

To stimulate the production of nanowires by *S. oneidensis*, cells were removed from an aerobic culture and resuspended in an anaerobic, chemically-defined medium with lactate as an electron donor and 100 nM ferric chloride as an electron acceptor. Some samples had 30 mM of fumarate added to limit electron acceptor concentration without starving the cells. No noteworthy difference was observed between samples that had supplemental fumarate and those that did not. 133 nM riboflavin was also present in the media, presumably in mixed oxidation states. With this method, appendages could be observed on the cells by scanning electron microscopy (**Figure 2-1A**) and AFM (**Figure 2-1B**). Similar appendages were observed from *Geobacter sulfurreducens* grown in an anaerobic reactor (**Figure 2-1C**).

The appendages observed on the cells when exposed to an anaerobic environment do not appear to be mono-polar flagella, which are observed on *S. oneidensis* in both aerobic and anaerobic conditions. Flagella are several cell lengths long and typically have either a sinusoidal shape or are linear if pulled in one direction. The anaerobically produced appendages had a diameter of 70 nm for both *S. oneidensis* and *G. sulfurreducens*, as measured by AFM. The appendages were shorter and wider than the flagella, and have an apparently smaller persistence length as well, resulting in bends with smaller radii of curvature and less regular vacillations. The thickness of these appendages is consistent with reports of membrane extensions but not pili.

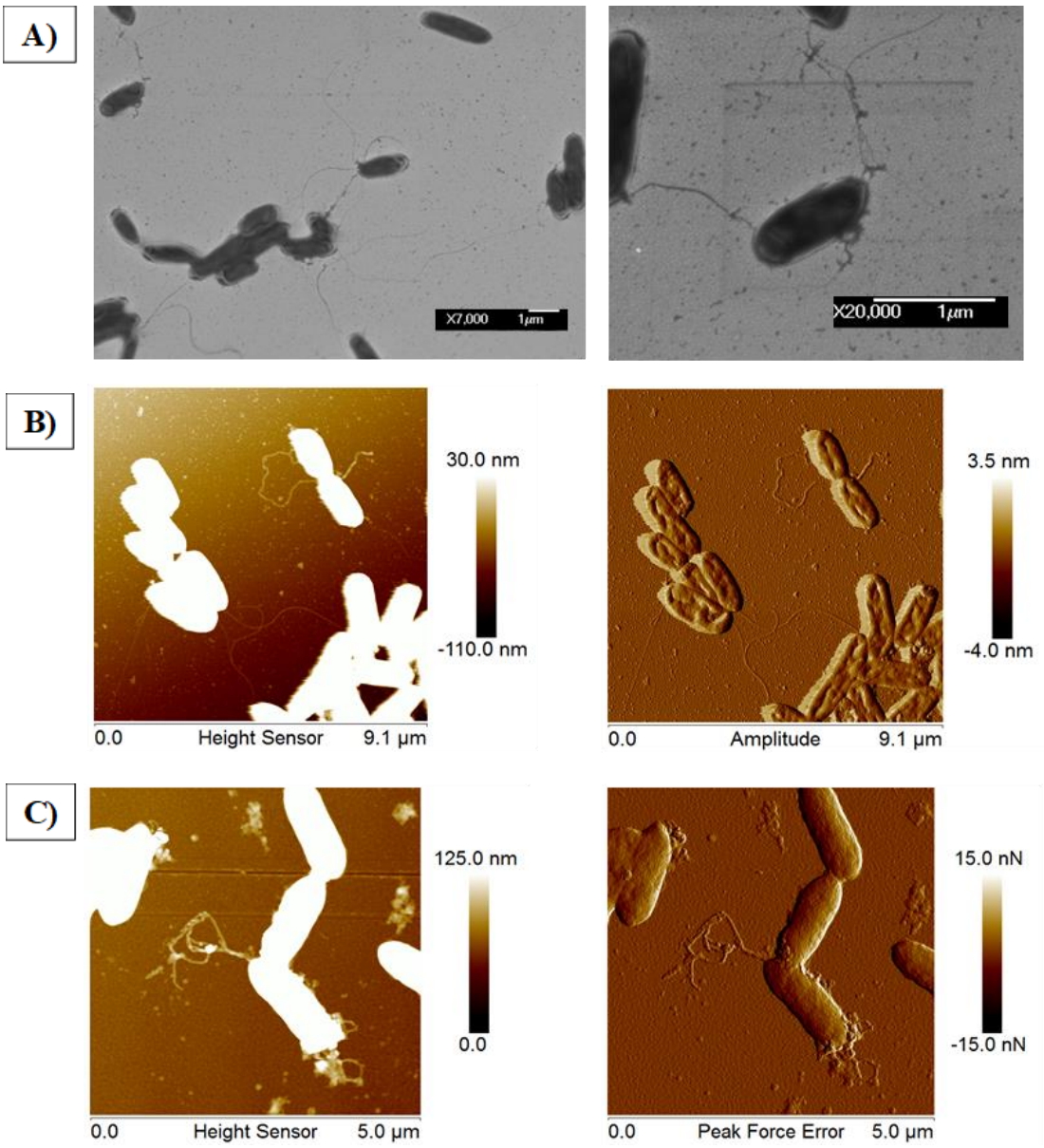

Figure 2-1. (A) Scanning electron micrographs of *Shewanella oneidensis* cells that were resuspended in anaerobic media. Flagella are seen across surface as well as other appendages that are shorter with more irregular curvature. Atomic force micrographs of **(B)** *S. oneidensis* and **(C)** *G. sulfurreducens* cells with appendages.

2.2.2 Conductance Measurements with Atomic Force Microscopy

Adhesiveness and conductance mapping of *G. sulfurreducens* are shown in **Figure 2-2** along with the spatial dimensions reproduced from **Figure 2-1**. Peak force tapping mode was used with AFM to obtain further information on the intrinsic nature of the appendages. In peak force tapping, atomic force spectra are recorded in a spatial array producing images of mechanical properties simultaneously with topographic measurements. Adhesiveness is one of several mechanical properties that can be recorded with AFM imaging. Adhesion, the amount of force that the AFM cantilever experiences upon retraction just before the contact is lost with the sample, is shown in **Figure 2-2B**. The PtIr-coated AFM probe tip experiences a greater magnitude of adhesive force with the *G. sulfurreducens* appendages than the cell bodies or the surrounding gold surface. Other material on the surface is less distinguishable from the background adhesion. Circular spots across the image, which have similar diameter and height to the cellular appendages, match the adhesiveness of the appendages and may be secreted membrane vesicles.

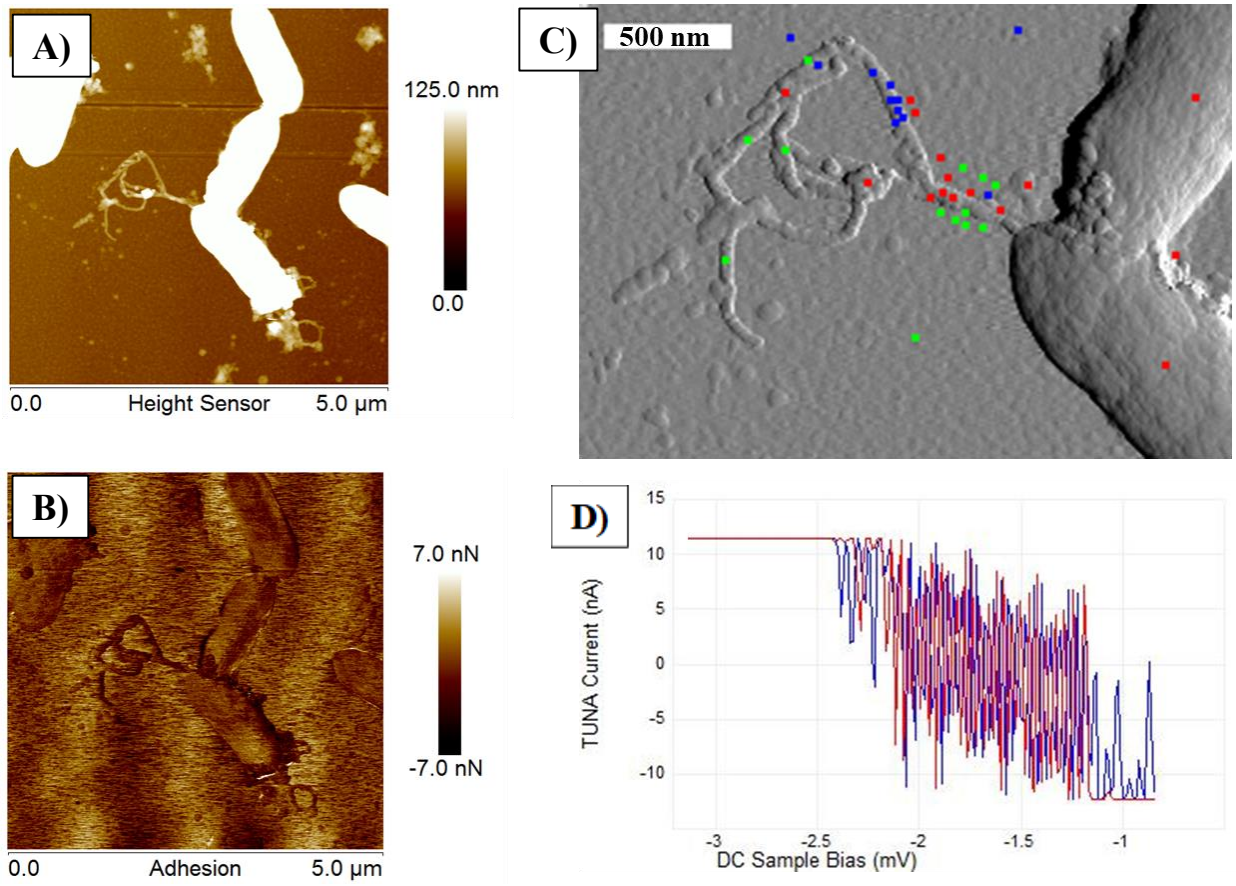

Figure 2-2. Electrical measurements of *G. sulfurreducens* appendage. **(A)** Sample topography. (reproduced from **Figure 2-1**) **(B)** Map of adhesive force measured by retraction of the AFM probe. **(C)** Map of current-voltage measurements with high conductance (>10^{-4} S) marked green, low conductance (<10^{-8} S) marked red, and intermediate conductance marked blue. **(D)** Representative voltage ramp measurement of intermediate conductivity (with inverted instrument current). The estimated resistivity from this measurement is 5 x10^{-6} Ω·m.

Conductance was measured by setting the AFM probe tip to a fixed location, sweeping the voltage difference between the tip and the sample, and recording the resulting electrical current. Conductance values were plotted on the image from peak force error channel of the *G. sulfurreducens* sample (**Figure 2-2C**). Areas with low conductance produced negligible current that did not emerge above the noise limit over the measured voltage range. These locations are marked with red dots in **Figure 2-2C**. This insulating character is consistently observed over cell bodies. Low conductance was also observed over some unidentified debris on the sample and in parts of the putative nanowires. Conductive points, where the change in

current per volt exceeds the sensitivity of the atomic force microscope, are marked with green dots. These locations generally correspond to areas that show the grain texture of the gold substrate, which presumably are not covered by adsorbents from the culture solution. Some areas on the bacterial appendages also show high conductance.

Locations with intermediate conductance are marked with blue dots. Most of these points appear over the bacterial appendages. **Figure 2-2D** is a representative measurement of current as a function of voltage at one of the locations marked with a blue dot. Conductance is represented by the slope of the line relating current and voltage. Conductivity can be calculated from conductance using the height measurements from peak force tapping mode as the distance between the tip and sample electrodes and estimating the cross sectional area of the sample to be similar to the AFM probe's tip diameter. This approximation yields a resistivity of 5×10^{-6} Ω·m for the measurement shown in **Figure 2-2D**. The resistivity suggests the sample is less conductive than most metals but more conductive than semiconductors. However, the conductivity is likely overestimated, because the tip radius used for the calculation is an underestimate of the cross section of the electron's pathway through the sample. The distribution of geometries that electrons traverse across the sample junction is not known. The current goes across the width of the appendage, and most electrons presumably traverse the shortest path, but an undetermined amount of electrons have the opportunity to move about the entire length of the appendage.

Some measurements on the cell appendages showed low conductance. Increased resistance may be the result of stochastic adsorption of insulating material. Salts that failed to be removed during sample preparation could be one such contaminant. Variations in the geometry of the interface between the tip and the surface may also lead to anomalous contact resistance.

Other points on the bacterial appendages showed high conductance. The AFM tip pushing through the appendage or drift of the probe location would, in either case, cause the gold substrate to be detected. The uncertainty of whether or not the probe is cutting into the appendage or sampling the gold substrate is a major obstacle for determining nanowire conductivity using current measurements across the width of the appendages.

Recording conductive AFM measurements over an insulating surface and measuring current along the length of a bacterial appendage prevents measurements of an underlying conductor and reduces the effects of contact resistance and importance of tip geometry. Calculations of conductivity are also more reliable when measuring across the length of a nanowire, because the path length is larger relative to the uncertainties of the measured quantities.

Conductivity along the length of *S. oneidensis* appendages was demonstrated in 2010 by El-Naggar and co-workers.[44] Resistance was shown to have a linear relationship with the distance between electrodes and extrapolation provided the contact resistance of the system. Nanowire resistivity was determined to be 1 Ω·cm by these measurements. Mutants lacking the OmcA and MtrC cytochromes produced appendages that were not conductive. The precise electrical measurements performed by El-Naggar and co-workers did not characterize the composition of the nanowires or other identifying features besides size and shape.

Replicating the results of El-Naggar and co-workers was attempted to serve as a basis to combine with mechanical information and chemical information from fluorescent probes. **Figure 2-3** shows *S. oneidensis* applied to an array of silicon dioxide interspersed with gold.

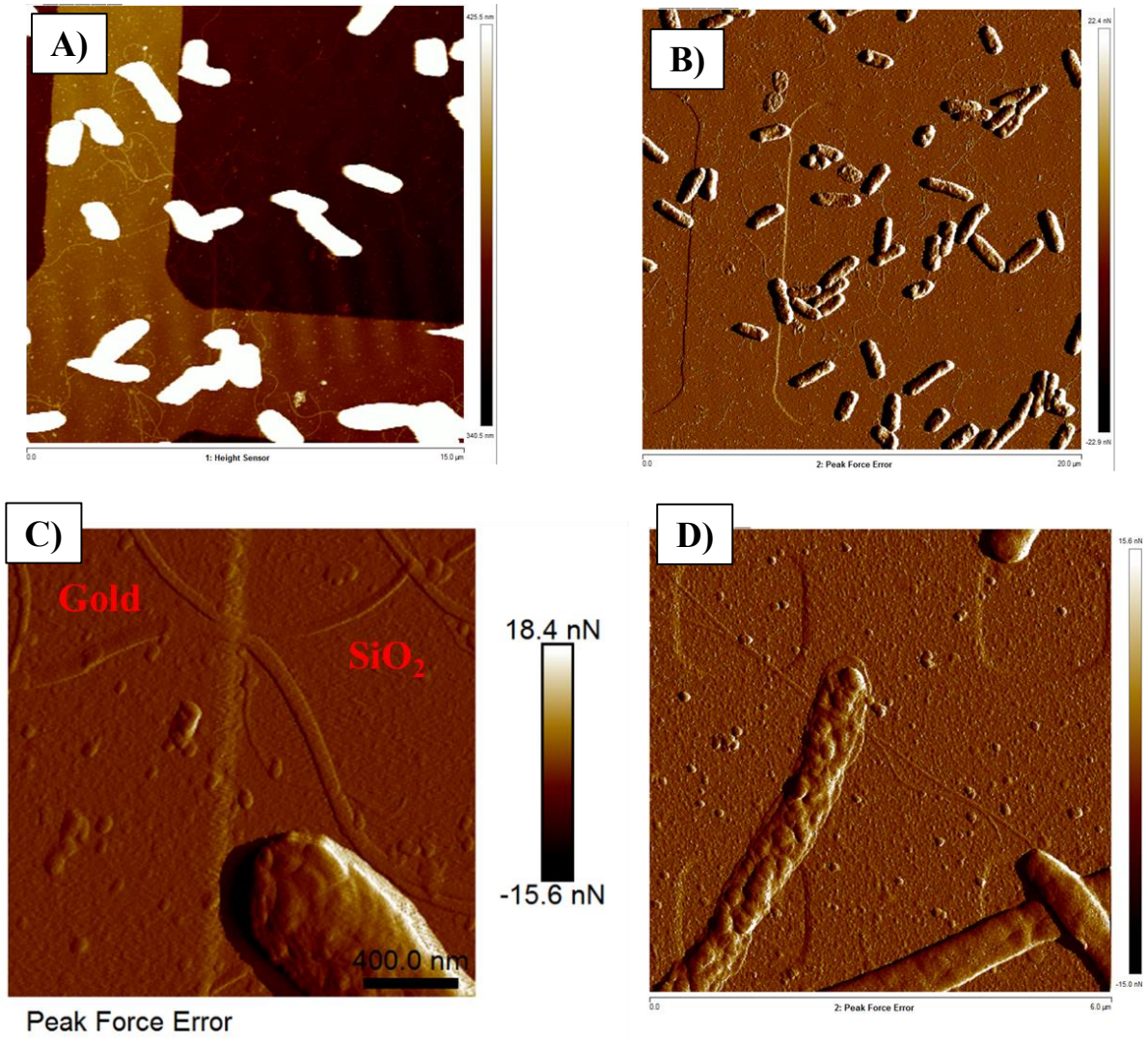

Figure 2-3. Patterned gold surfaces to measure conductivity along filament length. *S. oneidensis* was applied to the surface, which featured recessed areas of insulating silicon dioxide surrounded by gold that is electrically connected to an atomic force microscope. The placement of appendages across a metal oxide junction is demonstrated with flagella.

Appendages were found stretching across areas of silicon dioxide to gold regions. The appendages appear similar to flagella and appreciable current was not measured. Observing electrical conduction along the length of bacterial nanowires compounds several unpredictable aspects of the sample preparation. First, nanowires need to be produced as a metabolic response. Next, the nanowires need to be positioned to cover a length of insulator before a section of gold. The deposition of the appendage must also have a good connection with the gold electrode.

Finally, conductive AFM measurements need to be performed with enough force to form electrical contact, but not too much force so as to disrupt the nanowires. After many attempts, a sample where nanowires were produced and were placed across a boundary of gold and silicon dioxide was not observed by my AFM measurements. The probability of creating an adequate sample for conductive AFM measurements becomes prohibitive when introducing additional measurements to characterize the nanowire composition. Fluorescence stains such as FM 4-64FX, which was used to identify the membrane extensions of *S. oneidensis*, are designed to be applied to living cells in a hydrated state and imaged soon after. Integrating fluorescence probes with AFM measurements may therefore require AFM to be performed after optical microscopy, further complicating the experimental procedure. Devising methods to increase the reliability of useful samples will improve reproducibility and enable more complex experimentation. Controlling the placement of the bacteria and their appendages is one strategy to reduce the rate of samples being unsuitable. Methods for guiding bacterial surface attachment and spatial placement were explored as described in the following chapters.

Damage of bacterial appendages by AFM is demonstrated in **Figure 2-4**. Possible sample disruption from scanning probe measurements is an important consideration. Electrical measurements across the length of a filament require that the entire length remains intact and undisrupted. However, perturbation from AFM can change the sample and move appendages. Flagella from the archaea *Methanospirillum hungatei*, which are hypothesized to have electrical conductivity, were scanned with the peak force tapping imaging and conductive AFM ramping method used for *G. sulfurreducens* above. Strands of flagella observable on the initial scan of the surface were no longer present upon another scan that followed numerous electrical measurements.

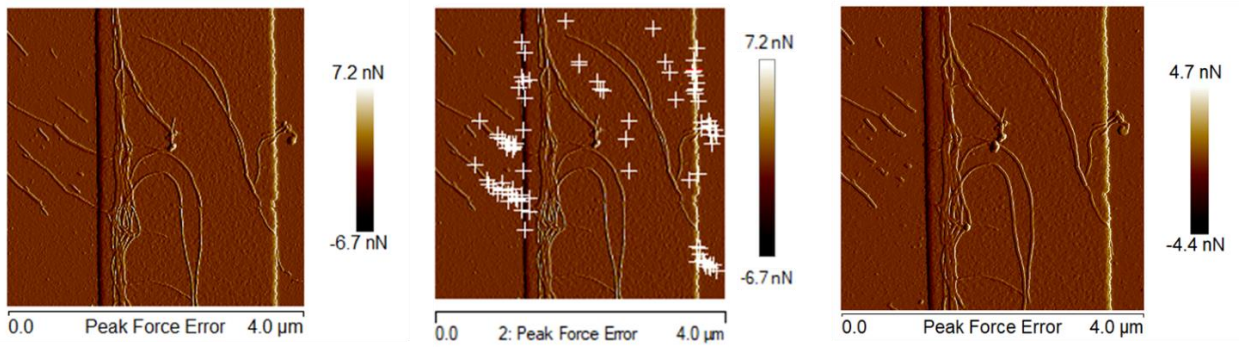

Figure 2-4. Change in filaments from *Methanospirillum hungatei* after scanning. **(Left)** Initial AFM scan. **(Middle)** Positions of electrical measurements. **(Right)** AFM scan after electrical measurements.

The issue of sample perturbation from the AFM tip can compound the problems of unreliable nanowire formation and arrangement of the nanowire across a conductor-insulator junction. Techniques needed for mechanistic investigation can be particularly sensitive to perturbation by scanning probes. For example, determination of the temperature dependence of nanowire conductivity requires many measurements of the same sample, with the possibility of disturbing the appendage structure each time. Such an experiment is more practical when samples are easily available. Another strategy for avoiding perturbation from the AFM tip is to use non-contact AFM modes. One such mode to probe electrical properties is electrostatic force microscopy (EFM).

2.2.3 Electrostatic Force Microscopy of Isolated Pili

Malvankar *et al.* used electrostatic force microscopy to measure the capacitance of *G. sulfurreducens* appendages in response to an injection of electrical charge.[45] Generation of force from isolated *G. sulfurreducens* fibers in response to the presence of electrical charge was verified by my independent measurements (**Figure 2-5**). This response indicates charge mobility or polarizability of electron density. However, unlike the symmetrical response to positive and negative voltages of the EFM probe reported by Malvankar *et al.*, the response here shows

greater phase shift of the EFM cantilever's oscillation at –5 V than +5 V. Here the voltage is relative to the sample. These results may indicate a propensity for the nanowires to accumulate positive charge, possibly by oxidation of redox groups within the nanowire. If these supposed redox groups do not easily become reduced, the movement of electrons toward the positively charged EFM probe would be limited and a smaller response expected, as observed.

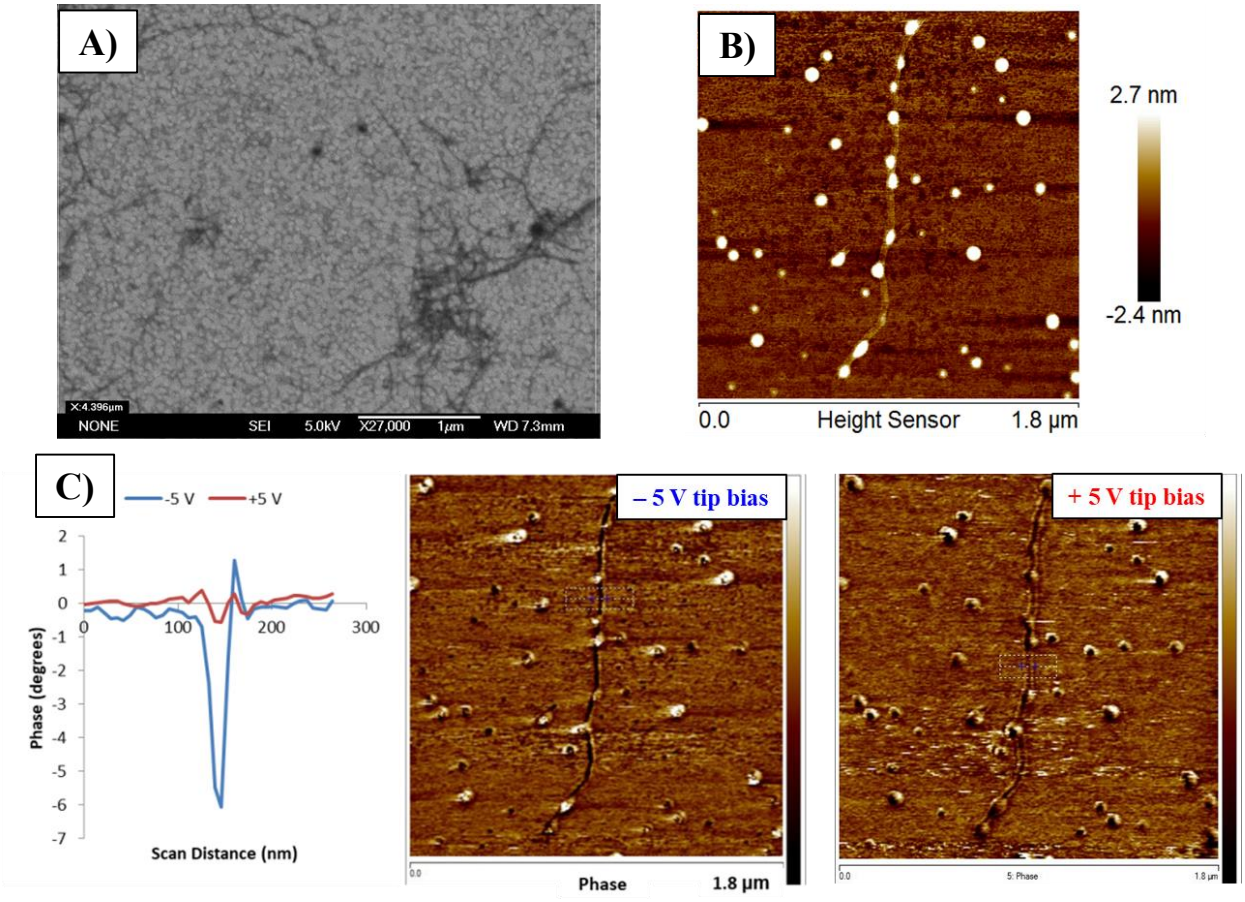

Figure 2-5. Electrostatic force microscopy of isolated *G. sulfurreducens* appendages. **(A)** Scanning electron micrograph of appendages supposed to be pili drop-cast onto a gold surface. **(B)** Atomic force micrograph of an appendage, height sensor channel. **(C)** Electrostatic force measurement of the same appendage. The phase of the AFM cantilever is shown as the sample was scanned while the tip was poised to –5 V and +5 V. Lines sections are displayed on the left.

2.2.4 Considerations for Optical and Electrical Measurements of the Same Samples

Correlated measurements of optical microscopy and atomic force microscopy, and related techniques, can be a powerful tool for the study of microbial appendages including nanowires. Fluorescence imaging can provide chemical information with membrane-specific, protein-specific, and other fluorescently active compounds that interact with particular material or chemical groups. Atomic force microscopy provides high resolution at the sub-cellular level and probes physical characteristics such as conductivity and mechanical properties.

Performing measurements by both optical microscopy and AFM necessitates transfer of the substrate carrying the bacteria between an optical microscope, in an aqueous state for many fluorescent probes, and an AFM stage where the sample is accessible to the AFM head. A flow cell with a surface that could be attached and removed by application of a vacuum pump was designed and fabricated, as shown in **Figure 2-6**, to allow the use of live imaging in culture media with optical microscopy. The flow cell is capped with a glass coverslip, which can have metal electrodes already produced by lithography. The body of the flow cell was created from transparent polyacrylate or polycarbonate. O-rings are inserted into the outer groove to seal the vacuum chamber. Solution containing the cells of interest is flowed through the inner channel for deposition or real-time imaging. The flat coverslip can be easily set on the AFM stage and scanned before or after attachment to the rest of the flow cell.

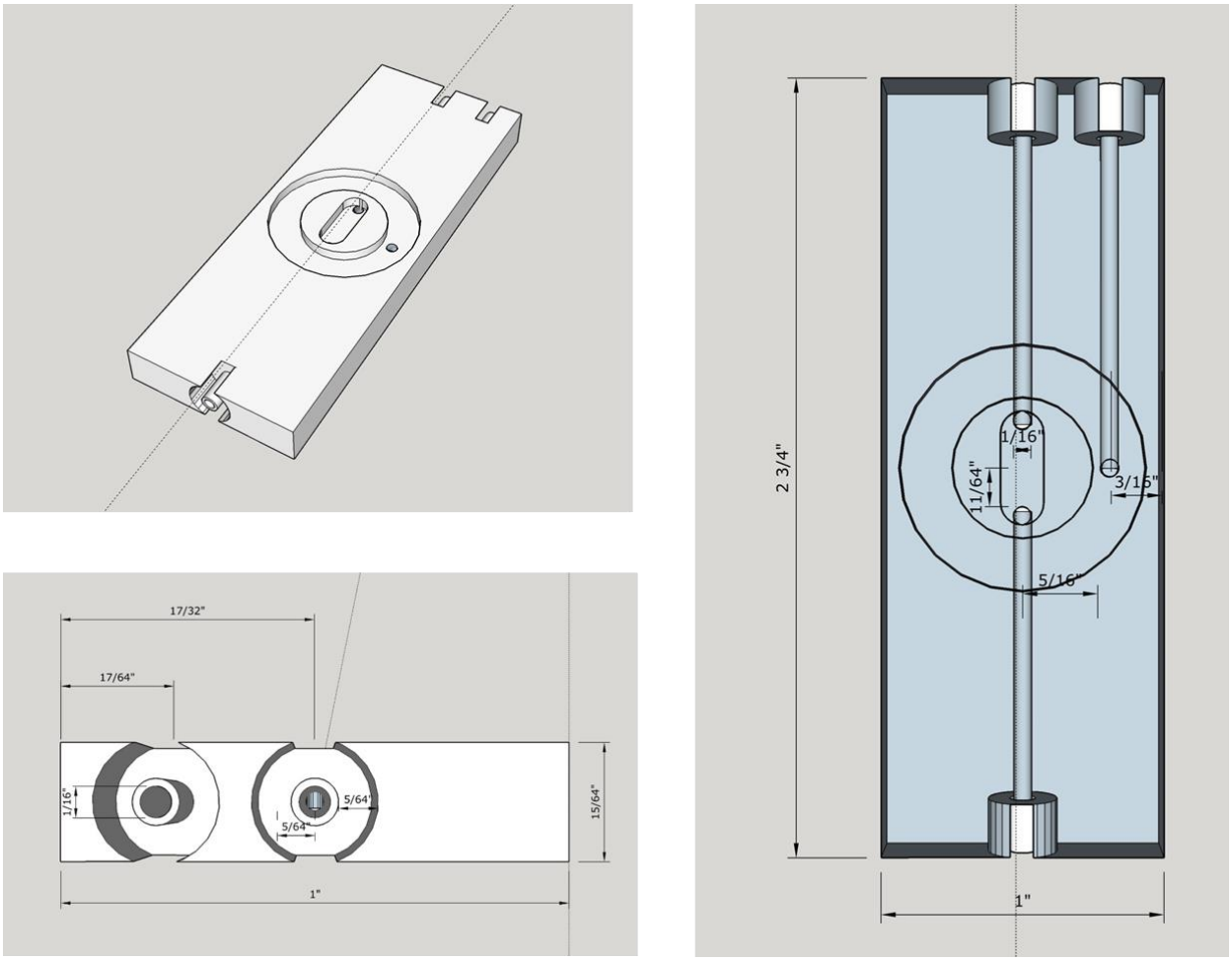

Figure 2-6. Design of vacuum flow cell for facile transfer of bacterial samples between optical and atomic force imaging. The top of the device supports a flat substrate, such as a glass slide, for cells to attach to, which can be removed by disconnecting the vacuum.

2.3 FUTURE DIRECTIONS FOR SCANNING PROBE MICROSCOPIES ON BACTERIAL APPENDAGES

Bacterial appendages are inherently difficult to purify. They are sub-cellular objects that have emergent properties beyond that of individual molecules and cannot be isolated into chemical components without losing the properties of the appendage. Therefore, it is difficult to separate identification from other kinds of analysis, and multiple types of measurement on the same sample are necessary for good characterization. One measurement to define the sample identity

and another to provide new information are a minimal requirement. In the case of nanowires, electrical conductivity is the defining feature. Association of conductivity with more readily measured properties has not yet been conclusively established.

Scanning probe techniques provide nanoscale, non-ensemblic measurements, without the need to isolate microbial appendages from cell culture. Utilizing force spectroscopy, through modalities such as peak force tapping, while imaging with atomic force microscopes is a powerful tool to characterize nanoscale objects. Mechanical properties, in addition to predicting mechanical behavior, can be used to identify specific appendage types and provide evidence for elucidating their material composition. In this chapter, the potential for adhesiveness to act as a nanowire identifier was shown. Adhesion measurement can easily be implemented in experiments where conductivity is being measured by AFM. Furthermore, adhesion can be measured with less conditions for sample preparation than electrical measurements and thus is more readily paired with other techniques. Fabricating electrodes and ensuring electrical contact without short circuits is a burden for using conductivity as an identifier of nanowires.

However, information from mechanical and topographical sources are less specific than chemical information. Reliability may also be compromised by the state of the sample. For example, when an appendage is pulled taut, it may alter mechanical properties. Atomic force microscopy correlated with fluorescence microscopy has been suggested here as a strategy to integrate chemical information into AFM experiments. Dehydration of samples is often employed for nanoscale microscopies, such as scanning probe or electron microscopy. Atomic force microscopy of liquid samples can be used to prevent distortion of the physical properties of nanowires. Change in the spacing between cytochromes in a nanowire may occur during desiccation and can have significant impact on electrical conductivity. Liquid AFM may be a

fruitful technique to pair with fluorescence microscopy for observation of the pristine state and native characteristics of microbial appendages.

Scanning ion conductance microscopy (SICM) and scanning electrochemical microscopy (SECM) are scanning probe techniques useful in liquid environments. The combination of SICM and SECM (SICM-SECM) with a double chambered probe can provide nanoscale resolution of cellular appendages while measuring local electrochemical states.[46] Scanning electrochemical microscopy alone has been applied to whole biofilms of *S. oneidensis,* but lacked the spatial resolution and direction of SICM for measurement of single cells.[47] These electrochemical states can determine not only that an appendage is conductive, but also what electrochemical potentials are relevant to the redox centers of an incoherent electron hopping system. Scanning ion conductance microscopy-scanning electrochemical microscopy is a non-contact scanning probe method that can avoid the sample perturbation demonstrated in **Figure 2-4**. Scanning ion conductance microscopy-scanning electrochemical microscopy is a promising tool for studying bacterial nanowires with the potential to localize charge carriers around the cell body and appendages.

The success of scanning probe techniques, such as AFM and SICM-SECM, in analyzing bacterial appendages can be improved by controlling the placement of cells on the surface. A well-defined array of cells can position nanowires between conductors for cAFM and prevent crowding of redox sites or pseudocapacitive material that may obscure imaging near the resolution limit of SICM.

2.4 CONCLUSIONS ON THE ORIGIN OF CONDUCTIVITY IN BIOFILMS OF *GEOBACTER SULFURREDUCENS* AND *SHEWANELLA ONEIDENSIS*

Debate has been active for years over whether bacterial nanowires are composed of pilin proteins or cytochrome containing membrane extensions, and whether the mechanism of conductivity is due to incoherent electron hopping or coherent superexchange.

The importance of cytochromes can be observed when cytochromes are knocked out genetically or located by microscopy with specific labeling. It has been shown *Geobacter* requires outer membrane cytochromes to reduce iron III oxide,[48] and cytochromes are associated with *G. sulfurreducens* nanowires.[37] So perhaps the cluster of iron-containing heme groups in the cytochromes are the critical component for EET through bacterial nanowires. The hypothesis that *S. oneidensis* nanowires are cytochrome-containing membrane extensions[40] may also apply to *Geobacter*. The similarity of the appendages between the two species in **Figure 2-1** supports the possibility of *G. sulfurreducens* also producing membrane extension appendages. Indeed, a recent report has claimed *G. sulfurreducens* nanowires are composed of the OmcS cytochrome and derive their conductivity from closely spaced heme groups.[49]

Could the pili-based nanowire hypothesis have been based on misleading experimental results? In the original report of *Geobacter* nanowires by Reguera *et al.* in 2005, the premise that the PilA pilin protein formed the nanowires was based on the reduced iron reduction rate of a PilA deficient mutant.[10] However, the iron reduction measurement appears to be based on a single trial and susceptible to the natural variation of cell cultures. The diminished iron reduction rate was claimed to be the result of reduced EET and not due to lack of attachment to the mineral, yet the bacteria did show less attachment after 48 hours.

Possibilities for error allow doubt to persist regarding nanowires. However, Lovley and co-workers demonstrated conductivity of no less than 0.22 S/m for *Geobacter* pili that was expressed from *E. coli*.[50] This result demonstrates a previously non-conductive specimen developing conductivity from only a piece of the *G. sulfurreducens pilA* gene and nothing else related to *G. sulfurreducens*. While the nanowires secreted from *E. coli* suffer the same characterization difficulties as other bacterial filaments, the PilA protein does appear to be electrically conductive.

Two models for the conductivity of bacterial nanowires developed from the study of *G. sulfurreducens* and *S. oneidensis*. The literature on each species influenced the other. Controversies in the field seemed as if they might be resolved simply by treating the systems independently, with *Geobacter* nanowires being metal-like coherent conductors made of pili, and *Shewanella* nanowires being membrane extensions harboring redox centers that enable incoherent electron hopping. This solution does not resolve all inconsistencies nor explain the OmcS cytochrome related conductivity from *G. sulfurreducens*. Rather than each model being limited to a single system, perhaps multiple conductive appendages exist in one or both systems.

Microbes that occupy a niche where EET is needed to interact with electron reservoirs could benefit from having both a rapidly constructed and retractable appendage, such as type IV pili, that can sense electron acceptors or donors through the electrical current and a conductive membrane-based appendage, which may be able to produce greater rates of electron exchange by virtue of a lower resistance pathway and electron shuttling through the periplasm core. If multiple conductive appendages can be formed, it seems advantageous for microbes to produce them. In terms of electron transport through both soluble electron mediators and solid conduction, it has been calculated that multiple EET mechanisms will improve metabolic

performance.[9] Should multiple kinds of bacterial nanowires exist in a single species, the importance of rigorous analytical techniques that can characterize cellular appendages will be greater than ever.

2.5 MATERIALS AND METHODS

Bacterial Culture and Biological Materials

A *Shewanella oneidensis* MR-1 p519nGFP colony from lysogeny broth (LB) agar plates containing 50 mg/L kanamycin was cultured in 20 mL LB media in a 125 mL flask for 24 hours at 32 °C while shaking at 200 rpm. 1 mL of the resulting culture was used to inoculate fresh 20 mL LB medium and cultured for 15 h under the same conditions. The cells were washed by spinning at 2300*g* in a centrifuge for 5 min then resuspending in modified M1 medium (M1 media supplemented with the components listed below). Dibasic sodium fumarate was added to a final concentration of 30 mM for the samples shown in **Figure 2-1B** and **Figure 2-1Figure 2-3**. No fumarate was added for the sample shown in **Figure 2-1A**. Prior to use, the modified M1 media was stored in an anaerobic hood overnight vented with filtered needles. Cells were then spun down and resuspended for a total of three times. 200 μL of the resuspended cells was diluted into 2 mL of fresh modified M1 medium. The cell culture was incubated at 32 °C without shaking for 8 hours. The bacteria were then fixed by add glutaraldehyde to the culture solution for a final concentration of 2.5%. The fluorescent stain FM 4-64FX was added to the culture for 10 min prior to fixation for the samples shown in **Figure 2-3**. The cultures were left under anaerobic atmosphere overnight.

G. sulfurreducens PCA culture was provided by the Kenneth Nealson lab at the University of Southern California.

Isolated pili from *G. sulfurreducens* were provided by the Derek Lovley lab at the University of Massachusetts, Amherst.

Flagella from *M. hungatei* were provided by the Hong Zhou lab at the University of California, Los Angeles.

Modified M1 media: pH 7.2, 85 mM NaOH, 30 mM PIPES buffer, 28 mM NH_4Cl, 1.34 mM KCl, 4.35 mM NaH_2PO_4 monohydrate, 30.2 mM NaCl, 60 mM sodium DL-lactate, 20 mg/L L-glutamate, 20 mg/L L-arginine, 20 mg/L DL-serine, 100 nM $FeCl_3$ hexahydrate, 195 nM sodium bicarbonate, 78.6 μM trisodium nitrilotriacetate, 121.7 μM $MgSO_4$ heptahydrate, 29.6 μM $MnSO_4$ monohydrate, 3.6 μM $FeSO_4$ heptahydrate, 6.8 μM $CaCl_2$ dihydrate, 4.2 μM $CoCl_2$ hexahydrate, 9.5 μM $ZnCl_2$, 0.4 μM $CuSO_4$ pentahydrate, 0.2 μM $AlK(SO_4)_2$ dodecahydrate, 1.6 μM H_3BO_3, 1.0 μM Na_2MoO_4 dihydrate, 1.0 μM $NiCl_2$ hexahydrate, 0.8 μM Na_2WO_4, 81.9 nM D-biotin, 45.3 nM folic acid, 486.4 nM pyridoxine HCl, 132.8 nM riboflavin, 140.7 nM thiamine HCl, 406.2 nM nicotinic acid, 209.8 nM D-pantothenic acid hemicalcium salt, 0.7 nM cyanocobalamin, 364.6 nM *p*-aminobenzoic acid, and 242.4 nM α-lipoic acid, all buffered to a pH of 7.2.

Substrate Preparation

Gold surfaces were composed of a 100-nm gold layer adhered to a silicon wafer with a 5 nm layer of titanium, unless stated otherwise. Just before use, gold surfaces were flame annealed with a 4 cm hydrogen flame by sweeping the flame over the surface once per second for 45 s.

The fixed *S. oneidensis* cultures were poured onto the gold substrates. Pipetting was avoided to prevent sheering of the bacterial appendages. The gold surfaces were soaked in the fixed cell

solution for 80 min before submerging in deionized water for 5 min. The samples were gently dried with a stream of nitrogen.

G. sulfurreducens culture was grown in an anaerobic chemostat that was spiked with reduced cysteine every 12 h to maintain a reductive state. The culture was applied, without air exposure, directly to the gold surface, which was flame annealed before use.

Isolated *G. sulfurreducens* pili in aqueous solution were vortexed for 1 min before placing a drop onto a silicon piece with a 200-nm-thick oxide layer and allowed to dry.

M. hungatei flagella were drop cast onto a gold pattern on top of a silicon dioxide layer of a silicon wafer. The samples were rinsed with water and then dried with nitrogen.

Patterned Gold and Silicon Dioxide Pattern Fabrication by Photolithography

Silicon wafers (University Wafer, South Boston, Massachusetts, USA) that were p-type, 0.001–0.005 Ω·cm, and <100> orientation were baked in a tube furnace to produce a 210.1 nm thick oxide layer. The negative tone photoresist AZ nLOF 2020 (MicroChemicals, Ulm, Germany) was applied to the wafers using a track coater. The wafer was exposed to broadband ultraviolet light for 5.5 s with the desired photomask using a Karl Suss MA6 contact aligner. A post exposure bake was performed for 1 min at 110 °C. The photoresist was developed in AZ 300 MIF (metal ion free) developer for approximately 45 s with swirling. Descuming was performed with a Matrix 105-Downstream Asher at 100 °C for 1 min, three times. A 3.6 nm Cr adhesion layer was evaporated at a rate of 2 Å/s followed by 20.2 nm of Au at 3 Å/s using a CHA metal evaporator. The remaining photoresist was stripped in Baker photoresist stripper 3000 at ca. 50 °C for 4 h. The wafers were rinsed with millipore water and dried with a nitrogen stream.

The substrates were flame annealed then exposed to propyl trimethyoxysilane vapor in a vacuum flask at 40 °C. A house vacuum line was applied for 1 min and static vacuum was held for 1 h before the substrate was removed.

Scanning Electron Microscopy

A JEOL JSM-6700F field emission scanning electron microscope was used to image cells with an SEI secondary electron detector. A 3 kV accelerating voltage was applied at 10 μA emission. The working distance was set to 8 mm. Scanning electron microscopy was performed after AFM to prevent destruction of the sample by the electron beam.

Atomic Force Microscopy

A Dimension Icon atomic force microscope (Bruker, Billerica, Massachusetts, USA) in soft tapping mode was used to locate cells before electrical measurements were made. SCM-PIT probes (Bruker, Billerica, Massachusetts, USA) were used. **Figure 2-1B** was collected with soft tapping mode with 9.08 μm scan size, 0.897 Hz scan rate, and 512 x 512 image resolution. Integral gain was 2.0. Proportional gain was 6.0. The amplitude setpoint was 105 mV, drive frequency was 74.164 kHz, drive amplitude was 54.32 mV. The cantilever spring constant was measured to be 2.183 N/m.

G. sulfurreducens cells were also analyzed with a Dimension Icon atomic force microscope with SCM-PIT probes. Soft tapping mode was used first to locate cells. A 0.999 Hz scan rate was used for the 6.04 μm image with 512 x 512 image resolution. Integral gain was 2 and proportional gain 5.0. Amplitude setpoint was 120 mV with a drive frequency of 74.053 kHz Drive amplitude was 58 mV. The Peak Force TUNA mode was then used for electronic

measurements, as shown in **Figure 2-2**. The deflection sensitivity was 155.46 nm/V and the measured spring constant was 1.911 N/m. A 5 μm scan size with 0.488 Hz scan rate, 384 x 384 image resolution, feedback gain of 15.73, peak force setpoint of 25 nN, and current sensitivity of 1 nA/V were used. Voltage ramping at fixed locations was performed with a deflection setpoint of 0.75 V.

Peak Force TUNA measurements of the sample shown in **Figure 2-4** had the following settings. Scan rate was 0.908 Hz, the image resolution was 256 x 256, the peak force setpoint was 15 nN, the feedback gain was 15. The deflection error sensitivity was measured as 131.48 nm/V, the spring constant as 2.462 N/m, and the current sensitivity was 1 nA/V. Deflection setpoints ranging from 0.3 V to 1.5 V were applied during the voltage ramps.

Electrostatic force microscopy was performed with the same microscope and probe type. A scan rate of 1.52 Hz, 1.78 μm scan size, 256 x 256 image resolution, 3.284 integral gain, 5.449 proportional gain, 250 mV amplitude setpoint, 75.35 kHz drive frequency, 365.6 mV drive amplitude, and lift height of 15 nm was used.

2.6 REFERENCES

1. Jiang, X.; Hu, J.; Fitzgerald, L. A.; Biffinger, J. C.; Xie, P.; Ringeisen, B. R.; Lieber, C. M., Probing electron transfer mechanisms in *Shewanella oneidensis* MR-1 using a nanoelectrode platform and single-cell imaging. *Proceedings of the National Academy of Sciences* **2010,** *107* (39), 16806–16810.

2. Logan, B. E., Exoelectrogenic bacteria that power microbial fuel cells. *Nature Reviews Microbiology* **2009,** *7* (5), 375–381.

3. Shi, L.; Dong, H.; Reguera, G.; Beyenal, H.; Lu, A.; Liu, J.; Yu, H.-Q.; Fredrickson, J. K., Extracellular electron transfer mechanisms between microorganisms and minerals. *Nature Reviews Microbiology* **2016,** *14* (10), 651–662.

4. McGlynn, S. E.; Chadwick, G. L.; Kempes, C. P.; Orphan, V. J., Single cell activity reveals direct electron transfer in methanotrophic consortia. *Nature* **2015,** *526* (7574), 531–535.

5. Pfeffer, C.; Larsen, S.; Song, J.; Dong, M.; Besenbacher, F.; Meyer, R. L.; Kjeldsen, K. U.; Schreiber, L.; Gorby, Y. A.; El-Naggar, M. Y.; Leung, K. M.; Schramm, A.; Risgaard-Petersen, N.; Nielsen, L. P., Filamentous bacteria transport electrons over centimetre distances. *Nature* **2012,** *491* (7423), 218–221.

6. Kjeldsen, K. U.; Schreiber, L.; Thorup, C. A.; Boesen, T.; Bjerg, J. T.; Yang, T.; Dueholm, M. S.; Larsen, S.; Risgaard-Petersen, N.; Nierychlo, M.; Schmid, M.; Bøggild, A.; van de Vossenberg, J.; Geelhoed, J. S.; Meysman, F. J. R.; Wagner, M.; Nielsen, P. H.; Nielsen, L. P.; Schramm, A., On the evolution and physiology of cable bacteria. *Proceedings of the National Academy of Sciences* **2019,** *116* (38), 19116–19125.

7. Meysman, F. J. R.; Cornelissen, R.; Trashin, S.; Bonné, R.; Martinez, S. H.; van der Veen, J.; Blom, C. J.; Karman, C.; Hou, J.-L.; Eachambadi, R. T.; Geelhoed, J. S.; Wael, K. D.; Beaumont, H. J. E.; Cleuren, B.; Valcke, R.; van der Zant, H. S. J.; Boschker, H. T. S.; Manca, J. V., A highly conductive fibre network enables centimetre-scale electron transport in multicellular cable bacteria. *Nature Communications* **2019,** *10* (1), 4120.

8. Kappler, A.; Benz, M.; Schink, B.; Brune, A., Electron shuttling via humic acids in microbial iron(III) reduction in a freshwater sediment. *FEMS Microbiology Ecology* **2004,** *47* (1), 85–92.

9. Renslow, R.; Babauta, J.; Kuprat, A.; Schenk, J.; Ivory, C.; Fredrickson, J.; Beyenal, H., Modeling biofilms with dual extracellular electron transfer mechanisms. *Phys Chem Chem Phys* **2013,** *15* (44), 19262–19283.

10. Reguera, G.; McCarthy, K. D.; Mehta, T.; Nicoll, J. S.; Tuominen, M. T.; Lovley, D. R., Extracellular electron transfer *via* microbial nanowires. *Nature* **2005,** *435* (7045), 1098–1101.

11. Fronzes, R.; Remaut, H.; Waksman, G., Architectures and biogenesis of non-flagellar protein appendages in Gram-negative bacteria. *EMBO J* **2008,** *27* (17), 2271–2280.

12. Allen, R. D.; Baumann, P., Structure and arrangement of flagella in species of the genus *Beneckea* and *Photobacterium fischeri*. *Journal of bacteriology* **1971,** *107* (1), 295–302.

13. Paranchych, W.; Frost, L. S., The Physiology and Biochemistry of Pili. In *Advances in Microbial Physiology*, Rose, A. H.; Tempest, D. W., Eds. Academic Press: 1988; Vol. 29, pp 53–114.

14. Díaz-Guerrero, M. Á.; Gaytán, M. O.; González-Pedrajo, B., Structure: Function of Transmembrane Appendages in Gram-Negative Bacteria. In *Biogenesis of Fatty Acids, Lipids and Membranes*, Geiger, O., Ed. Springer International Publishing: Cham, 2019; pp 671–689.

15. Hu, B.; Khara, P.; Christie, P. J., Structural bases for F plasmid conjugation and F pilus biogenesis in *Escherichia coli*. *Proceedings of the National Academy of Sciences* **2019,** *116* (28), 14222–14227.

16. Craig, L.; Forest, K. T.; Maier, B., Type IV pili: Dynamics, biophysics and functional consequences. *Nature Reviews Microbiology* **2019,** *17* (7), 429–440.

17. Wagner, J. K.; Setayeshgar, S.; Sharon, L. A.; Reilly, J. P.; Brun, Y. V., A nutrient uptake role for bacterial cell envelope extensions. *Proceedings of the National Academy of Sciences* **2006,** *103* (31), 11772–11777.

18. Galkina, S. I.; Romanova, J. M.; Bragina, E. E.; Tiganova, I. G.; Stadnichuk, V. I.; Alekseeva, N. V.; Polyakov, V. Y.; Klein, T., Membrane tubules attach *Salmonella Typhimurium* to eukaryotic cells and bacteria. *FEMS Immunology & Medical Microbiology* **2011,** *61* (1), 114–124.

19. Remis, J. P.; Wei, D.; Gorur, A.; Zemla, M.; Haraga, J.; Allen, S.; Witkowska, H. E.; Costerton, J. W.; Berleman, J. E.; Auer, M., Bacterial social networks: structure and composition of *Myxococcus xanthus* outer membrane vesicle chains. *Environmental Microbiology* **2014,** *16* (2), 598–610.

20. Devaraj, A.; Buzzo, J. R.; Mashburn-Warren, L.; Gloag, E. S.; Novotny, L. A.; Stoodley, P.; Bakaletz, L. O.; Goodman, S. D., The extracellular DNA lattice of bacterial biofilms is structurally related to Holliday junction recombination intermediates. *Proceedings of the National Academy of Sciences* **2019,** *116* (50), 25068–25077.

21. Böckelmann, U.; Janke, A.; Kuhn, R.; Neu, T. R.; Wecke, J.; Lawrence, J. R.; Szewzyk, U., Bacterial extracellular DNA forming a defined network-like structure. *FEMS Microbiology Letters* **2006,** *262* (1), 31–38.

22. Barnes, A. M. T.; Ballering, K. S.; Leibman, R. S.; Wells, C. L.; Dunny, G. M., *Enterococcus faecalis* produces abundant extracellular structures containing DNA in the absence of cell lysis during early biofilm formation. *mBio* **2012,** *3* (4), e00193–12.

23. Ibáñez de Aldecoa, A. L.; Zafra, O.; González-Pastor, J. E., Mechanisms and regulation of extracellular DNA release and its biological roles in microbial communities. *Frontiers in microbiology* **2017,** *8*, 1390.

24. Danese, P. N.; Pratt, L. A.; Kolter, R., Exopolysaccharide production is required for development of *Escherichia coli* K-12 biofilm architecture. *Journal of Bacteriology* **2000,** *182* (12), 3593–3596.

25. Limoli, D. H.; Jones, C. J.; Wozniak, D. J., Bacterial extracellular polysaccharides in biofilm formation and function. *Microbiology spectrum* **2015,** *3* (3), 10.1128/microbiolspec.MB-0011-2014.

26. Costa, O. Y. A.; Raaijmakers, J. M.; Kuramae, E. E., Microbial extracellular polymeric substances: Ecological function and impact on soil aggregation. *Frontiers in Microbiology* **2018,** *9*, 1636.

27. Rehm, B. H. A., Bacterial polymers: Biosynthesis, modifications and applications. *Nature Reviews Microbiology* **2010,** *8* (8), 578-592.

28. Gorby, Y. A.; Yanina, S.; McLean, J. S.; Rosso, K. M.; Moyles, D.; Dohnalkova, A.; Beveridge, T. J.; Chang, I. S.; Kim, B. H.; Kim, K. S.; Culley, D. E.; Reed, S. B.; Romine, M. F.; Saffarini, D. A.; Hill, E. A.; Shi, L.; Elias, D. A.; Kennedy, D. W.; Pinchuk, G.; Watanabe, K.; Ishii, S. i.; Logan, B.; Nealson, K. H.; Fredrickson, J. K., Electrically conductive bacterial nanowires produced by *Shewanella oneidensis* strain MR-1 and other microorganisms. *Proceedings of the National Academy of Sciences* **2006,** *103* (30), 11358–11363.

29. Dohnalkova, A. C.; Marshall, M. J.; Arey, B. W.; Williams, K. H.; Buck, E. C.; Fredrickson, J. K., Imaging hydrated microbial extracellular polymers: Comparative analysis by electron microscopy. *Applied and Environmental Microbiology* **2011,** *77* (4), 1254–1262.

30. Kiviet, D. J.; Nghe, P.; Walker, N.; Boulineau, S.; Sunderlikova, V.; Tans, S. J., Stochasticity of metabolism and growth at the single-cell level. *Nature* **2014,** *514* (7522), 376–379.

31. Barchinger, S. E.; Pirbadian, S.; Sambles, C.; Baker, C. S.; Leung, K. M.; Burroughs, N. J.; El-Naggar, M. Y.; Golbeck, J. H., Regulation of gene expression in *Shewanella oneidensis* MR-1 during electron acceptor limitation and bacterial nanowire formation. *Applied and Environmental Microbiology* **2016,** *82* (17), 5428–5443.

32. Malvankar, N. S.; Lovley, D. R., Microbial nanowires for bioenergy applications. *Current Opinion in Biotechnology* **2014,** *27*, 88–95.

33. Malvankar, N. S.; Vargas, M.; Nevin, K. P.; Franks, A. E.; Leang, C.; Kim, B.-C.; Inoue, K.; Mester, T.; Covalla, S. F.; Johnson, J. P.; Rotello, V. M.; Tuominen, M. T.; Lovley, D. R., Tunable metallic-like conductivity in microbial nanowire networks. *Nature Nanotechnology* **2011,** *6* (9), 573–579.

34. Vargas, M.; Malvankar, N. S.; Tremblay, P.-L.; Leang, C.; Smith, J. A.; Patel, P.; Synoeyenbos-West, O.; Nevin, K. P.; Lovley, D. R., Aromatic amino acids required for pili conductivity and long-range extracellular electron transport in *Geobacter sulfurreducens*. *mBio* **2013,** *4* (2), e00105–13.

35. Malvankar, N. S.; Vargas, M.; Nevin, K.; Tremblay, P.-L.; Evans-Lutterodt, K.; Nykypanchuk, D.; Martz, E.; Tuominen, M. T.; Lovley, D. R., Structural basis for metallic-like conductivity in microbial nanowires. *mBio* **2015,** *6* (2), e00084–15.

36. Pirbadian, S.; El-Naggar, M. Y., Multistep hopping and extracellular charge transfer in microbial redox chains. *Physical Chemistry Chemical Physics* **2012,** *14* (40), 13802–13808.

37. Leang, C.; Qian, X.; Mester, T.; Lovley, D. R., Alignment of the *c*-type cytochrome OmcS along pili of *Geobacter sulfurreducens*. *Applied and Environmental Microbiology* **2010,** *76* (12), 4080–4084.

38. Margoliash, E.; Lustgarten, J., Interconversion of horse heart cytochrome C monomer and polymers. *The Journal of Biological Chemistry* **1962,** *237*, 3397–3405.

39. Polizzi, N. F.; Skourtis, S. S.; Beratan, D. N., Physical constraints on charge transport through bacterial nanowires. *Faraday Discussions* **2012,** *155*, 43–61.

40. Pirbadian, S.; Barchinger, S. E.; Leung, K. M.; Byun, H. S.; Jangir, Y.; Bouhenni, R. A.; Reed, S. B.; Romine, M. F.; Saffarini, D. A.; Shi, L.; Gorby, Y. A.; Golbeck, J. H.; El-Naggar, M. Y., *Shewanella oneidensis* MR-1 nanowires are outer membrane and periplasmic extensions of the extracellular electron transport components. *Proceedings of the National Academy of Sciences* **2014,** *111* (35), 12883–12888.

41. Leung, K. M.; Wanger, G.; El-Naggar, M. Y.; Gorby, Y.; Southam, G.; Lau, W. M.; Yang, J., *Shewanella oneidensis* MR-1 bacterial nanowires exhibit p-type, tunable electronic behavior. *Nano Letters* **2013,** *13* (6), 2407–2411.

42. El-Naggar, M. Y.; Gorby, Y. A.; Xia, W.; Nealson, K. H., The molecular density of states in bacterial nanowires. *Biophysical Journal* **2008,** *95* (1), L10–L12.

43. Boesen, T.; Nielsen, L. P., Molecular dissection of bacterial nanowires. *mBio* **2013,** *4* (3), e00270–13.

44. El-Naggar, M. Y.; Wanger, G.; Leung, K. M.; Yuzvinsky, T. D.; Southam, G.; Yang, J.; Lau, W. M.; Nealson, K. H.; Gorby, Y. A., Electrical transport along bacterial nanowires from *Shewanella oneidensis* MR-1. *Proceedings of the National Academy of Sciences* **2010,** *107* (42), 18127–18131.

45. Malvankar, N. S.; Yalcin, S. E.; Tuominen, M. T.; Lovley, D. R., Visualization of charge propagation along individual pili proteins using ambient electrostatic force microscopy. *Nature Nanotechnology* **2014,** *9* (12), 1012–1017.

46. Takahashi, Y.; Shevchuk, A. I.; Novak, P.; Babakinejad, B.; Macpherson, J.; Unwin, P. R.; Shiku, H.; Gorelik, J.; Klenerman, D.; Korchev, Y. E.; Matsue, T., Topographical and electrochemical nanoscale imaging of living cells using voltage-switching mode scanning electrochemical microscopy. *Proceedings of the National Academy of Sciences* **2012,** *109* (29), 11540–11545.

47. Zhang, W.; Wu, H.; Hsing, I. M., Real-time label-free monitoring of *Shewanella oneidensis* MR-1 biofilm formation on electrode during bacterial electrogenesis using scanning electrochemical microscopy. *Electroanalysis* **2015,** *27* (3), 648–655.

48. Mehta, T.; Coppi, M. V.; Childers, S. E.; Lovley, D. R., Outer membrane *c*-type cytochromes required for Fe(III) and Mn(IV) oxide reduction in *Geobacter sulfurreducens*. *Applied and Environmental Microbiology* **2005,** *71* (12), 8634–8641.

49. Wang, F.; Gu, Y.; O'Brien, J. P.; Yi, S. M.; Yalcin, S. E.; Srikanth, V.; Shen, C.; Vu, D.; Ing, N. L.; Hochbaum, A. I.; Egelman, E. H.; Malvankar, N. S., Structure of microbial nanowires reveals stacked hemes that transport electrons over micrometers. *Cell* **2019,** *177* (2), 361–369.

50. Ueki, T.; Walker, D. J. F.; Woodard, T. L.; Nevin, K. P.; Nonnenmann, S. S.; Lovley, D. R., An *Escherichia coli* chassis for production of electrically conductive protein nanowires. *ACS Synthetic Biology* **2020,** *9* (3), 647–654.

Chapter 3. Microbial Adhesion to Solid Surfaces

3.1 MICROBIAL SURFACE COLONIZATION AND BIOFILMS

3.1.1 Microbial Modes of Life: Biofilm and Planktonic

Interactions of micro-organisms with surfaces are fundamental components of microbial life and activity. Microbes can be planktonic, meaning suspended in fluid, or associated with a solid. When microbes aggregate on a surface they can form a biofilm, which is the collection of microbes and surrounding material that symbiotically form on surfaces. Biofilms are often the natural and scientifically relevant state of bacteria and other microbes.[1] Most microbes on Earth exist in biofilms, and planktonic cells occur primarily in oceans.[2]

Surface sensing and adhesion to surfaces by planktonic cells are the first steps of surface colonization and formation of microbial biofilms. As such, understanding adhesion, surface sensing, and colonization are crucial to understanding biofilms. In addition to providing physical connections, surface interactions by bacteria produce cellular responses that influence colonization behaviors, including modulation of motility appendages and production of secreted adhesives.[3] Colonization can be affected by bacterial interactions with surfaces, even when the microbe is no longer in close proximity.[4] Where a robust biofilm and microbial colony is desirable, irreversible attachment of cells after surface interaction is essential.[5] Unstable biofilms may disperse or become non-active, particularly in the event of temporary nutrient insufficiency.[6] Manipulation of microbial colonization of surfaces enables much potential for fundamental study and technological advances.

3.1.2 Beneficial Biofilms and Control of Attachment

As noted in chapter 1, there are several examples of beneficial microbial processes. Processes that cause net reduction of the culture medium, and may be anabolic, can produce high value chemicals by biosynthesis. Such chemicals may include fuels,[7,8] polymers,[9] surfactants,[10] and anything else a metabolic pathway can be engineered to produce. Catabolic processes that cause net oxidation to the culture medium can capture energy or remove unwanted materials from the environment.[11] These processes occur in microbial biofilms, and colonization of solid electrodes can couple the microbial metabolism to electronic devices, producing bioelectrical systems.

Beneficial biofilms can be improved by making colonization dynamics more favorable, which may be the result of enriching the types of microbes populating a surface or increasing the total adhered cells. There are three major components of a microbial community on a surface. The amount of microbial presence, the relative composition of the community, and the homogeneity of the surface. In terms of being able to control attachment, these factors correspond to the ability to modulate total attachment, change the ratio of strains of microbes, and pattern the surface so as to influence the first two items of this sentence. Functionalizing surfaces to control bacterial attachment is shown schematically in **Figure 3-1**. Surface design can either promote cells into well-defined geometries or enrich desired cells on a surface.

Increasing microbial attachment is necessary at least to the point where colonization is reliably initiated. Having a high number of cells on a surface may also maximize desirable metabolic processes. Simply increasing the total number of cells on a surface can increase microbial device performance. *Geobacter sulfurreducens* biofilm thicknesses of about 20 μm have shown maximal current output, indicating the need for multiple cell layers.[12] The linkage

between an inorganic substrate and a first layer of cells sets the foundation for the biofilm. Forming a robust interaction between a surface and microbes is imperative to have full surface coverage by adhered cells, and may also induce closer packing of cell layers further from the surface.

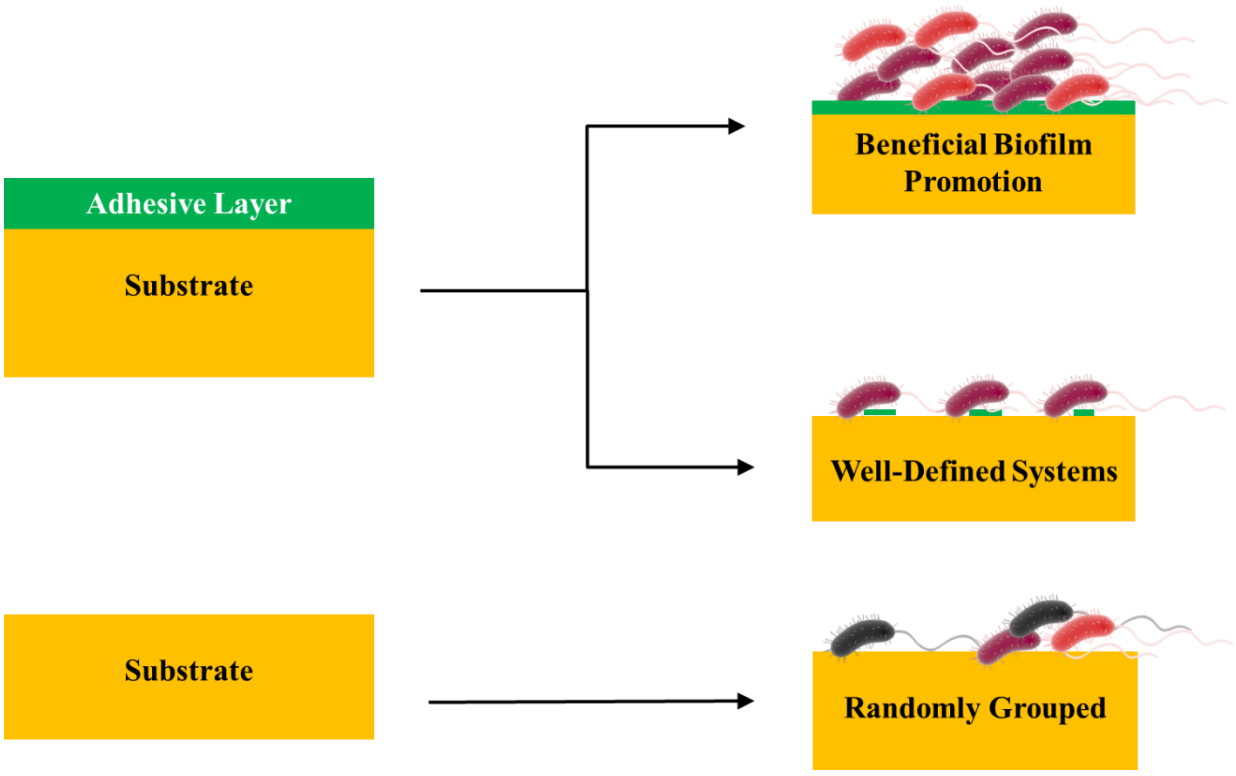

Figure 3-1. Control over microbe surface colonization. Higher densities of cells and cells of a strain of interest can be introduced on functionalized surfaces. Rather than unpredictable and erratic positioning of cells, well-defined systems can be created by promoting and reducing adhesion selectively.

Strengthening a microbe's attraction to a particular surface not only increases the number of cells on the surface, but could also change the *fraction* of that microbe in the surface community. Microbial community composition is a key indicator of a biofilm's functionality. The metabolically crucial members of a biofilm may be desired in high abundance and ancillary microbes may be necessary in appropriate ratios or diversity. Electroactive biofilms, as an

example, produce a large range of cell voltages possible from various soil microbiomes.[13] Furthermore, a single family within a microbial consortium may inordinately increase electroactivity.[11] A culture of one species may not be sufficient for maximal performance without ancillary microbes. Significant increases in fuel cell current have been reported with an *Enterococcus faecium* ancillary strain versus pure electroactive cultures.[14] Promoting surface adhesion of particular species of bacteria is one way to select for biochemical reactivity in a biofilm. Selective microbial adhesion could also prevent colonization of pathogens or otherwise deleterious microbes through promotion of adhesion of benign species used as an inert layer.[15] Understanding choices that influence a microbial biofilm composition may therefore be critical to harnessing microbial utility.

The composition of a biofilm can be pre-determined, to an extent, by the type of surface that bears it.[16] As an example, polypropylene surfaces from different production batches, with differing filament diameters and contact angle, have shown varied biofilm diversity due to higher or lower adhesion attachment dynamics.[17] This observation of biofilm dynamics on the polypropylene surfaces is empirical; a thoughtfully designed system is expected to expand greatly the control over biofilm formation. The deterministic nature of surface colonization by bacteria means thoroughly grasping the range of possible surface modifications is essential to engineered biofilms. The initial adhesion of cells is particularly important as microbes in these devices are often received from the environment rather than deposited procedurally. Microbial interfaces capable of selective control of adhesion by cell type over time may be particularly powerful. Additionally, releasing cells may be an important consideration in utilizing the products of biosynthesized chemicals and preventing inactive cells from occluding an electrode or other functional part of a device.

Manipulation of surface colonization can also be used to define cell attachment spatially across surfaces. Controlling colonization to form well-defined monolayers of cells enables observation and measurement of nanoscale features, especially with surface sensitive techniques. On uncontrolled surfaces, the fundamental study of nanoscopic features in microbial communities is difficult as they can be buried or hidden in clusters of cells. Additionally, intercellular interactions can be instigated when one cell type is spatially arranged and another cell type is placed next to it. As cells can have a wide variety of interactions, there may be various opportunities for technological advances and fundamental studies presented by the ability to position cells at will.

3.2 METHODS FOR PROMOTING AND PHYSICAL MODELS OF MICROBIAL ADHESION

There are a diverse range of strategies to enhance microbial adhesion to surfaces and therefore a rich area to explore for fundamental study and technological optimization.[18,19] Methods have been used to promote microbial adhesion to surfaces have varied from physical forces to general chemical interaction to specific biochemical adhesion. Derjaguin–Landau–Verwey–Overbeek (DLVO) theory describes combined Coulombic and Lifshitz–van der Waals forces of micrometer-scale particles, and predicts increased attraction of negatively charged bacteria to positive surfaces due to attraction from both Coulombic and van der Waals forces.[20] As most bacterial cell membranes are negatively charged, DLVO theory predicts increased attraction to positively charged surfaces.[21] Realizing this, several positively charged surfaces have been produced that promote the adhesion of bacteria.[22] Poly-L-lysine is a standard polycationic

coating, and poly(ethyleneimine) deposition on glass surfaces increased *Escherichia coli* adhesion 215-fold.[23,24]

A modification of DLVO theory further includes hydrophobic effects and osmotic interactions on the attraction of cell suspensions.[25] The influence of hydrophobic effects on bacterial attachment has since been experimentally established.[26,27] The effect depends on how hydrophobic the microbial cell membrane is along with the polarity and ionic strength of the liquid medium and nature of the solid surface.[28] Generally, the interaction energy of bacteria correlates with the surface energy, as has been shown for *E. coli*.[29] *Staphylococcus epidermidis* was found to bind hydrophilic polyacrylamide less than other polymers and have a variable preference for hydrophobic surfaces over the course of 24 hours. However, when the bacteria were deposited on the same surfaces in serum, as opposed to phosphate-buffered saline (PBS), only the anionic and cationic samples showed appreciable bacterial adsorption.[30] These findings suggest that the formation of a conditioning layer of material, deposited from the serum, can screen adhesion of cells that results from the system's hydrophobicity.

Other properties of a surface have also been shown to influence bacterial adhesion, such as: roughness, which increases surface area and shields against shear forces,[31-33] larger topographic features,[34] and elastic modulus.[35,36] The physiochemical properties described above can be tailored to increase the attachment of bacteria to electrodes and consequently increase the performance of devices such as microbial fuel cells created thereafter. Such improvements have been observed by treating carbon electrodes with ammonia or plasma treatment to increase the positive charge on the surface among other properties.[37-39]

Methods of controlling microbial attachment may have similar effects for different species. If the physical properties of the cell, such as charge, modulus, or size are conserved between species, then the adhesiveness that is derived from these properties is also expected to be conserved across species. However, physical properties can vary from species to species.[40,41] To understand of the adhesive properties of a species of interest precisely, one should consider the different modes of adhesion for that particular species. We now consider surface adhesion of *Shewanella oneidensis*. As an electroactive bacterium, the formation of *S. oneidensis* biofilms has technological relevance, which was discussed in chapter 1. Enriching key species, like *S. oneidensis*, in a microbial community can make useful genes functionally abundant and make beneficial biofilms more effective.[42]

Increased attachment of *Shewanella* has been achieved by air plasma pre-treatment of carbon-based electrodes. The surface treatment concurrently increased current output of the associated fuel cell with a lower Coulombic efficiency.[43] Alterations to the microbes have also been employed to facilitate surface attachment. *S. oneidensis* has been engineered to express a gold-binding peptide on an outer membrane protein, LamB-5rGBP, which increased the attachment of the cells to the surface, but was associated with the loss of certain outer membrane proteins required for extracellular respiration.[44] DNA has been used to direct attachment of *S. oneidensis* as well.[45] Conductivity of complementary DNA strands appeared to facilitate electron transport between the cells and gold surfaces. Current approximately quadrupled for cells linked to surfaces with DNA duplexes versus cells deposited without linkers. This method of DNA-facilitated attachment requires the cells to be chemically conjugated with complementary DNA through cleavage of bacterial saccharides with sodium periodate, however.

Many combinations of microbial species and surface properties still have not been tested for adhesiveness. Even the discovery of materials that facilitate attachment, such as plasma-treated carbon, leave many unknowns about what causes the microbial adhesion. Processes, such as plasma treatment, can change many properties of a surface. Simple, rapid methods for testing microbial adhesion would be beneficial for exploring the space of adhesive materials by enabling large-scale screening of individual material properties and their interactions with various microbial strains. In this chapter, a colony counting method is demonstrated for testing the adhesiveness of surfaces to microbes.

3.3 RESULTS: ADHESION OF *SHEWANELLA ONEIDENSIS* TO SURFACES OF VARIOUS CHEMICAL IDENTITY

A method for measuring surface adhesiveness was developed, as shown in **Scheme 3-1**. Adherence in this method is measured by counting the number of colony-forming units that are removed by sonication from a surface exposed to bacterial culture. *S. oneidensis* bacteria were exposed to surfaces to initiate cell attachment. Non-adherent cells were removed with several rinses of PBS. The bacteria remaining on the surface were sonicated to remove them with more PBS rinses. The cells that were removed after sonication were diluted and cultured until their colonies became visible, then counted. Several dilution ratios were cultured to provide samples that did not have overlapping colonies but did have enough colonies for precise results. Each colony represents a colony-forming unit—something that, when cultured, forms a colony. A colony-forming unit may be a single cell or a cluster of cells. Some cells in a culture may fail to multiply, so the number of colony-forming units in a sample may be higher or lower than the number of individual cells. The number of colony-forming units provides a representation of the

number of bacteria that were adhered to the surface, where the colony-forming units represent the number of cells removed from the surface, and the number of cells removed by sonication approximately represents the number of cells that were on the surface. Samples were prepared on the bottoms of well plates to standardize the surface areas of the exposed surfaces.

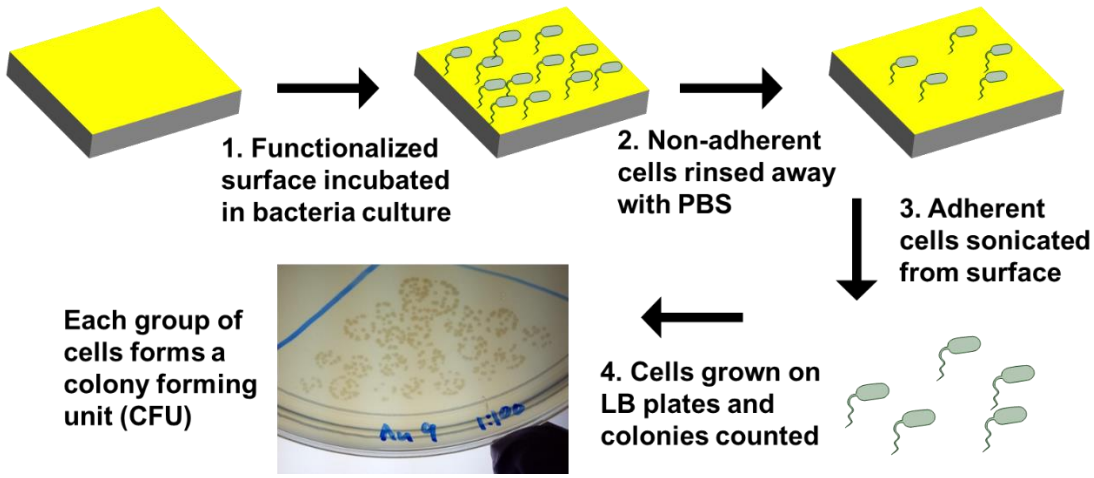

Scheme 3-1. Experimental design for testing bacterial surface adhesion by sonicated removal and colony counting.

This method is label free, does not require fluorescent reporters, and can be performed without microscopes. It also enables the measurement of initial cell attachment. The effect of sonication time on the number of cells recovered from the surface with this method was tested (**Figure 3-2**). Culturable cells were recovered after ten minutes of sonication, indicating the resilience of *S. oneidensis* to sonication. Three minutes of sonication produced the highest average number of colony-forming units but was not significantly different from the other sonication times.

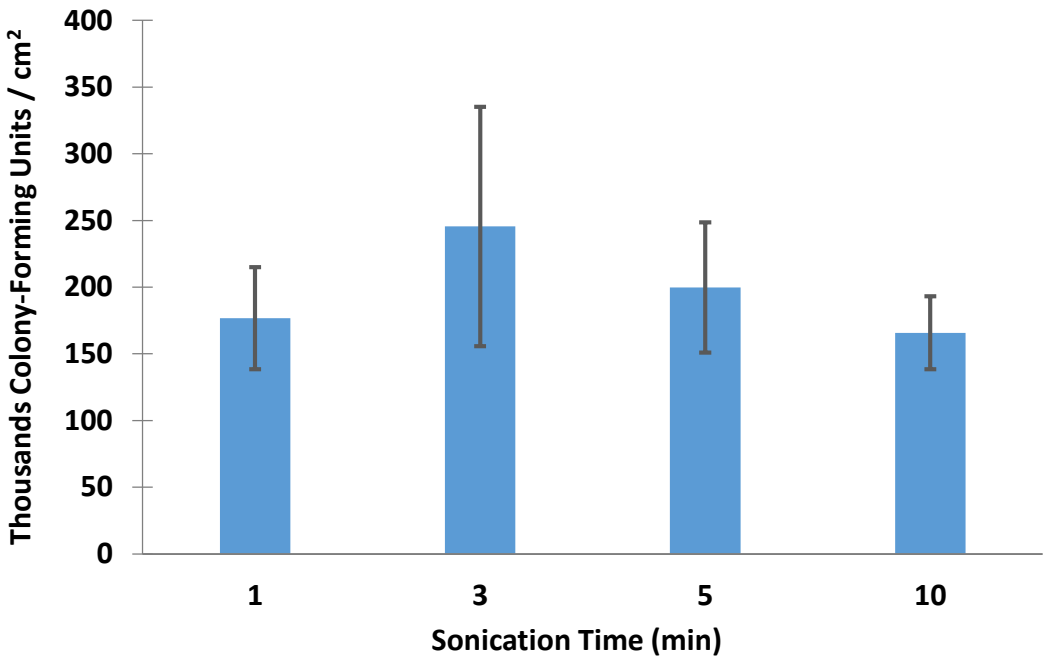

Figure 3-2. Test of sonication effects on cell removal. Error bars indicate standard error of the mean (N=4).

Various surface types were tested with the colony counting method described above. In **Figure 3-3**, alkanethiols on gold were compared to bare gold surfaces. The functional termini exposed to the culture solutions were, hydrophobic methyl groups of dodecanethiol, positively charged quaternary amines groups of (11-mercaptoundecyl)-*N*,*N*,*N*-trimethylammonium bromide, and ethylene glycol units of (11-mercaptoundecyl)hexa(ethylene glycol) ($HS\text{-}(CH_2)_{11}\text{-}(OCH_2CH_2)_6\text{-}OH$). Dodecanethiol surfaces yielded significantly more colony-forming units than bare gold surfaces (p value = 0.0231 by unpaired t-test).

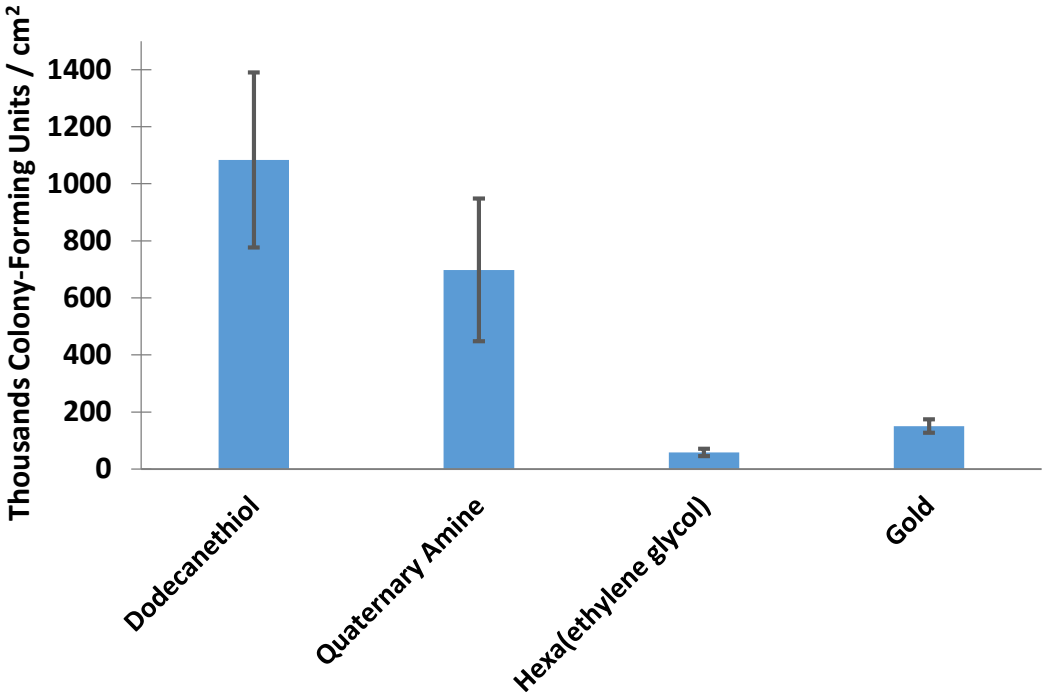

Figure 3-3. Adhesion of *Shewanella oneidensis* on various types of self-assembled monolayers as determined by colony-forming units sonicated from the surfaces. Error bars show standard error of the mean (N=4).

The adhesiveness of *S. oneidensis* to self-assembled monolayers terminated with methyl groups and quaternary amine groups has also been measured by Artyushkova *et al.* with a microscopy and X-ray photoelectron spectroscopy approach. In that report, methyl-terminated self-assembled monolayers were found to produce the thickest biofilms, while electron transfer was found to be most efficient on quaternary-amine-terminated surfaces.[46] The findings of Artyushkova *et al.* suggest that our findings that initial cell attachment is increased on methyl-functionalized surfaces may also lead to increased attachment of mature biofilms.

The adhesiveness of methyl-terminated surfaces was further investigated by measuring alkanethiols of different lengths (**Figure 3-4**). Dodecanethiol, with 12 methylene units, and decanethiol, with 10, produced more colony-forming units than octanethiol and hexanethiol, with 8 and 6 methylene units respectively.

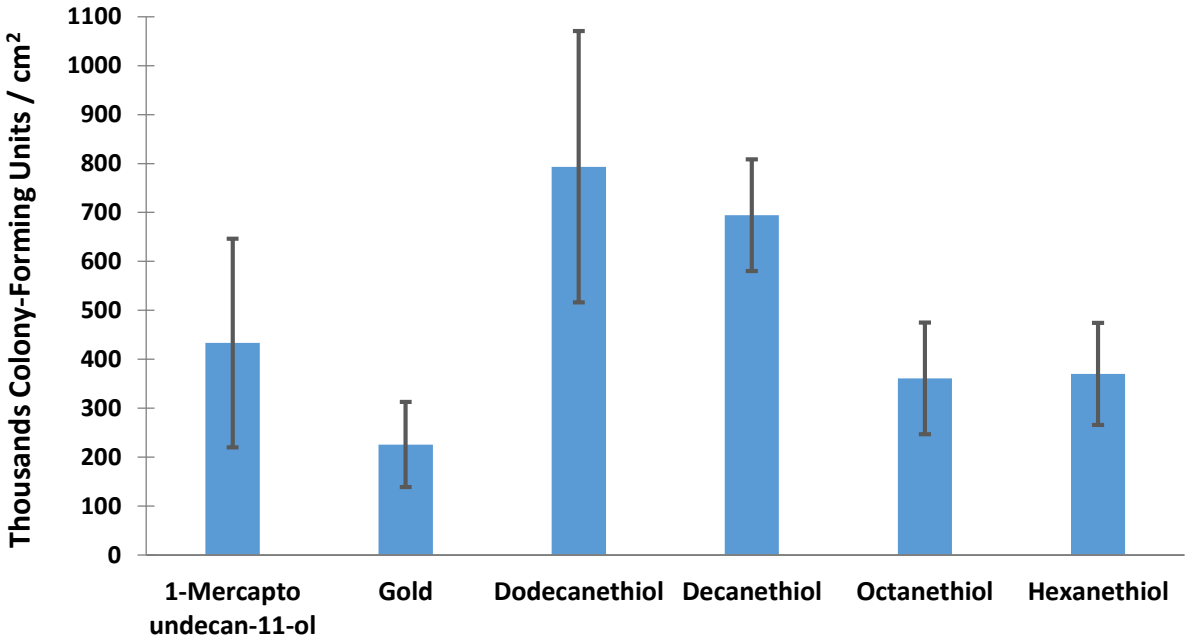

Figure 3-4. Adhesion of *Shewanella oneidensis* on various thicknesses of self-assembled monolayers as determined by colony-forming units rinsed from the surfaces. Error bars show standard error of the mean (N=4).

A trend is observed of longer alkanethiol molecules yielding more colony-forming units. It may be that the longer alkyl chains have more flexibility and can either expose more of the molecule to the bacteria or the materials properties of the monolayer facilitates attachment to the cells.

The sonication and colony counting method was applied to several materials typically used as anodes, as well (**Figure 3-5**). Fuel cell anodes are typically evaluated based on power output, however by independently optimizing cell attachment and substrate conductivity, better anodes and anode materials can be intelligently designed. Tungsten carbide, which has been used in a microbial fuel cell,[47] appeared to have almost no attached cells. The limited initial attachment may indicate unreliable or slow biofilm growth. The low cell count on tungsten

carbide may indicate toxicity with the solution volume used. Gold surfaces yielded more colony-forming units than either of the other materials.

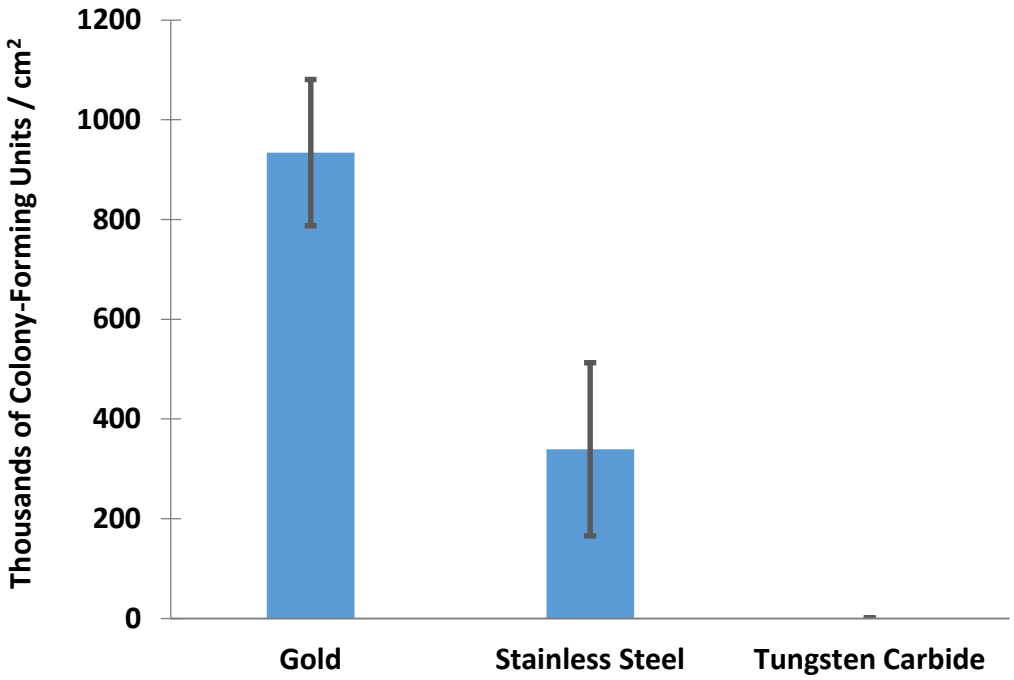

Figure 3-5. Adhesion of *Shewanella oneidensis* on anode materials as determined by colony forming units removed from the surfaces by sonication. Error bars show standard error of the mean (N=4).

Topographically, the gold surface is flatter than the unpolished stainless steel or tungsten carbide. As bacteria are expected to catch on edges and corners of materials, the topographical features can be important for both the initial attachment of bacteria and the release of cells during sonication. To check for cells that remained on the surface after sonication, the anode materials were observed with fluorescence microscopy (**Figure 3-6**).

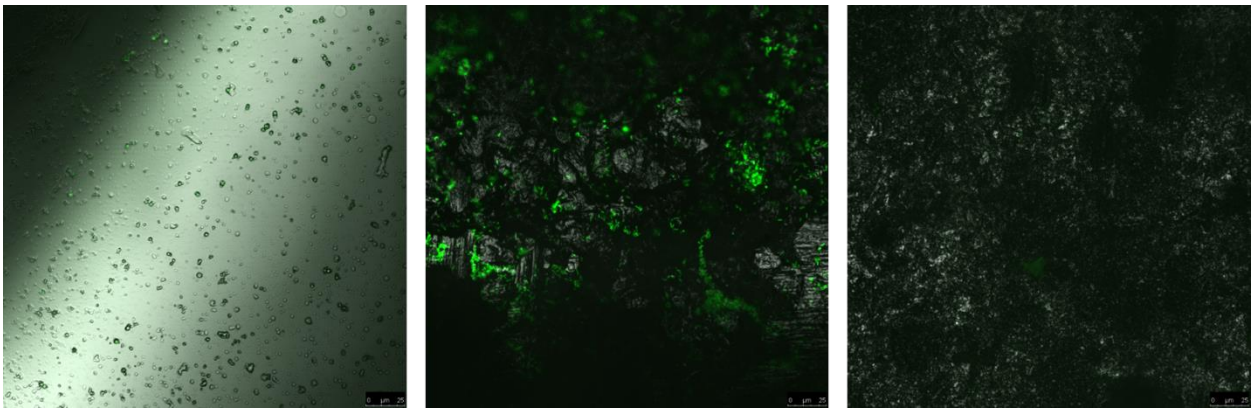

Figure 3-6. Confocal fluorescence micrographs of anode materials after removal of *S. oneidensis* cells by sonication. **(Left)** Gold. **(Middle)** Stainless steel. **(Right)** Tungsten carbide.

The gold surfaces had some fluorescent cells scattered across them, but fewer than the steel surfaces, which seem to accumulate cells in the crevices of the material. The tungsten carbide surfaces showed some patches of diffuse fluorescence but almost no cells in any of the locations imaged. The fluorescence on the tungsten carbide surfaces may have been GFP released from dead cells. The high number of cells retained on the steel surfaces indicates that the colony counting measurement displayed in **Figure 3-5** underestimates the adhesiveness of the steel and suggests the sonication-based method used here has limited applicability for rough surfaces. For accurate measurements of surfaces that can strongly retain cells, a method that directly probes the surface without removing cells is desired. The use of a fluorescent plate reader, described in the next chapter, enabled a faster, easier, and more accurate method for testing bacterial adhesion to surfaces. Another notable feature is that the gold samples represented in **Figure 3-5** suggested much more attached cells than the other experiments, which may be indicative of a lack of precision with the sonication and colony counting method.

Gold surfaces in the experiments presented in this chapter had greater *S. oneidensis* attachment than tungsten carbide. In addition to guiding the developing biofilm's taxonomic and

functional composition, the microbe-device interface of a microbial technology is important for facilitating transfer of material between the micro-organisms and the rest of the device. In the case of bioelectrical systems, electrons must be able to transfer to electrodes with little resistance. The results here indicate gold produces relatively good bacterial attachment. As gold is also one of the highly conductive metals, it may be particularly useful for some bioelectrical applications.

The results presented here indicate that surfaces terminated with long alkyl chains can promote initial attachment of *S. oneidensis*. The greater attachment reflects the ability to increase the fraction of *S. oneidensis* in a mixed species population, where the other species do not have increased attachment to alkyl-terminated or hydrophobic surfaces.

The advantages and disadvantages of the sonication and colony counting method have been analyzed in this chapter. The method is an accessible, easy to perform option that could be particularly useful with non-fluorescent microbial strains, especially on visually complex, heterogeneous surfaces where cells can be mis-identified by microscopy. The sonication and colony counting method is less reliable on rough surfaces and may be less precise that other methods, due to the variability possible in each experimental step.

3.4 MATERIALS AND METHODS

Self-Assembled Monolayer Formation

Gold surfaces were functionalized with alkanethiol molecules by solution deposition. An adhesion layer of 7.5 nm of titanium, followed by 75 nm of gold, were evaporated onto a black polystyrene 96-well microtiter plate or silicon wafers. The gold surfaces were submerged in a

1 mM ethanolic solution of the appropriate alkanethiol overnight. The surfaces were removed from solution then rinsed with ethanol and dried with a nitrogen stream.

Bacterial Growth

Pre-culture of *Shewanella oneidensis* MR-1 p529nGFP was made by inoculation of 20 mL of lysogeny broth (LB) medium from LB-agar plates. The bacterial suspensions were incubated at 32 °C for 14 h with 200 rpm of shaking. New cultures were then prepared by diluting 1 mL of pre-culture into 20 mL of fresh LB media and 40 μL of 25 g/L kanamycin solution (50 mg/L final kanamycin concentration). The cultures were incubated for 2.3 h at 32 °C with 200 rpm of shaking, until it reached an optical density at 600 nm of 1.20.

The cells were pelleted by centrifugation (2300 *g*) for 5 min and resuspended in pH 7.2 1× PBS. Centrifugation and resuspension were repeated for a total of three times. The resulting bacterial suspensions were diluted 1:10 in PBS and 250 μL were added to each sample well in the sample well plates.

Preparation of Anode Materials

ProPlates (Electron Microscopy Sciences, Hatfield, Pennsylvania, USA), bottomless 96-well plates, were used to apply bacterial solutions to anode materials. The materials, rectangular lengths of unpolished 304 stainless steel and tungsten carbide (McMaster-Carr, Santa Fe Springs, California, USA), and gold coated silicon wafers, were washed with 70% ethanol and dried. Then the materials were adhered to the well plate by the ProPlate adhesive. Graphite samples were also prepared but would not retain the bacteria solutions and the results were excluded. The sample wells were filled with 100% ethanol for approximately 5 min to sterilize then rinsed with

PBS three times. After the addition of bacteria, the plates were covered with a petri dish and incubated for 20.5 h at 32 °C without agitation.

Colony Counting

Solutions on the bacteria-exposed surfaces were removed from the sample wells and replaced with 250 μL of PBS four times to remove non-adherent cells. The PBS-filled wells were floated in a sonicator and sonicated for 3 min. The solutions were then transferred to blank well plates. Serial decimal dilutions were performed until samples of 1:10,000 dilution were prepared. 80 μL of the diluted solutions were applied to LB agar plates by micropipette as a series of droplets. The droplets were allowed to dry for 30 min before the plates were flipped upside down and incubated overnight. Colonies were counted manually.

Optical Microscopy

After the anode material samples were sonicated and the solutions removed, the substrates were removed from the ProPlate and imaged. The sample was imaged with a Leica TCS-SP5 AOBS confocal microscope (Leica Microsystems, Wetzlar, Germany). Laser excitation at 488 nm with emission recorded over 500–555 nm was used for the fluorescence channel. Laser excitation at 633 nm recorded over the same wavelength was used for the reflection channel. Both emission measured with photomultiplier tubes.

3.5 REFERENCES

1. Jefferson, K. K., What drives bacteria to produce a biofilm? *FEMS Microbiology Letters* **2004,** *236* (2), 163–173.

2. Flemming, H.-C.; Wuertz, S., Bacteria and archaea on Earth and their abundance in biofilms. *Nature Reviews Microbiology* **2019,** *17* (4), 247-260.

3. O'Toole, G. A.; Wong, G. C. L., Sensational biofilms: Surface sensing in bacteria. *Current Opinion in Microbiology* **2016,** *30*, 139–146.

4. Lee, C. K.; de Anda, J.; Baker, A. E.; Bennett, R. R.; Luo, Y.; Lee, E. Y.; Keefe, J. A.; Helali, J. S.; Ma, J.; Zhao, K.; Golestanian, R.; O'Toole, G. A.; Wong, G. C. L., Multigenerational memory and adaptive adhesion in early bacterial biofilm communities. *Proceedings of the National Academy of Sciences* **2018,** *115* (17), 4471–4476.

5. Petrova, O. E.; Sauer, K., Sticky situations: Key components that control bacterial surface attachment. *Journal of Bacteriology* **2012,** *194* (10), 2413–2425.

6. Thormann, K. M.; Saville, R. M.; Shukla, S.; Spormann, A. M., Induction of rapid detachment in *Shewanella oneidensis* MR-1 biofilms. *Journal of Bacteriology* **2005,** *187* (3), 1014–1021.

7. Li, H.; Opgenorth, P. H.; Wernick, D. G.; Rogers, S.; Wu, T.-Y.; Higashide, W.; Malati, P.; Huo, Y.-X.; Cho, K. M.; Liao, J. C., Integrated electromicrobial conversion of CO_2 to higher alcohols. *Science* **2012,** *335* (6076), 1596–1596.

8. Kumar, M.; Morya, R.; Gnansounou, E.; Larroche, C.; Thakur, I. S., Characterization of carbon dioxide concentrating chemolithotrophic bacterium *Serratia* sp. ISTD04 for production of biodiesel. *Bioresource Technology* **2017,** *243*, 893–897.

9. Jiang, X.-R.; Yao, Z.-H.; Chen, G.-Q., Controlling cell volume for efficient PHB production by *Halomonas*. *Metabolic Engineering* **2017,** *44*, 30–37.

10. Maheshwari, N.; Kumar, M.; Thakur, I. S.; Srivastava, S., Recycling of carbon dioxide by free air CO_2 enriched (FACE) *Bacillus* sp. SS105 for enhanced production and optimization of biosurfactant. *Bioresource Technology* **2017,** *242*, 2–6.

11. Bond, D. R.; Holmes, D. E.; Tender, L. M.; Lovley, D. R., Electrode-reducing microorganisms that harvest energy from marine sediments. *Science* **2002,** *295* (5554), 483–485.

12. Sun, D.; Chen, J.; Huang, H.; Liu, W.; Ye, Y.; Cheng, S., The effect of biofilm thickness on electrochemical activity of *Geobacter sulfurreducens*. *International Journal of Hydrogen Energy* **2016,** *41* (37), 16523–16528.

13. Ringelberg, D. B.; Foley, K. L.; Reynolds, C. M., Electrogenic capacity and community composition of anodic biofilms in soil-based bioelectrochemical systems. *Applied Microbiology and Biotechnology* **2011,** *90* (5), 1805–1815.

14. Read, S. T.; Dutta, P.; Bond, P. L.; Keller, J.; Rabaey, K., Initial development and structure of biofilms on microbial fuel cell anodes. *BMC Microbiology* **2010,** *10*, 98.

15. Chen, Q.; Zhu, Z.; Wang, J.; Lopez, A. I.; Li, S.; Kumar, A.; Yu, F.; Chen, H.; Cai, C.; Zhang, L., Probiotic *E. coli* Nissle 1917 biofilms on silicone substrates for bacterial interference against pathogen colonization. *Acta Biomaterialia* **2017,** *50*, 353–360.

16. Chia, T. W. R.; Nguyen, V. T.; McMeekin, T.; Fegan, N.; Dykes, G. A., Stochasticity of bacterial attachment and its predictability by the extended Derjaguin-Landau-Verwey-Overbeek theory. *Applied and Environmental Microbiology* **2011,** *77* (11), 3757–3764.

17. Felföldi, T.; Jurecska, L.; Vajna, B.; Barkács, K.; Makk, J.; Cebe, G.; Szabó, A.; Záray, G.; Márialigeti, K., Texture and type of polymer fiber carrier determine bacterial colonization and biofilm properties in wastewater treatment. *Chemical Engineering Journal* **2015,** *264*, 824–834.

18. Hori, K.; Matsumoto, S., Bacterial adhesion: From mechanism to control. *Biochemical Engineering Journal* **2010,** *48* (3), 424–434.

19. Costello, C. M.; Yeung, C. L.; Rawson, F. J.; Mendes, P. M., Application of nanotechnology to control bacterial adhesion and patterning on material surfaces. *Journal of Experimental Nanoscience* **2012,** *7* (5-6), 634–651.

20. Derjaguin, B.; Landau, L., Theory of the stability of strongly charged lyophobic sols and of the adhesion of strongly charged particles in solutions of electrolytes. *Progress in Surface Science* **1993,** *43* (1), 30–59.

21. Hermansson, M., The DLVO theory in microbial adhesion. *Colloids and Surfaces B: Biointerfaces* **1999,** *14* (1), 105–119.

22. Terada, A.; Yuasa, A.; Kushimoto, T.; Tsuneda, S.; Katakai, A.; Tamada, M., Bacterial adhesion to and viability on positively charged polymer surfaces. *Microbiology* **2006,** *152* (12), 3575–3583.

23. Colville, K.; Tompkins, N.; Rutenberg, A. D.; Jericho, M. H., Effects of poly(L-lysine) substrates on attached *Escherichia coli* bacteria. *Langmuir* **2010,** *26* (4), 2639–2644.

24. Xia, B.; Shi, J.; Dong, C.; Zhang, W.; Lu, Y.; Guo, P., Covalent assembly of poly(ethyleneimine) *via* layer-by-layer deposition for enhancing surface density of protein and bacteria attachment. *Applied Surface Science* **2014,** *292*, 1040–1044.

25. van Oss, C. J., Energetics of cell-cell and cell-biopolymer interactions. *Cell biophysics* **1989,** *14* (1), 1–16.

26. Gilbert, P.; Allison, D.; Brading, M.; Verran, J.; Walker, J., *Biofilm Community Interactions: Chance or Necessity?* BioLine Cardiff, UK: 2001.

27. Krasowska, A.; Sigler, K., How microorganisms use hydrophobicity and what does this mean for human needs? *Frontiers in cellular and infection microbiology* **2014,** *4*, 112.

28. Bruinsma, G. M.; van der Mei, H. C.; Busscher, H. J., Bacterial adhesion to surface hydrophilic and hydrophobic contact lenses. *Biomaterials* **2001,** *22* (24), 3217–3224.

29. Liu, Y.; Zhao, Q., Influence of surface energy of modified surfaces on bacterial adhesion. *Biophysical Chemistry* **2005,** *117* (1), 39–45.

30. MacKintosh, E. E.; Patel, J. D.; Marchant, R. E.; Anderson, J. M., Effects of biomaterial surface chemistry on the adhesion and biofilm formation of *Staphylococcus epidermidis in vitro*. *Journal of Biomedical Materials Research Part A* **2006,** *78A* (4), 836–842.

31. Scheuerman, T. R.; Camper, A. K.; Hamilton, M. A., Effects of substratum topography on bacterial adhesion. *Journal of Colloid and Interface Science* **1998,** *208* (1), 23–33.

32. Harris, L. G.; Richards, R. G., *Staphylococcus aureus* adhesion to different treated titanium surfaces. *Journal of Materials Science: Materials in Medicine* **2004,** *15* (4), 311–314.

33. Jeyachandran, Y. L.; Venkatachalam, S.; Karunagaran, B.; Narayandass, S. K.; Mangalaraj, D.; Bao, C. Y.; Zhang, C. L., Bacterial adhesion studies on titanium, titanium nitride and modified hydroxyapatite thin films. *Materials Science and Engineering: C* **2007,** *27* (1), 35–41.

34. Song, F.; Koo, H.; Ren, D., Effects of material properties on bacterial adhesion and biofilm formation. *Journal of Dental Research* **2015,** *94* (8), 1027–1034.

35. Lichter, J. A.; Thompson, M. T.; Delgadillo, M.; Nishikawa, T.; Rubner, M. F.; Van Vliet, K. J., Substrata mechanical stiffness can regulate adhesion of viable bacteria. *Biomacromolecules* **2008,** *9* (6), 1571–1578.

36. Saha, N.; Monge, C.; Dulong, V.; Picart, C.; Glinel, K., Influence of polyelectrolyte film stiffness on bacterial growth. *Biomacromolecules* **2013,** *14* (2), 520–528.

37. He, Y.-R.; Xiao, X.; Li, W.-W.; Sheng, G.-P.; Yan, F.-F.; Yu, H.-Q.; Yuan, H.; Wu, L.-J., Enhanced electricity production from microbial fuel cells with plasma-modified carbon paper anode. *Physical Chemistry Chemical Physics* **2012,** *14* (28), 9966–9971.

38. Cheng, S.; Logan, B. E., Ammonia treatment of carbon cloth anodes to enhance power generation of microbial fuel cells. *Electrochemistry Communications* **2007,** *9* (3), 492–496.

39. Wei, J.; Liang, P.; Huang, X., Recent progress in electrodes for microbial fuel cells. *Bioresource Technology* **2011,** *102* (20), 9335–9344.

40. Dickson, J. S.; Koohmaraie, M., Cell surface charge characteristics and their relationship to bacterial attachment to meat surfaces. *Applied and Environmental Microbiology* **1989,** *55* (4), 832–836.

41. Auer, G. K.; Weibel, D. B., Bacterial Cell Mechanics. *Biochemistry* **2017,** *56* (29), 3710–3724.

42. Hermon, L.; Hellal, J.; Denonfoux, J.; Vuilleumier, S.; Imfeld, G.; Urien, C.; Ferreira, S.; Joulian, C., Functional genes and bacterial communities during organohalide respiration of chloroethenes in microcosms of multi-contaminated groundwater. *Frontiers in Microbiology* **2019**, *10*, 89.

43. Epifanio, M.; Inguva, S.; Kitching, M.; Mosnier, J.-P.; Marsili, E., Effects of atmospheric air plasma treatment of graphite and carbon felt electrodes on the anodic current from *Shewanella* attached cells. *Bioelectrochemistry* **2015,** *106*, 186–193.

44. Kane, A. L.; Bond, D. R.; Gralnick, J. A., Electrochemical analysis of *Shewanella oneidensis* engineered to bind gold electrodes. *ACS Synthetic Biology* **2013,** *2* (2), 93–101.

45. Furst, A. L.; Smith, M. J.; Lee, M. C.; Francis, M. B., DNA hybridization to interface current-producing cells with electrode surfaces. *ACS Central Science* **2018,** *4* (7), 880–884.

46. Artyushkova, K.; Cornejo, J. A.; Ista, L. K.; Babanova, S.; Santoro, C.; Atanassov, P.; Schuler, A. J., Relationship between surface chemistry, biofilm structure, and electron transfer in *Shewanella* anodes. *Biointerphases* **2015,** *10* (1), 019013–019013.

47. Rosenbaum, M.; Zhao, F.; Quaas, M.; Wulff, H.; Schröder, U.; Scholz, F., Evaluation of catalytic properties of tungsten carbide for the anode of microbial fuel cells. *Applied Catalysis B: Environmental* **2007,** *74* (3), 261–269.

Chapter 4. Adhesion of *Shewanella oneidensis* to Glycopolymer Layers

This chapter is based on *ACS Appl. Mater. Interfaces* **2020**, 12, 35767–35781.

4.1 INTRODUCTION

While physical properties such as electrical charge, surface energy, and roughness can influence microbial adhesion, these physical properties are susceptible to adulteration by the adsorption of a conditioning layer of material. Specifically recognized chemical motifs may be less influenced by changing general properties of the overall surface. Saccharides are specifically recognized by microbes and have the advantages of water solubility, large stereochemical space, and abundant biosynthetic availability. Bacterial bonds to saccharides also have the ability to become even more adherent to a surface under high shear force.[1] Accordingly, saccharides are known to be used by bacteria to mark surfaces for colonization.[2] The secretion of the exopolysaccharide (EPS) matrix is among the aspects of surface colonization affected by the internal signaling cascade in bacteria that is activated upon surface contact and detection.[3] Mannose and other saccharide monomers, such as galactose and glucose, are common motifs found in EPS molecules.[4]

Saccharide-binding proteins, known as lectins, may be presented by bacteria on the ends of hair-like appendages, known as pili. Several attachment pili, known as fimbriae, have been discovered that recognize surfaces and contribute to biofilm formation.[5] One well-studied fimbria is the type I pili that is composed mostly of FimA proteins and terminated with the FimH lectin.[6,7] This type I pilus binds the sugar mannose, and is known to exist in *Escherichia coli* and several other gammaproteobacteria.[5,8,9] The attachment of bacteria that express FimH-terminated type I pili can be enhanced by engineering mannose-presenting surfaces. Whitesides and

co-workers demonstrated the ability to attract *E. coli* to a surface covered with alkanethiols terminated with a mannose residue.[10]

The presence of multivalency can increase binding strength or rate more than the sum of an equivalent number of monovalent bonds.[11] The results of multivalent interactions between saccharides and their targets have been referred to as the cluster glycoside effect.[12] Between saccharides and isolated proteins, multivalency has been widely studied and thermodynamics and kinetics have been characterized.[13,14] On the scale of bacteria, it has been reported that increasing the density of mannose on a flat surface nonlinearly increases the number of *E. coli* cells that are adsorbed.[15,16]

Assembly on two-dimensional surfaces provides multiple binding sites of the saccharide of interest across the surface. However, these sites are limited in how densely they can be packed before steric crowding prevents further insertion of saccharides or occludes binding to the biological targets. To increase the valency of saccharides beyond the limit of a planar conformation, polymer scaffolding can be used. By extending the molecular layer further away from the surface, more of the three-dimensional space is occupied by saccharide units in a given surface area. The increased multivalency may then augment the interactions to saccharide binding partners. Such extension of mannose residues into three dimensions has been accomplished using branching oligosaccharides. Textor and co-workers reported that multivalent branched trimannose molecules adhered much more *E. coli* compared to monolayers of monovalent mannose-terminated molecules.[15] However, the size of the mannose cluster was optimal as a trimer and less *E. coli* attached to branched oligosaccharides with six or nine mannoses. The lower binding by the longer molecules may be due to the α-1,2 glycosidic bonding used on the outer mannose residues or because FimH is well fitted to trisaccharides, as

has been described previously.[6] It has not yet been determined whether the increased adhesiveness of oligosaccharide mannose is due to increased valency, moiety density, or shape and receptor binding fit.

A glycopolymer can be constructed to present multiple monosaccharides rather than linking saccharide units in the manner of a polysaccharide, which is created by binding saccharide units directly to each other. This repeating monosaccharide polymer construction avoids the convolution between the alterations to the saccharide structure and the effects of multivalency. The availability of each of the saccharide unit's four hydroxyl groups is preserved and the multivalent saccharide binding can be tested independently of effects due to modification of the saccharide structure. Surfaces functionalized with tethered polymers decorated with monosaccharide mannose pendants have been shown to enhance *E. coli* attachment while not enhancing attachment of *Staphylococcus aureus*.[17,18] These observations did not compare adhesion to mannose monomer layers that were not a part of polymeric protrusions.

As discussed in the previous chapter, the adhesiveness of surfaces to *Shewanella oneidensis*, and other bacteria capable of transferring electrons directly to electrodes, is of particular interest. Enhancing the interfaces of these cells and surfaces could help provide consistent current output to electrodes and improve the performance of devices utilizing electroactive microbes. Attachment of key species may also be important in consortia of microbes where the ability to enrich the abundance of key species may have technological utility.

To promote adhesion specifically, mannosylated surfaces can be employed for *S. oneidensis* as it contains a mannose-binding lectin known as mannose-sensitive hemagglutinin (MSH).[19] Mannose-sensitive hemagglutinin is a type IV pilus that extends from the cell body and

influences the motility and surface attachment of bacteria.[20] It has been described in a number of other gammaproteobacteria including *Vibrio cholerae*,[21,22] *Pseudoalteromonas tunicata*,[23] and *Aeromonas salmonicida*.[24] In *V. cholerae* El Tor, mannose-sensitive hemagglutinin has been shown to be used in forming biofilms on borosilicate surfaces.[22] Mannosylated surfaces can influence surface colonization, not only by providing a physical attachment point, but also by modulating cellular colonization processes. In *V. cholerae*, MSH pili biogenesis can be affected by surface interactions as well as their internal signaling molecule cyclic-di-GMP, which means pilus biogenesis can act as a function of multiple inputs.[25]

In this chapter, the complex behavior of surface colonization is approached by modifying a key component of surface interaction: the specific interaction between the MSH pili in *S. oneidensis* and mannose sugar motifs. Glycopolymers are used as the mannoside agent in the work described in this chapter and are compared with analogs of different saccharides. The considerations for the glycopolymers, described above, are summarized here. Saccharides are chosen for their biochemical specificity which has more enduring adhesiveness in the presence of adsorbents and fluctuating ion concentration than surface charge and other physical properties. Each saccharide unit is presented as a monosaccharide, with four free hydroxyls available, to test changes in valency independently from effects due to modification of the saccharide structure. To increase the valency of saccharides beyond the limit of a planar conformation, a polymer scaffolding is used, which extends into three dimensions above the surface. We seek an approach of pre-assembled glycopolymers to keep the density of saccharides per polymer and local structure known.

By grafting the mannose glycopolymer to surfaces, we successfully promoted surface adhesion of *S. oneidensis*, enriched the percentage of one strain over another during

co-deposition, and induced where the bacteria attach on a molecular pattern. When adherent bacteria were rinsed with methyl α-D-mannopyranoside, the glycopolymer-functionalized surfaces retained more cells than self-assembled monolayers terminated by a single mannose unit. These results suggest the three-dimensional multivalency of the glycopolymers both promotes and retains bacterial attachment. When the methyl α-D-mannopyranoside competitor was co-deposited with the cell culture, however, the mannose-based polymer was not significantly different from bare gold surfaces. The necessity for equilibration between methyl α-D-mannopyranoside and the cell culture to remove the enhancement suggests the retention of cells on glycopolymer surfaces is kinetically controlled, and not a thermodynamic result of the cluster glycoside effect. The MshA lectin appears to facilitate the improved adhesion observed. Our findings, that the surfaces studied here can induce stable initial attachment and influence the ratio of bacterial strains on the surface, may be applied to harness useful microbial communities.

4.2 RESULTS AND DISCUSSION

4.2.1 Characterization of Glycopolymer Synthesis and Surface Assembly

Collaborators from the Prof. Andrea Kasko group synthesized the glycopolymers decorated with various saccharides, **Scheme 4-1**, using a reversible addition-fragmentation chain transfer (RAFT) reaction. A related method has been reported previously where mannose units are attached to a polymer scaffold through the hydroxyl on the sixth carbon of mannose.[26] Here, we have attached each saccharide residue to the acrylate scaffold by the anomeric carbon. The glycosidic bond formed through the anomeric carbon not only stabilizes the α isomer of the saccharide, but is also the configuration typically found in natural saccharide molecules.

Non-reducing saccharides, which are bound through the anomeric carbon, tend to have increased biological activity compared to reducing saccharides.[27]

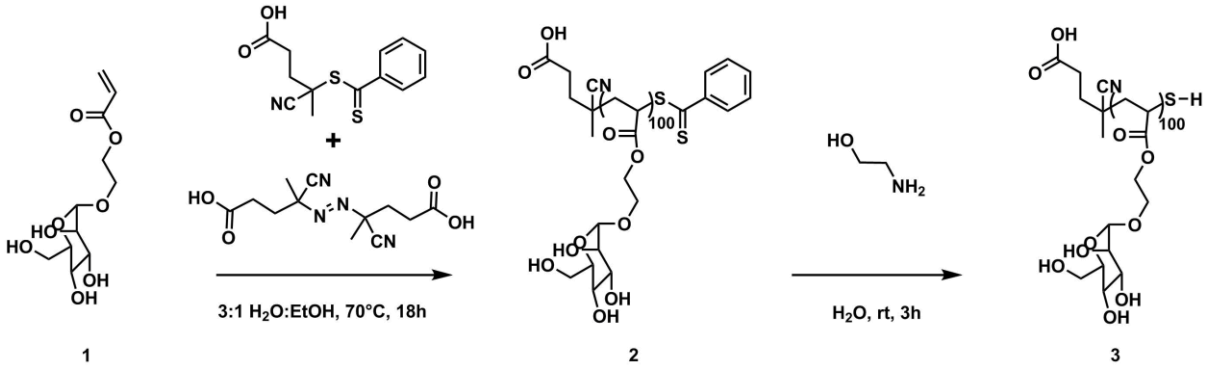

Scheme 4-1. The structure of poly(mannose acrylate)thiol, referred to below as polymannose, is shown. The hydroxylethylacrylate center of the polymer has a general non-adhesiveness, while the monosaccharide pendants provide specific adhesiveness. The polymer is produced by reversible addition-fragmentation chain transfer, which provides a thiol upon aminolysis. Corresponding polymers with glucose, galactose, and *N*-acetylglucosamine were prepared with the same process with analogous starting monomers.

The polymeric structure is, as described above, intended to increase the number of saccharide binding sites along the surface normal as well as along the two dimensions parallel to the substrate surface. One saccharide residue was incorporated into the polymer chain per acrylate repeat unit to conserve the recognizability of the monosaccharide. Mannose, glucose, galactose, and *N*-acetylglucosamine saccharides were functionalized with an acrylate moiety and polymerized. For brevity, the poly(acrylate saccharide)s are referred to below by their saccharide type, *e.g.*, polymannose. The polymerizable acrylate group of the glycopolymer monomer is linked to the saccharide unit by a hydroxyethyl group. The poly(2-hydroxyethyl acrylate) core structure that results when the glycopolymers form is analogous to polymers that have reported low adhesiveness.[28,29]

Methods for producing polymers on a surface include physisorption, chemisorption of the formed polymer (known as "grafting to" the surface), and chemisorption of an initiator from which the polymer is formed *in situ* (known as "grafting from" the surface). The method used in this work is grafting to the surface, where the polymers are formed in solution then bound to the surface through chemical bonding. The covalently bound chemisorption methods provide a stable bond to the surface that is not susceptible to changes in ion concentration and other factors of the medium.[30] Methods grafting from a surface, although providing higher polymer density, may suffer from variable reaction completeness.[30,31] Polymer length is more homogeneous across the surface and surface-recombination side reactions are avoided when grafting to the surface rather than grafting from the surface.[32] The grafting to approach provides known molecular structure and density of saccharides per polymer. Glycopolymers synthesized by RAFT featuring lactose and glucose have previously been grafted to surfaces to study *E. coli* adhesion.[33] Like other controlled polymerizations, RAFT offers better control over molecular weight and polydispersity than traditional chain polymerizations.[34]

Polymers synthesized by RAFT are conveniently terminated with a dithioester. The dithioester produces a free thiol upon aminolysis with ethanolamine, enabling facile self-assembly to gold surfaces. Gold is useful for electrodes in bioelectrical test systems because of its resistance to corrosion and high conductivity.[35] Electrodes of other metals and carbon are also used—compromising intrinsic conductivity for adhesiveness.[36–41] By functionalizing gold surfaces with glycopolymer, we can introduce colony-promoting character to the conductive surface. The opposite end of the polymer from the sulfur group is terminated with a carboxylic acid group, which can be utilized for facile conjugation to amine-terminated surfaces or additional functionalization of the assembled poly(saccharide acrylate) layer.[42,43]

Saccharide	M_w[a]	M_n[a]	Đ[a]	DP_n[a]	DP_n[b]
glucose	9600	6800	1.42	24	65
galactose	12000	8500	1.41	31	76
mannose	28700	16400	1.75	59	108
N-acetylglucosamine	14200	8400	1.68	27	76

Table 4-1. Glycopolymer weight average and number average molecular weight (M_w and M_n, respectively), dispersity (Đ) and degree of polymerization (DP_n) as determined by [a]aqueous gel permeation chromatography (GPC) relative to pullulan standards and by [b]comparison of the chain end and saccharide protons integrals with ^{1}H nuclear magnetic resonance (^{1}H NMR) spectroscopy.

The degree of polymerization (DP_n), weight average and number average molecular weight (M_w and M_n, respectively), and dispersity (Đ) of the various glycopolymers used in these experiments are shown in **Table 4-1**. A linear relationship was observed between the DP_n of the polymers when measured by gel permeation chromatography (GPC) and when calculated from ^{1}H nuclear magnetic resonance (^{1}H NMR) spectroscopy. Degree of polymerization and molecular weight measurements by ^{1}H NMR spectroscopy were higher than by GPC. This difference is likely due to the glycopolymer backbone and RAFT chain end being more hydrophobic than any component of pullulan, and thus the glycopolymer having a smaller hydrodynamic volume than the polysaccharide of similar length. The glycopolymers would be expected to be more compact to minimize unfavorable interactions between its hydrophobic components and the aqueous solvent used in GPC.

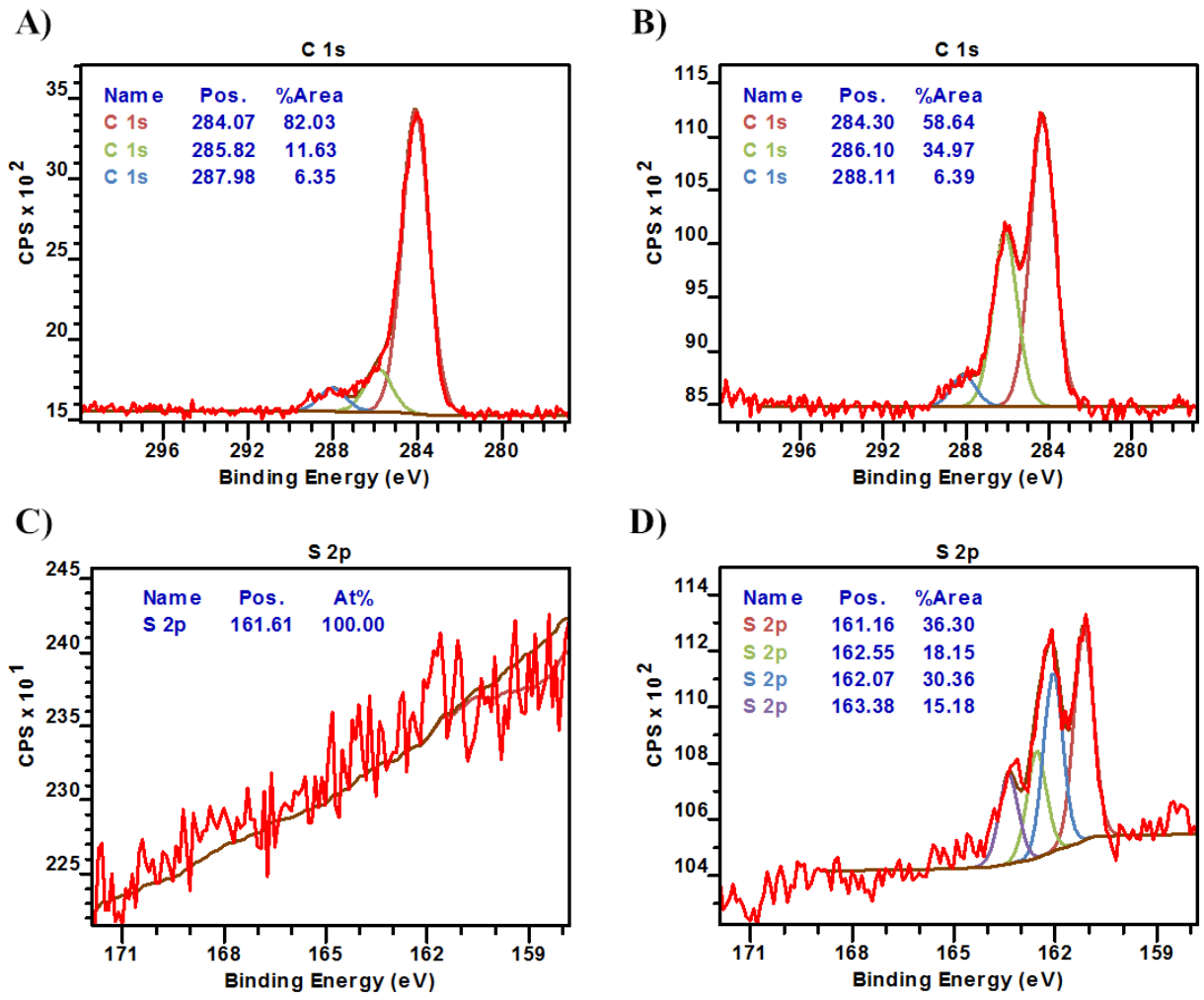

Figure 4-1. X-ray photoelectron spectra of glycopolymer surfaces. Bare gold **(A)** and polymannose on gold **(B)** carbon 1s spectra. C–C/C–H peaks of adventitious carbon and the deposited polymer are present at 284 eV in the bare gold and glycopolymer spectra. C–O bound carbon, present at 286 eV, as well as C=O bound carbon, present at 288 eV, increase in relative and total intensity as glycopolymer is added to the surface. Bare gold **(C)** and polymannose **(D)** sulfur 2p spectra demonstrate the emergence of surface sulfur as the thiol-containing glycopolymer self-assembles.

Characterization of the glycopolymers after self-assembly on a surface was primarily achieved by X-ray photoelectron spectroscopy (XPS). The surfaces were measured after dissolving the glycopolymer in water with ethanolamine and exposing the solution to the gold surface for several days. **Figure 4-1A** shows the change in the line shape of the carbon 1s signal. Adventitious carbon, which adsorbs randomly on surfaces, is present in the spectrum of bare

gold as a single peak at 284 eV.[44] The polymannose spectrum (**Figure 4-1B**) has three peaks corresponding to the C–C, C–O, and C=O sections of the polymer. The ratio of C–O to O–C–O and C=O is about 4:1, which corresponds roughly to the proportion of carbon species in the polymannose samples. Similar carbon spectra for the other glycopolymers are shown in **Figure 4-2**.

Sulfur can be observed in the XPS spectra of the thiolated surfaces in the expected energy region at 162 eV (**Figure 4-1D**). The sulfur peak appears split into two doublets, with each doublet having an intensity ratio of 2:1 due to spin-orbit coupling. The two signals imply two metal sulfide binding modalities. Minimal oxidized sulfur is observed in the 166–171 eV window, even after weeks of storage in air. This result indicates good stability of the covalent bonding of the glycopolymers to the surface. No appreciable sulfur peak is observed on the bare gold substrate (**Figure 4-1C**). X-ray photoelectron spectra of the other glycopolymers are shown in **Figure 4-3**.

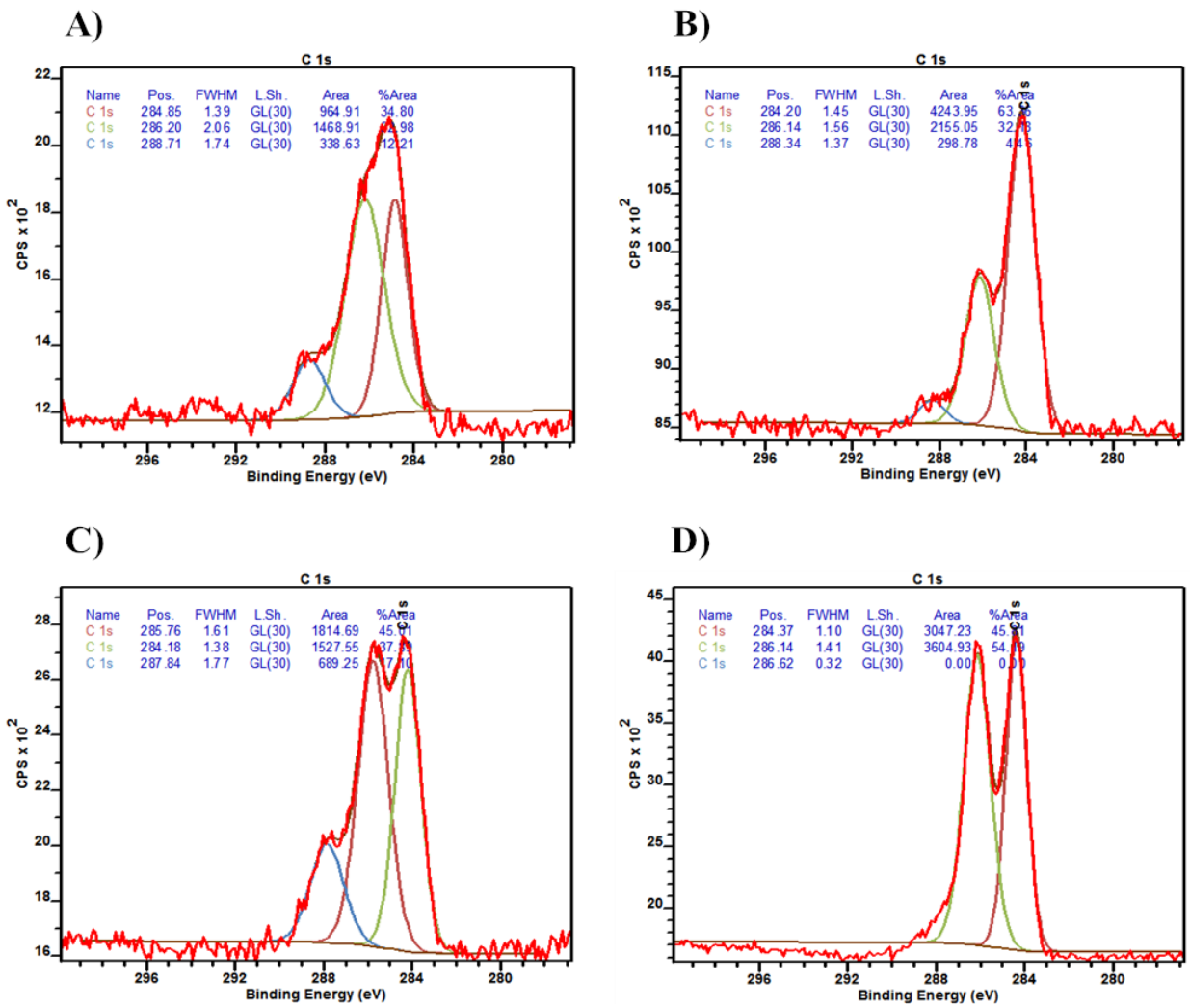

Figure 4-2. Carbon 1s X-ray photoelectron spectra of **(A)** polygalactose **(B)** polyglucose **(C)** poly(*N*-acetylglucosamine) and **(D)** tethered mannose monomer.

Monolayers of (11-[(*p*-phenyl-α-D-mannopyranosyl) aminocarbonyl methoxy hexa(ethoxy)]undec-1-yl-thiol), which will be referred to from here on as tethered mannose monomers, were produced on gold surfaces to compare to the mannose glycopolymer. The tethered mannose monomers have a single mannoside residue per molecule assembled on the surface. Functionalization of the gold surfaces with the mannose monomers provides a roughly two-dimensional array of mannosides to compare to the three-dimensional distribution of saccharides produced on the glycopolymer surfaces. The carbon 1s XPS spectrum of a tether

mannose monomer surface is shown in **Figure 4-2D**, which does not show the C=O associated peak seen in the glycopolymer spectra. The sulfur 2p XPS spectrum of a tether mannose monomer surface is shown in **Figure 4-3D**.

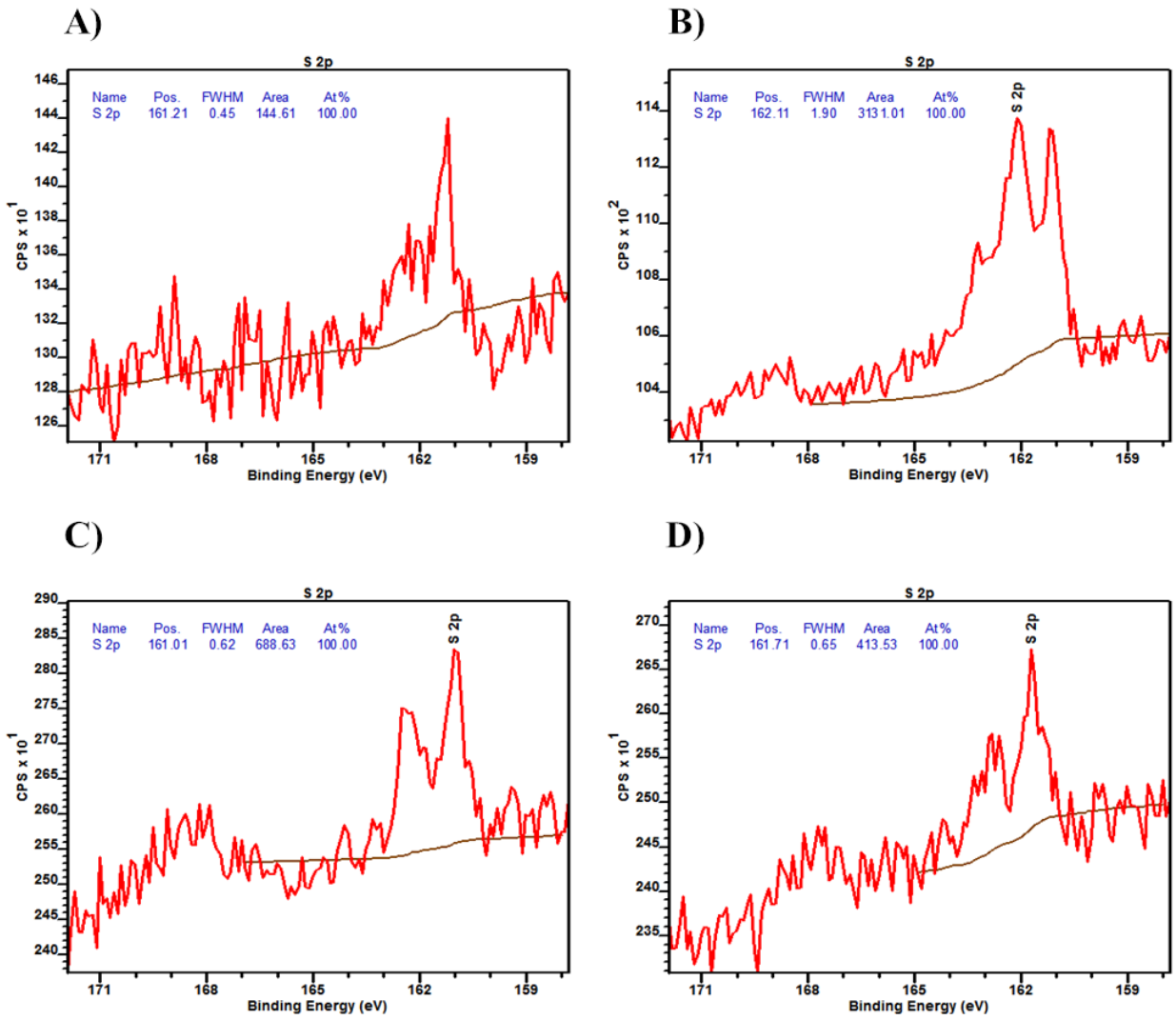

Figure 4-3. Sulfur 2p X-ray photoelectron spectra of **(A)** polygalactose **(B)** polyglucose **(C)** poly(*N*-acetylglucosamine) and **(D)** tethered mannose monomer.

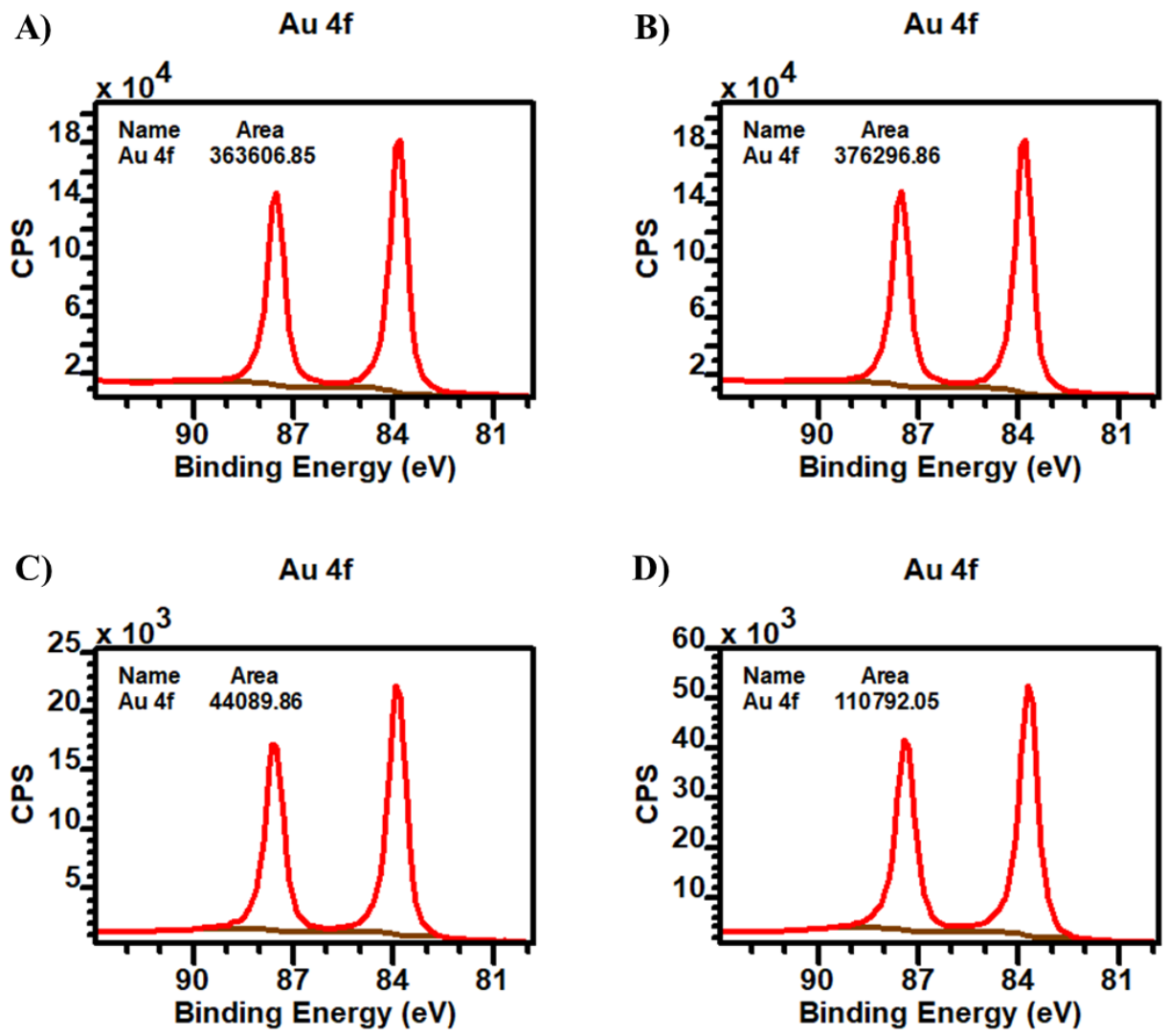

Figure 4-4. Au 4f X-ray photoelectron spectra of **(A)** polymannose **(B)** polyglucose **(C)** polygalactose and **(D)** poly(*N*-acetylglucosamine).

The density of glycopolymer molecules can be estimated by comparing the amount of sulfur and gold at the surface as measured from x-ray photoelectron spectroscopy. The gold 4f XPS spectra of glycopolymer surfaces is shown in **Figure 4-4**. The raw areas of the integrated signals are scaled by the relative sensitivity factor of the orbital, 6.25 for Au 4f and 0.668 for S 2p. Taking the ratio of these corrected areas provides the ratio of gold to sulfur atoms detected by the instrument. Gold atoms per sulfur atoms are 15 ± 4 by standard deviation (SD) for

polymannose, 13 ± 3 (SD) for polyglucose, 33 ± 61 (SD) for polygalactose, and 17 ± 5 (SD) for poly(*N*-acetylglucosamine). X-ray photoelectron spectroscopy is a surface sensitive technique, however, detection of gold atoms beneath the surface layer can contribute to the magnitude of the gold signal, which means the ratio of gold atoms on the molecular interface to sulfur atoms is likely smaller than the ratio of total gold and sulfur atoms.

Polymannose assembled onto gold surfaces was measured by ellipsometry to have an average dry height of 2.0 ± 0.6 nm. Poly(galactose acrylate) surfaces were measured to have an average dry height of 1.2 ± 0.9 nm. The polymannose surfaces had water contact angles of 56.9° ± 0.6° (SD) advancing and 36.2° ± 0.7° (SD) receding. Tethered mannose monomer surfaces had 38.9° ± 1.5° (SD) advancing and 29.0° ± 2.0° (SD) receding water contact angles.

Electrochemical desorption of polymannose was employed to verify chemisorption and determine the density of polymannose molecules on the surface. (**Figure 4-5**) The anodic peak near 0.8 V matches the electrochemical potential of thiol reduction during one-electron desorption.[45] The integration of this peak provides the total charge of electrons accepted by the surface. Factoring in the scan rate of 20 mV/s and the surface area of 0.08 cm^2 that was exposed to the electrochemical cell, the density of thiol molecules was calculated to be 14.8/nm^2.
A control sample, which was exposed to only ethanolamine solution without any glycopolymer, was measured to determine background current and subtracted from the polymannose sample during the calculation.

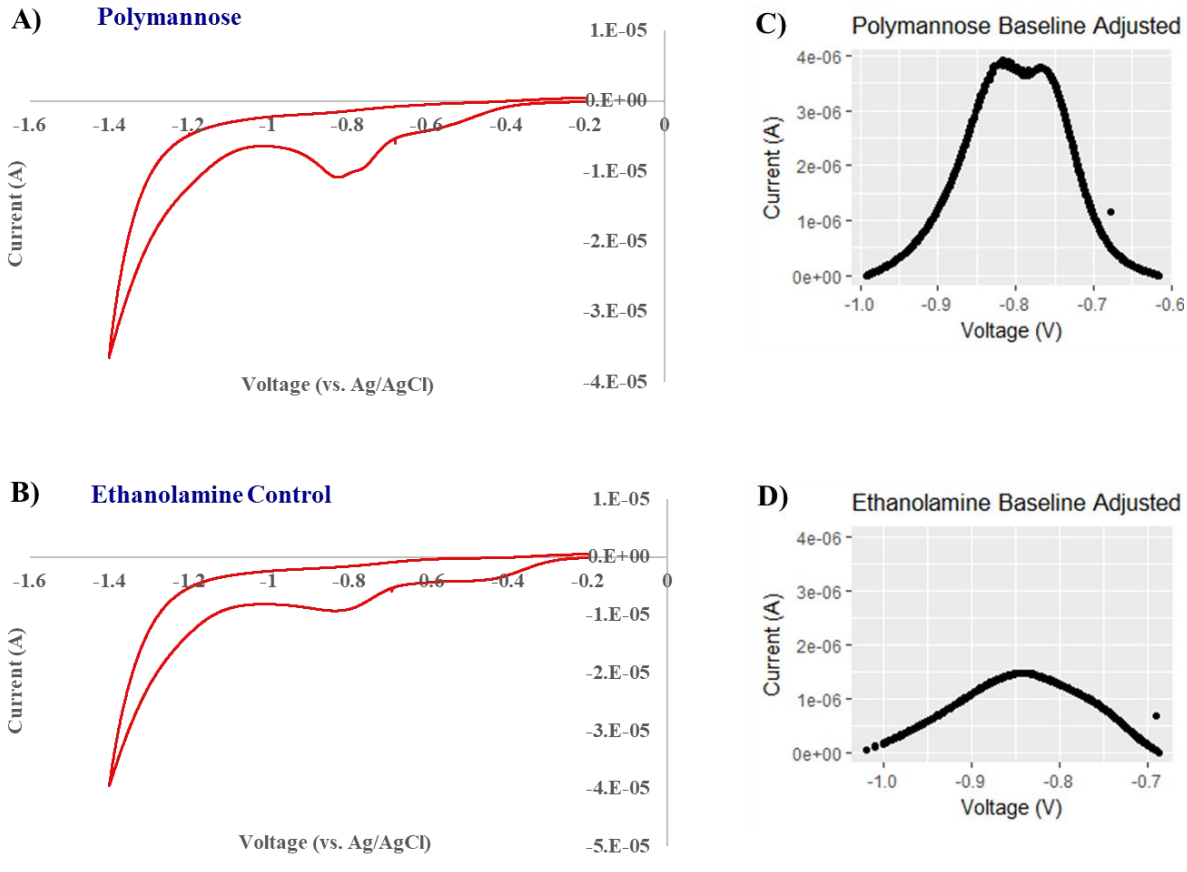

Figure 4-5. Electrochemical desorption of **(A)** polymannose self-assembled monolayer **(B)** and a control sample exposed to the same ethanolamine solution without glycopolymer. Anodic peak around -0.8 V represents desorption of thiols from the surface. Isolated sections of the desorption peak with baseline removed for **(C)** polymannose and **(D)** the ethanolamine control. The scan rate was 20 mV/s and surface area was 0.08 cm^2.

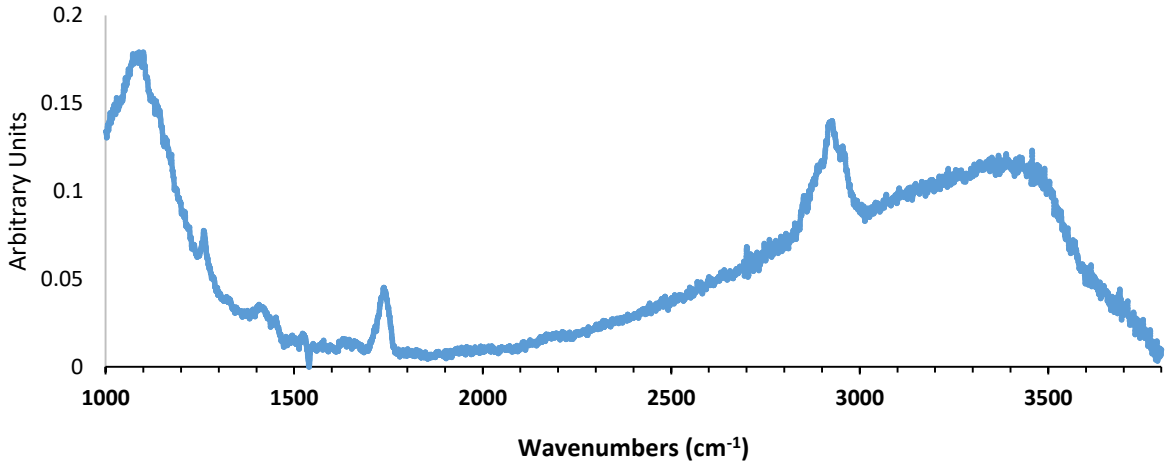

Figure 4-6. Polymannose spectrum by polarization modulation-infrared reflection-absorption spectroscopy (PM-IRRAS). Several vibrational modes are present: ether stretching at 1100 cm^{-1}, carbonyl stretching of the ester at 1750 cm^{-1}, alkyl C-H stretch at 2900 cm^{-1}, and a broad peak for alcohol stretching at 3400 cm^{-1}. The spectral baseline has been removed.

Polarization modulation-infrared reflection-absorption spectra of the glycopolymer assemblies on gold surfaces showed characteristic vibrational frequencies. A representative spectrum for polymannose is shown in **Figure 4-6**. The expected peaks from the tethered mannose monomer assemblies also appear in their spectra. (**Figure 4-7**)

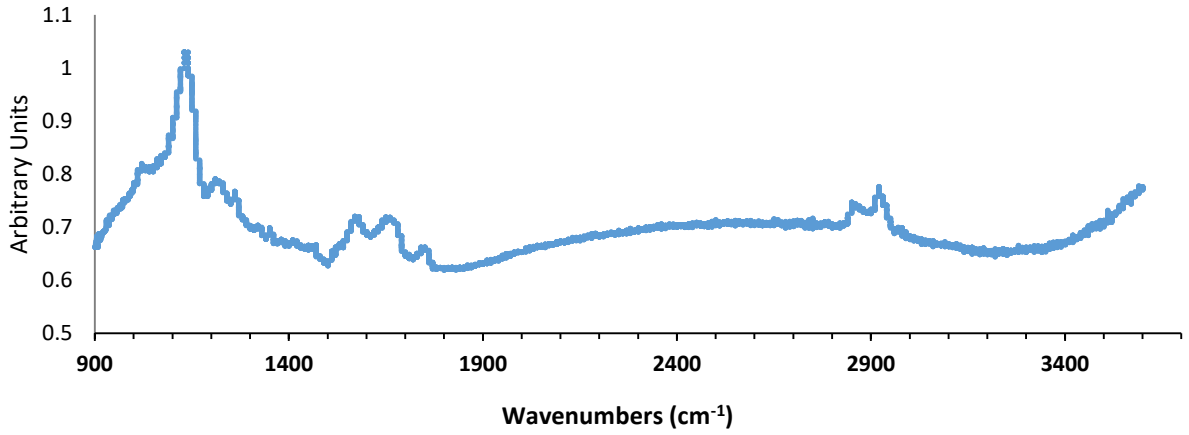

Figure 4-7. Tethered mannose monomer PM-IRRAS spectrum. Ether stretching modes from the ethylene glycol units are visible at 1100 cm^{-1}. Carbonyl of the carboxylic acid is mostly removed at 1750 cm^{-1} and replaced by the amide carbonyl stretch at 1650 cm^{-1} as the mannoside is added by amide bond formation. Alkyl and aromatic C-H stretching is present around 2900 cm^{-1}. The spectral baseline has been removed.

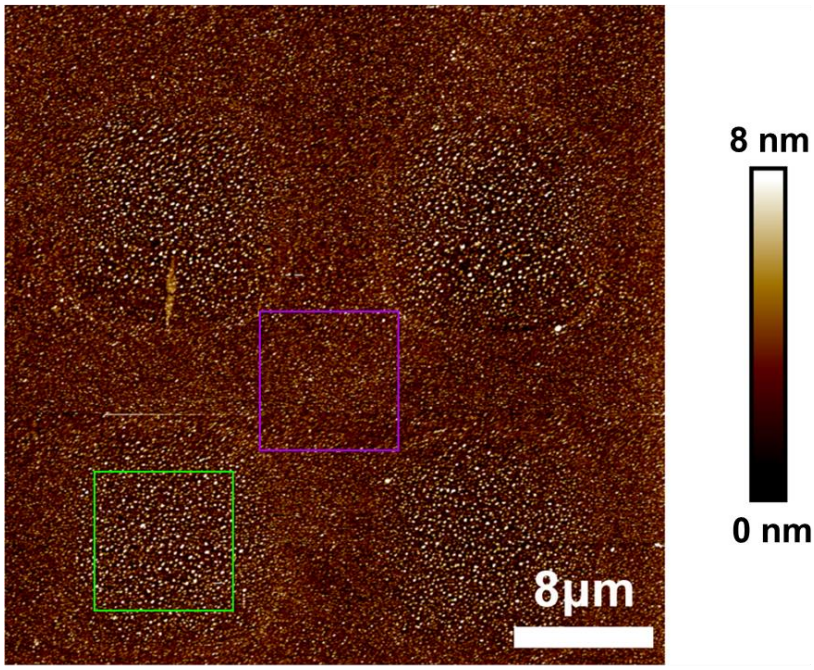

Figure 4-8. Atomic force micrograph of polymannose pattern on gold surface. The region outlined with the green box corresponds to a polymannose functionalized area and has a root-mean-square surface roughness of 4.4 nm. The region outlined with the purple box corresponds to a bare gold area and has a root-mean-square surface roughness of 4.2 nm.

4.2.2 Interactions of *S. oneidensis* and the Glycopolymer Surfaces

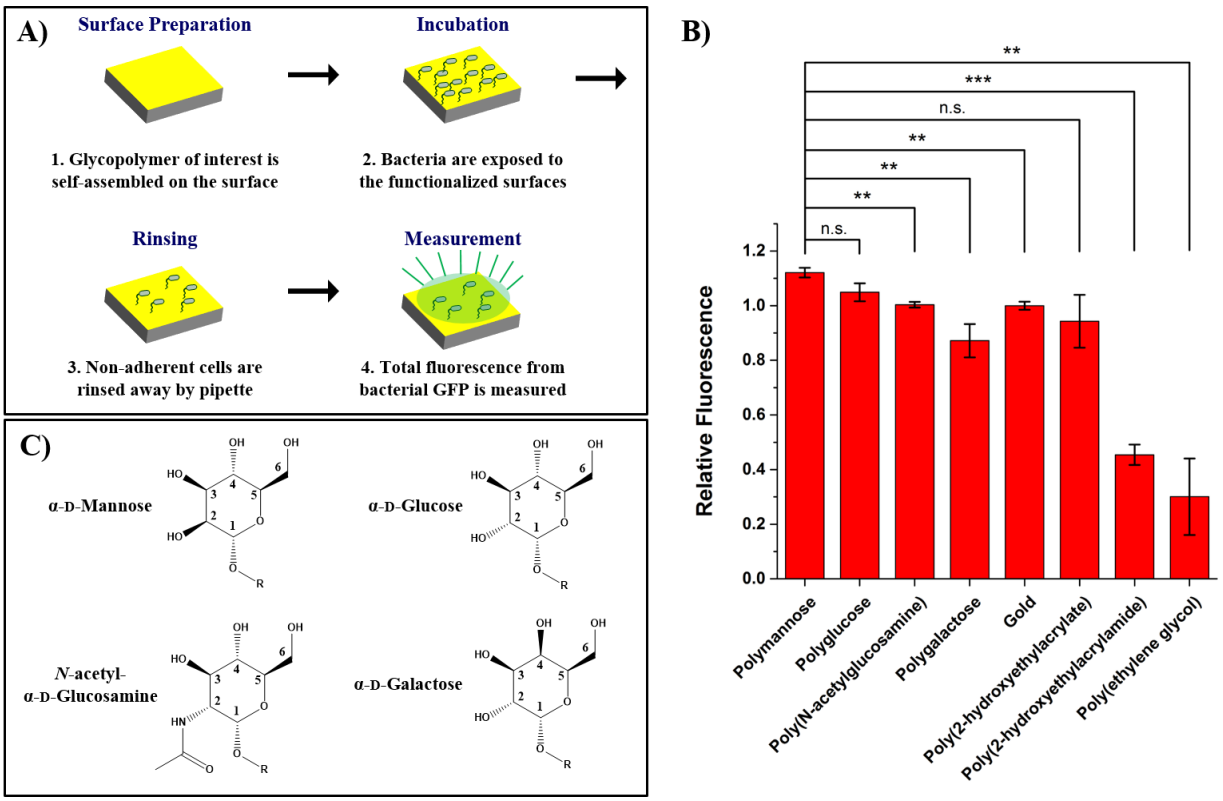

Figure 4-9. Adhesiveness of *Shewanella oneidensis* cells to various surfaces as measured by total fluorescence. **(A)** Adhesiveness was measured by incubating fluorescent cells over polymer functionalized surfaces and rinsing away non-adherent cells. Fluorescence is plotted relative to signal of cells adhered to bare gold. **(B)** Polymannose enables greater adhesion of *S. oneidensis*, which is diminished by changing the chirality of the second and fourth carbons of the poly(acrylate saccharide)s. Error bars indicate standard error of the mean (N = 4). **(C)** Saccharide motifs of the glycopolymers.

Adhesiveness of various polymers and saccharide moieties is shown in **Figure 4-9**. Monolayers of the glycopolymers were prepared and exposed to cultures of *S. oneidensis* that express green fluorescent protein (GFP). Non-adherent cells were rinsed away with phosphate-buffered saline (PBS) and the remaining cells were quantified by measuring the total fluorescence from the surface. Variances in GFP measurements as a result of cell proliferation was limited by exposing the cells to the surfaces while in nutrient poor solution, controlling the

cell density and growth phase of cells applied to the surfaces, and measuring cells remaining on the surfaces immediately after rinsing away non-adherent cells. Polymannose shows the highest total fluorescence and is significantly brighter than the polygalactose and poly(*N*-acetylglucosamine) glycopolymers. The polymannose surfaces had 12.1 ± 2.3%, by standard error of the mean (SEM), more fluorescence intensity than bare gold surfaces. Poly(2-hydroxyethylacrylate), which has the same core structures of the glycopolymers, showed similar fluorescence as bare gold surfaces. Poly(2-hydroxyethylacrylamide) and poly(ethylene glycol)-treated surfaces demonstrated lower fluorescence than all other samples.

The greater fluorescence indicates polymannose promotes surface adhesion by *S. oneidensis* on this timescale of 18 hours. Polyglucose has the most similar fluorescence to polymannose of the series of hexoses tested. Glucose differs from mannose by the stereochemistry of the hydroxyl on the second carbon, which faces towards the backbone of the polymer. Changing the chirality of only the second carbon hydroxyl is insufficient to significantly change bacterial recognition of the surface. Galactose, however, has inverted chirality at both the second and outward-facing fourth carbon with respect to mannose and binds significantly fewer bacteria. The *N*-acetylglucosamine glycopolymer retains an intermediate number of bacteria between polyglucose and polygalactose. The stereochemistry of the saccharide residues appears to be more important than their size and functionality for *S. oneidensis* recognition of surface saccharides, because the acetyl group appended to the second carbon substituent of poly(*N*-acetylglucosamine) is less impactful than the additional inversion of the fourth carbon chirality in polygalactose.

The greater influence of the fourth carbon hydroxyl over the second carbon hydroxyl we observed in *S. oneidensis* is consistent with the binding of *V. cholerae* cytolysin, which bonds to

methyl α-D-mannose through the third and fourth carbon hydroxyls.[46] The related stereochemical importance may indicate the *S. oneidensis* mannose-binding lectin (MshA) is homologous to *V. cholerae* lectins and form β-prism domains.[46–48] The importance of fourth carbon hydroxyl also suggests glycans with (1,4) glycosidic linkages are not as impactful for *S. oneidensis* colonization as saccharides that maintain a free hydroxyl on the fourth carbon.

Methyl α-D-mannopyranoside is a non-metabolizable form of mannose which can compete for binding of MSH lectin sites.[20] The methyl group is bound to the oxygen on the anomeric carbon of the mannose residue analogous to the core of the glycopolymers. The methyl α-D-mannopyranoside inhibitor dissolved in PBS was used to rinse bacteria from the various surfaces to test the strength of attachment. During these rinses, the culture medium was removed and replaced with solution without cells, which greatly diminishes the attachment rate of the bacteria. The detachment rate thus becomes the governing factor in net attachment rate.

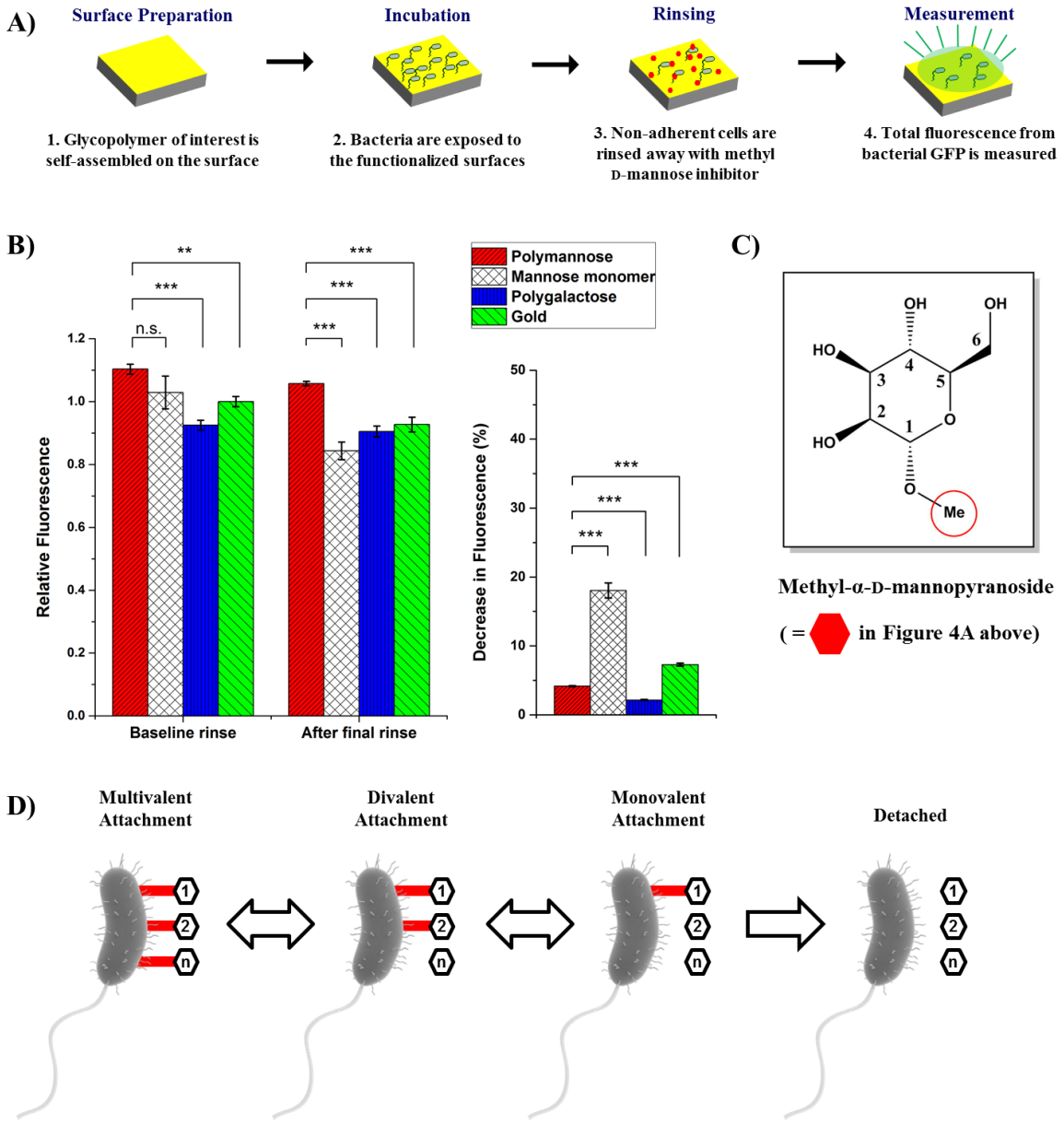

Figure 4-10. Persistence of cell adhesion after rinsing samples with methyl α-D-mannopyranoside, an analog of the surface-bound mannose units. **(A)** Method for testing robustness of cell adhesion using green fluorescent protein (GFP). **(B)** Both before and after mannoside inhibitor rinsing, more cells remained adhered to the polymannose surface than either polygalactose or bare gold. Tethered mannose monomer surfaces presenting a single mannoside residue per thiol head group originally adhered a similar amount of *S. oneidensis* as polymannose but lost more cells during methyl α-D-mannopyranoside rinsing. Error bars indicate standard error of the mean (N = 5). **(C)** Structure of methyl α-D-mannopyranoside inhibitor. **(D)** Schematic of multivalent detachment.

Rinsing the bacteria laden surfaces with methyl α-D-mannopyranoside solution caused a decrease in the total GFP fluorescence, suggesting fewer cells were adhered (**Figure 4-10**). The decrease in total fluorescence caused by rinsing with methyl α-D-mannopyranoside solution was disproportionately larger for tethered mannose monomer (11-[(*p*-phenyl-α-D-mannopyranosyl) aminocarbonyl methoxy hexa(ethoxy)]undec-1-yl-thiol) surfaces, which have a single mannoside residue per molecule assembled on the surface. Tethered mannose monomers became statistically distinguishable from polymannose after rinsing. Both glycopolymer samples tested retained more of the initially adhered cells than bare gold surfaces. The percentage decrease in total fluorescence from before rinsing with methyl α-D-mannopyranoside was as follows: 4.2 ± 1.6% (SEM) for polymannose surfaces, 18.1 ± 5.8% (SEM) for tethered mannose monomer, 2.2 ± 2.5% (SEM) for polygalactose, and 7.3 ± 2.9% (SEM) for bare gold. The decrease in fluorescence indicates faster detachment of cells adhered to tethered mannose monomer surfaces than the glycopolymer surfaces.

The three-dimensional multivalency of the glycopolymers seems to be responsible for slowing the detachment rate of adherent cells considering the monovalent mannose-terminated monolayers were more easily removed. With multivalent attachment, the rupture of one bond does not fully detach the binding partners and time is allowed for rebinding to occur. On the scale of the bacteria, this means the detachment of one saccharide-lectin pair does not fully release a cell from the surface (**Figure 4-10D**). Other saccharides and bacterial recognition sites remain localized and reattachment of the unbound lectin can occur more rapidly. By having multiple binding sites, a cell is therefore kinetically hindered from releasing from the surface. In addition to the mannose bonds directly holding a bacterium in place, the multivalent effect may act indirectly through surface sensing. As more sensory receptors are bound to target molecules,

integration of their signal over time would be larger. Multivalent attachment of surface sensory receptors could then increase colonization response and more rapidly establish strong attachment of the cell to the surface through secondary binding sites.

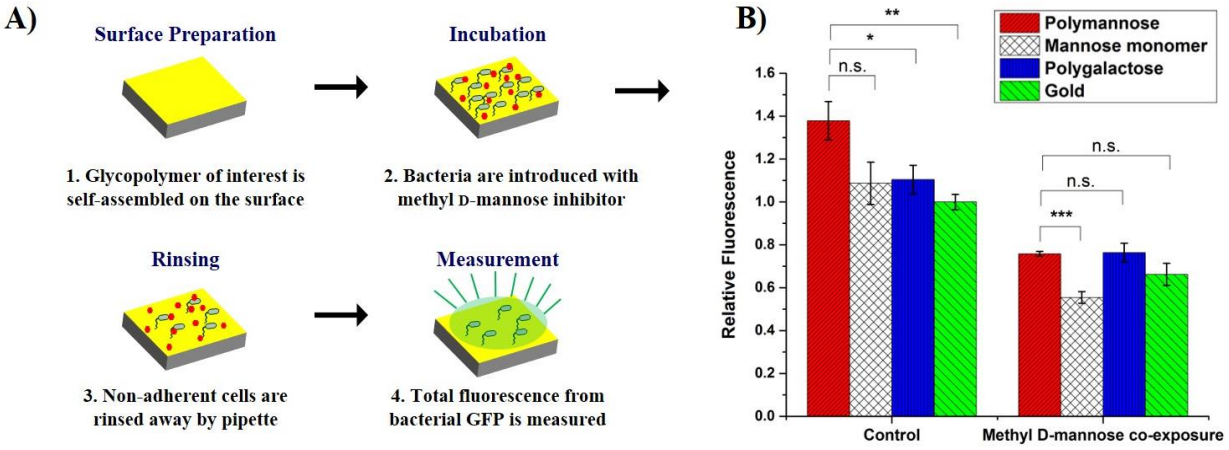

Figure 4-11. Inhibition of initial adhesion. **(A)** Simultaneous introduction of inhibitor with cell culture. **(B)** With no methyl α-D-mannopyranoside, results are as observed with other measurements and polymannose samples have the greatest fluorescence. Mixing methyl α-D-mannopyranoside into the original cell culture, before exposure to the substrate surfaces, removes the difference between polymannose, polygalactose, and bare gold in adhered cells. All samples, particularly tethered mannose monomer, adhere less *S. oneidensis* when incubated with methyl α-D-mannopyranoside. Error bars indicate standard error of the mean (N = 4).

When methyl α-D-mannopyranoside was added to the bacterial culture before exposure to a surface, less adhesion was observed (-0.62 ± 0.09 (SEM) for polymannose, -0.53 ± 0.10 (SEM) for tethered mannose monomers, -0.34 ± 0.08 (SEM) for polygalactose, and -0.34 ± 0.06 (SEM) for bare gold surfaces, all in arbitrary units of relative fluorescence), and the difference between adhesiveness of glycopolymers surfaces and bare gold was no longer significant (**Figure 4-11**). Tethered mannose monomer surfaces showed the lowest fluorescence of all surface types when *S. oneidensis* is incubated with methyl α-D-mannopyranoside.

Rinsing with the mannose inhibitor after cells have attached to the surfaces, as presented in **Figure 4-10**, shows the robustness of *S. oneidensis* colonization on polymannose, once established. Concurrent exposure of the methyl α-D-mannopyranoside and the cell culture to the surface (**Figure 4-11**) probes the importance of steady-state mannose binding and sensing, and provides some mechanistic insights. The resistance to methyl α-D-mannopyranoside-induced detachment observed in **Figure 4-10** appears to be kinetic in nature, because the enhanced persistence of adhered cells on polymannose is removed when the system is provided time to equilibrate as in **Figure 4-11**. Transiently introducing methyl α-D-mannopyranoside with rinsing produces a more dynamic system than concurrent exposure lasting the entire incubation period. Both cell-surface association rates and dissociation rates of the systems represented in **Figure 4-11** are influenced by methyl α-D-mannopyranoside. Whereas in **Figure 4-10** the inhibitor is largely affecting the dissociation rate as cells are already attached when methyl α-D-mannopyranoside is introduced and planktonic cells are removed. Our results suggest that previously reported kinetic descriptions of multivalency in cluster glycosides, also concern systems at the scale of microbial cells.[11,14,49]

Mechanistically, the ability of methyl α-D-mannopyranoside to inhibit the enhanced cellular attachment on polymannose surfaces implicates the structures of the mannoside units as the causative agents that enhance attachment. The free methyl α-D-mannopyranoside can occlude recognition sites on the bacteria; once the receptors are blocked, mannose-dependent adhesiveness is presumably diminished. Furthermore, it appears the attachment enhancement is the result of a direct physical linkage between the bacteria and the surface, rather than the result of signaling cascades responding to sensing of mannoside units, because the addition of

dissolved mannoside units decreased attachment and the addition of surface-tethered mannoside units increased attachment.

Tethered mannose monomer surfaces appear less adhesive to *S. oneidensis* than polymannose or polygalactose with methyl α-D-mannopyranoside present. One explanation for this result is that tethered mannose monomer surfaces have lower mannose-lectin-independent—thus, non-specific—adhesiveness than the glycopolymers. The ethylene glycol linkage in the tether that attaches the mannose monomer to the gold surface could reduce surface adhesiveness. Non-specific multivalency between the glycopolymers and non-MSH binding sites could also contribute to the differences between tethered mannose monomers and the glycopolymers. The glycopolymer saccharide pendants could undergo reattachment if multiple pendants are physisorbed to a particle. In other words, non-specific binding sites that are not lectins can allow reattachment of a severed bond, as long as other bacterium-surface bonds keep the saccharides pendants localized to either the previous binding location or a new one. If the galactose units of the polygalactose surfaces are binding to *S. oneidensis* nonspecifically, these interactions could also explain the resistance to methyl α-D-mannopyranoside rinses seen in polygalactose (**Figure 4-10**), which has similar relative magnitude to polymannose surfaces. If only non-specific interactions were involved, the adhesiveness of the mannose and galactose units to non-specific bonding partners is expected to be very similar as only the stereochemistry differs in the molecules. Dipole interactions and hydrogen bonding have similar opportunities for physical attachment in either type of saccharide pendant. The glycopolymers would then have similar levels of attached cells when the mannose-binding sites are filled by methyl α-D-mannopyranoside.

Another possibility for why tethered mannose monomers are more affected by the addition of methyl α-D-mannopyranoside is that polymannose may be able to interact with a partially filled array of lectins more effectively due to its expanded valency. Mannose-dependent attachment mechanisms may be present in reduced form, if the system is sub-saturated. Polygalactose may interact with other lectins produced by *S. oneidensis* and retain adhesiveness relative to tethered mannose monomers. Galactose-dependent binding could also explain the resistance to methyl α-D-mannopyranoside rinses in **Figure 4-10**. The differences between adhesiveness due to partial availability of mannose lectins binding to polymannose surfaces and galactose lectins binding to polygalactose surfaces is not distinguishable, if this is the case.

The inhibitory activity of methyl α-D-mannopyranoside presented above indicates the relevance of mannose binding in *S. oneidensis* surface interaction. The influence of mannose-sensitive hemagglutinin is suggested by the results shown in **Figure 4-12**, where the MSH containing wild-type strain was enriched as a fraction of the total cell population on the polymannose surfaces.

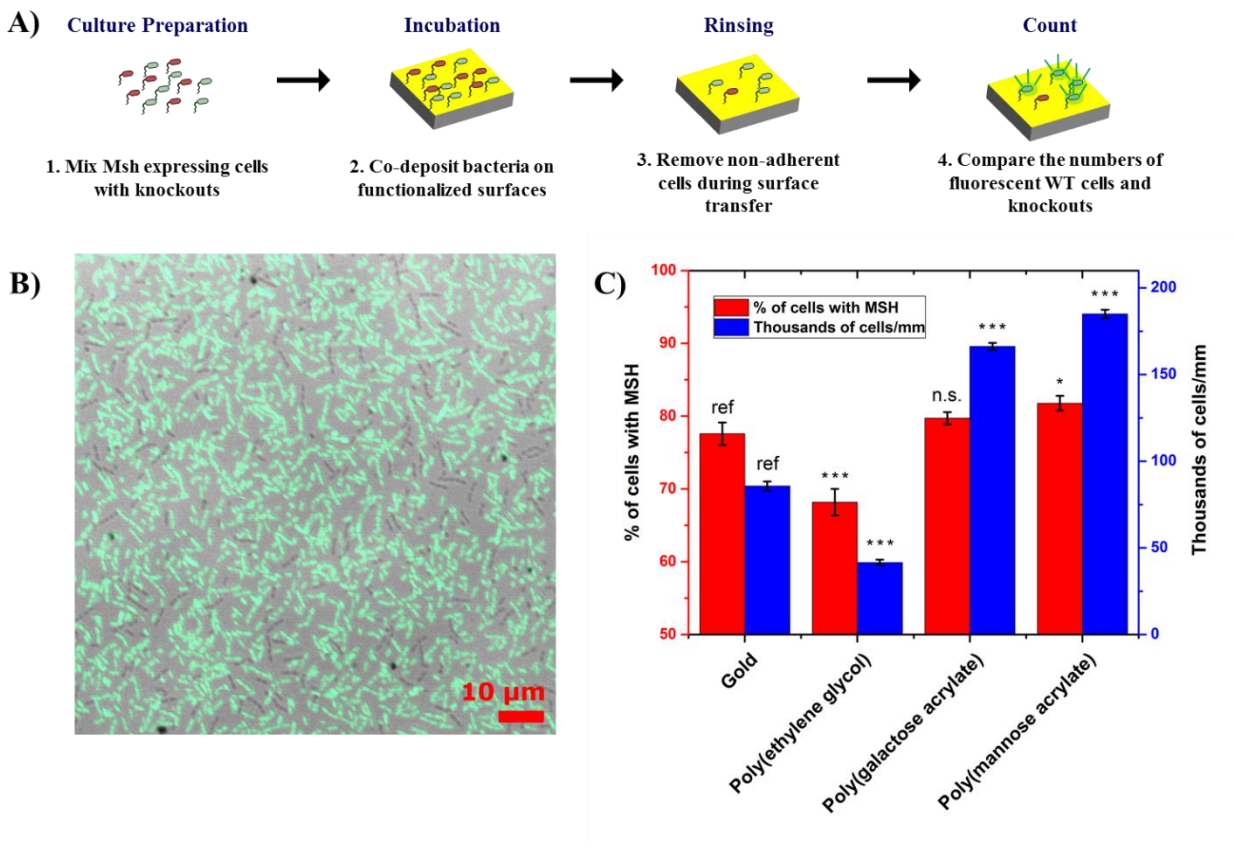

Figure 4-12. Surface colonization of competing *S. oneidensis* strains, containing *mshA-D* genes, and *ΔmshA-D* knockout. **(A)** Method for determining the fraction of *mshA-D* expressing cells on the surface. The fraction of a strain is measured by counting the fluorescent strain (wild type) of cells versus the non-fluorescent (*ΔmshA-D*) strain. **(B)** Example micrograph of the co-cultured surface. A fluorescence image is overlaid the concurrently taken brightfield image. The fluorescent strain is wild type, which produces mannose-sensitive hemagglutinin (MSH). **(C)** Fraction of fluorescent cells (red) and cell density (blue) on various surfaces. The *mshA-D* expressing strain is selectively enriched on polymannose surfaces compared to gold. Cell density is increased on the poly(saccharide acrylate) surfaces. Significance is marked by comparison to the bare gold reference. Error bars indicate standard errors of the mean.

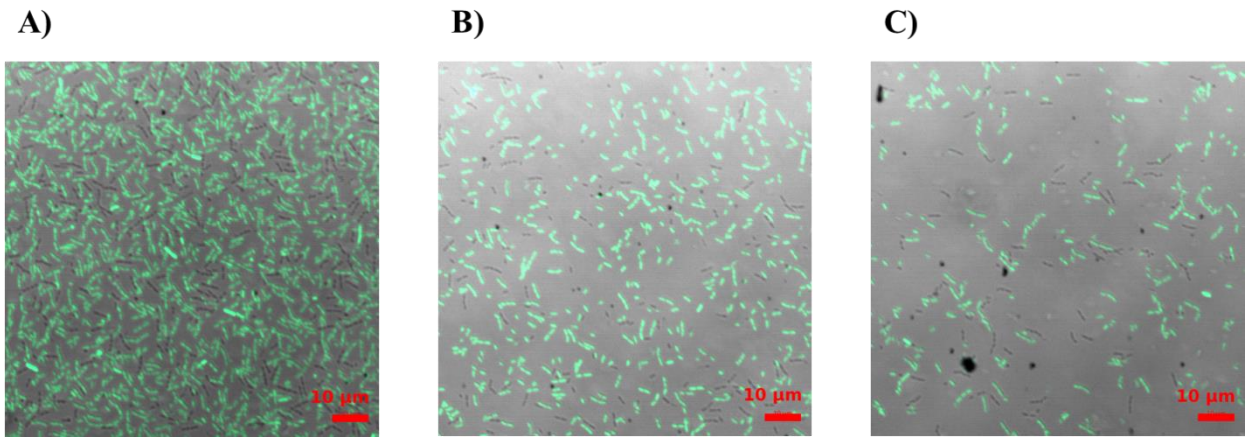

Figure 4-13. Representative micrographs of surfaces colonized by *S. oneidensis* wild type (fluorescent) and *ΔmshA-D* knockout (non-fluorescent) co-culture. **(A)** Polygalactose. **(B)** Bare gold. **(C)** Poly(ethylene glycol). Fluorescence images are overlaid with brightfield images that were taken concurrently.

Selective enhancement of surface colonization by natively MSH possessing bacteria versus *ΔmshA-D* genetic knockouts was possible on polymannose surfaces (**Figure 4-12**). Cultures of the two strains were mixed together with equal densities of the strains, then incubated on top of the various surfaces. The cultures were mixed and deposited simultaneously in an effort to standardize the concentration of signaling molecules secreted by the bacteria into the culture medium and reduce the variability in lag time before colonization. The number of cells for each strain were counted on the various surfaces. The cell density of both strains increased on the glycopolymer surfaces, with polymannose increasing the most, and decreased on poly(ethylene glycol) (PEG) surfaces versus bare gold. The cell density of wild-type cells was not proportional to the cell density of the *ΔmshA-D* knockout cells. Polymannose surfaces showed the fraction of bacteria containing the *mshA-D* genes increase by 5.4 ± 2.4% (SEM) versus bare gold surfaces.

Poly(ethylene glycol)-covered surfaces showed a reduction of the fraction of Msh expressing strain compared to bare gold surfaces. Poly(galactose) surfaces had a higher total cell density than gold (p-value < 0.001), whereas in the results presented in **Figure 4-9**, the two

sample types were not statistically distinguishable (p-value = 0.087). This result may be due to extracellular GFP, which enters the culture medium when the fluorescent cells lyse, increasing total fluorescence. There may be more adsorbed extracellular GFP on the gold surfaces than samples with less nonspecific adhesiveness. The higher precision of the microscopy measurements can also explain why the difference was distinguishable.

The net rate of appearance of wild-type cells was higher on average than *ΔmshA-D* knockouts from the time of initial exposure of the surfaces to the cell cultures to the time of imaging. The rate of net appearance of cells on a surface is the combination of the rate of cell division and death on the surface, and the net rate of cellular attachment. The rates for cellular division, death, and net attachment are likely time-dependent as factors such as metabolic rate, colonization signals, and dispersal signals vary in time. One way that a strain could be enriched in a mixture on a particular surface is if colonists on one type of surface grew and divided at a faster rate than another surface type. This difference may be possible if a surface signal, such as saccharide motifs, activates cell division. Differences merely between surface and bulk population growth rate would affect the samples proportionally and would not produce the enrichment we observed. Furthermore, it is known that the growth rate of bacteria on a surface reflects that of bulk solution while in a non-chemotactic environment.[50] If a surface does not influence bacterial growth rates, then the relationship of the strain proportions will depend only on the attachment and detachment rates and not on either strain's population growth rate.

The net rate of attachment can be influenced by direct physical bonds between a bacterium and the surface, as well as secondary responses from intracellular signaling ultimately resulting from surface sensing. Secondary responses, due to regulation of cellular systems that control colonization, are another way for surface interactions to influence net attachment.

Surface sensing by bacteria, including by MSH pili, is known to influence biofilm formation.[3] Retraction of pili has been found to stimulate bacterial secretion of adhesives.[51] Moreover, MSH retraction with the PilT protein is known to be associated with biofilm formation in *S. oneidensis*.[19] Therefore, colonization behavior favoring attachment and resisting dispersal may result from interaction of MSH and the mannose character of the surface. However, because methyl α-D-mannopyranoside reduces the number of surface-associated bacteria, it seems the physical linkage of the mannoside units to the bacteria may be the more important mechanism of attachment in this system.

The increased attraction of the wild type to polygalactose surfaces may be the result of the surfaces having more mannose character than bare gold. The mannose character of a surface, or how mannose-like a surface is, describes the combined density of mannose residues and molecular moieties that are similar enough in shape to mannose to be recognized nonspecifically by a mannose lectin. This recognition includes molecular groups existing on the surface before exposure to the cell culture medium, such as the glycopolymer films, as well as adsorbed molecules, such as extracellular polymeric substances secreted by the bacteria. With respect to adsorbed mannose, the gold surfaces are expected to accumulate more mannose character than PEG surfaces, which are resistant to the adsorption of mannose residue deposits. Surfaces that initially contained no mannose may demonstrate mannose-dependent adhesion by developing a mannose-containing conditioning layer after exposure to cellular secretions. The polygalactose surfaces may either be able to accumulate secreted mannose or to have some off-target adhesion to the MSH pili.

We observed the most even ratio of wild-type to *ΔmshA-D* knockout cells on the PEG surfaces. If mannose-independent forces—including Coulombic, van der Waals, and other

physical forces—affect both strains equally, then the fraction of each strain in the population would reach parity on an idealized mannose-free surface. The more even distribution of the strains on the PEG surfaces suggests that they have less adhesive interactions that depend on MSH.

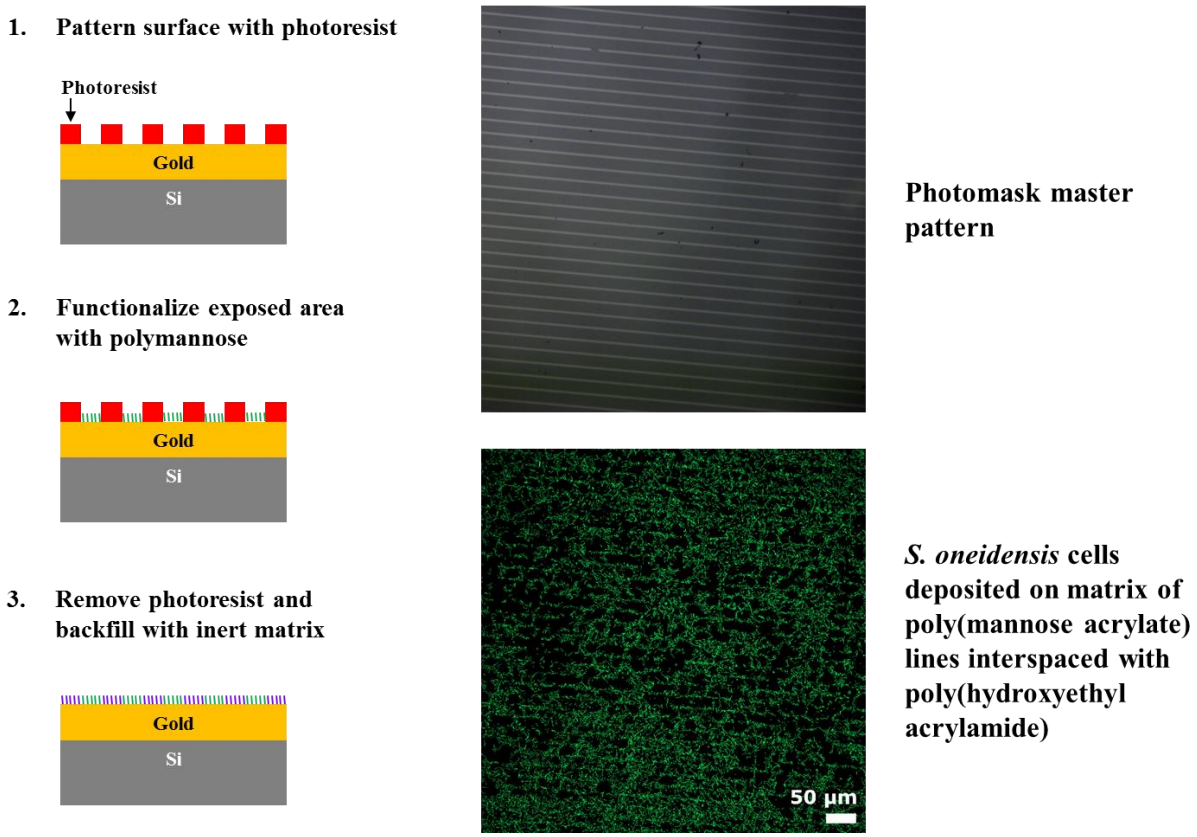

Figure 4-14. Demonstration of the ability to control *S. oneidensis* adhesion to a surface was performed with a molecular pattern of polymannose in a poly(2-hydroxyethylacrylamide) matrix. The polymannose was deposited as 2 µm lines interspersed with poly(2-hydroxyethylacrylamide) with a periodicity of 10 µm. The attraction of the polymannose retains cells over the area where it is deposited.

S. oneidensis was stimulated into a series of lines by molecularly patterning a gold surface with polymannose by conventional photolithography. (**Figure 4-14**) Polymannose was self-assembled around a photoresist layer. The photoresist was removed and the gaps between the polymannose regions were backfilled with poly(2-hydroxyethylacrylamide). The increased

adhesion of polymannose enables spatial control over bacteria surface colonization. With control over colonization, arbitrary patterns can be used for fundamental study of cell interaction with each other, co-culture interaction with successive deposition of various strains or species, or other spatially important properties such as bacterial appendages, which can be unidentifiable in a monolayer of cells. Polymannose was also found to direct the surface coverage of *Vibrio cholerae* (**Figure 4-15**). A different pattern of polymannose interspersed with (11-mercaptoundecyl)hexa(ethylene glycol) was used with *V. cholerae*.

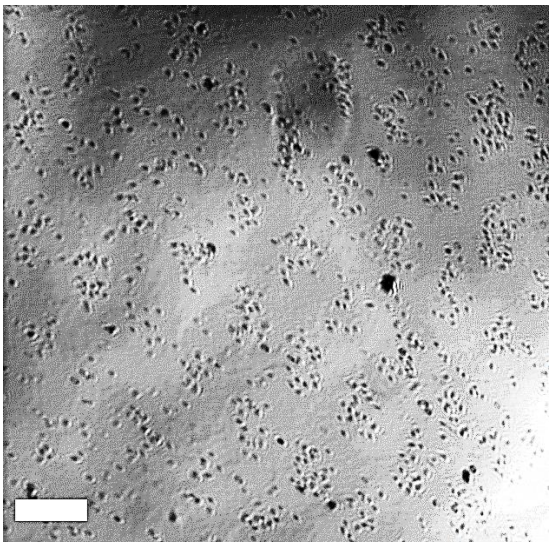

Figure 4-15. Cellular pattern of *Vibrio cholerae* directed by polymannose and ethylene glycol-terminated spacer molecules. Imaged with reflection mode of optical microscope. Scale bar is 20 μm.

4.3 CONCLUSIONS

We synthesized glycopolymers presenting branching monosaccharide units and assembled them onto gold surfaces to influence the surface colonization by the bacteria *Shewanella oneidensis.* The poly(mannose acrylate) glycopolymer promoted adhesion of 12.1 ± 2.3% (SEM) more cells versus bare gold surfaces. When the wild-type strain was

co-deposited with a Δ*mshA-D* knockout strain, the fraction of cells that contained the *mshA-D* genes was increased by 5.4 ± 2.4% (SEM). This enhancement indicates the strain selectivity of the surface and the importance of mannose-sensitive hemagglutinin pili's MshA lectin.

The persistence of the cellular attachment was investigated by rinsing the adhered cells with methyl α-D-mannopyranoside, an inhibitor of binding to the MSH attachment pili. Following the rinses with methyl α-D-mannopyranoside, the glycopolymer samples presented the smallest decrease of attached cells suggesting stable colonization (The decrease in total fluorescence was 4.2 ± 1.6% (SEM) for polymannose surfaces and 2.2 ± 2.5% (SEM) for polygalactose surfaces versus 18.1 ± 5.8% (SEM) for tethered mannose monomers and 7.3 ± 2.9% (SEM) for bare gold surfaces). By adding the inhibitor before surface exposure, the specific adhesiveness of polymannose is removed relative to polygalactose and bare gold surfaces. This result indicates that mannose-specific binding is the driving factor for the augmented *S. oneidensis* attachment to polymannose surfaces. The retention of cells adhering to polymannose in the presence of methyl α-D-mannopyranoside appears to be a kinetic effect, as the inhibitor must be concurrently incubated for several hours to equalize the samples. The three-dimensional multivalency of glycopolymer samples appears to be responsible for the enhanced adhesiveness because tethered mannose monomer surfaces do not retain as many cells upon inhibition of surface binding. The ability to pattern *S. oneidensis* on polymannose surfaces was also demonstrated in this work.

Using the glycopolymer surfaces, we have driven bacterial colonization, enriched one strain of the bacteria against another, and induced where bacteria attach. These capabilities enable new experimental design and technological innovation. Rational design of bioelectrical technologies is reliant on surface-colonizing microbes. Our model system targets bioelectrical

systems by using the metal-reducing *S. oneidensis* as the microbes and conductive, non-oxide forming gold as the solid surfaces. Generally, our findings that a poly(monosaccharide acrylate) functionalized surface can produce stable initial attachment, and that saccharide lectin pairs are promising for biofilm customization, can be applied to other types of beneficial or benign microbes.

4.4 PROSPECTS

Glycopolymers presenting a monosaccharide on each of their side chains are described in this chapter. These saccharides conserve hydroxyl groups by binding only with the anomeric carbon and thus preserve known monosaccharide recognition by bacteria. Further work could incorporate oligosaccharide units branching off of the polymeric support. Such oligosaccharides can be homooligosaccharide units utilizing the same saccharides or heterooligosaccharides using combinations of different saccharide types. As the trisaccharide motif has been found to increase *E. coli* binding significantly, other oligosaccharide configurations may offer substantial avidity and specificity for targeted microbes.[6] Psl is a polysaccharide used in bacterial surface sensing that may be worth emulating.[2] By multiplexing the design space of saccharide presenting surfaces we expect high specificity for chosen microbial targets.

The time dependence of bacterial attachment and growth dynamics should also be investigated. The kinetic nature of the resistance to methyl α-D-mannopyranoside inhibition by the glycopolymers studied here emphasizes the importance of cellular attachment and detachment rates. Studying the strength of equilibrium binding alone misses the dynamic features of microbial surface colonization. Real-time measurements are necessary to compare the dynamics of various surface types being colonized. Moreover, studies that measure only initial

and final timepoints have their conclusions limited by the convolution of cellular growth, death, attachment, and detachment. By separating the rates of each of these processes, mechanistic principles are derivable. The scope of polymannose's influence over the longer time course of mature biofilm formation can be determined, as well as the duration and optimal time of attachment influence. Flow cell studies could also investigate variation spatially and track individual cell lineages.

Interfacing microbial metabolism with solid-state devices requires association of microbes with solid surfaces and transfer of electrons through these junctions. In applying extracellular electron transport to create microbial bioelectrical systems, the improved adhesive qualities of the glycopolymer layer are balanced against the electrical conductivity of the material. Mannose-decorated polymers with a conductive backbone, such as polyaniline or poly(3,4-ethylenedioxythiophene) polystyrene sulfonate (PEDOT:PSS), could be synthesized to optimize both conductivity and adhesiveness of the biofilm-electrode interface. Different types of polymer layers, with varying molecular lengths and surface densities, should be investigated for the trade-off in interfacial electrical conductivity versus increased attachment and cellular meshing with the surface. This trade-off can be measured by the current output of a microbial fuel cell, where anodes functionalized with various mannosylated glycopolymer films are compared to unfunctionalized surfaces and tethered mannose monomers. The impact of adulterants in culture supernatant on the surface's conductivity over time should also be tested. Alternatively, conductivity can be increased by enabling electron transport around glycopolymer molecules rather than through them. Engineering the polymer layer to have submonolayer coverage and expose conductive patches of the substrate is one way to encourage cellular interaction without obscuring electron transport.

The cellular patterns described here demonstrate the directing capability of the polymer layer and can be used as a tool for further experimentation. When one cell type is spatially patterned and another cell type is placed next to it, interactions between cells, such as intercellular communication, can be observed. Measurement of nanoscale features, especially with surface-sensitive techniques, is facilitated with reproducible, well-defined colonization; nanoscopic features in microbial communities can be buried or hidden in clusters of cells. The cellular interactions with boundaries of surface types may also be observed on the chemically patterned surface.

The fidelity of the bacterial pattern on the molecular pattern may be further improved by investigating rinsing techniques. As rinsing is the mechanism used to remove cells in the undesired areas, it is an important parameter to understand. Improvements to bacterial patterning are also expected if the adhesiveness of the glycopolymer is improved as suggested above. Providing a more nutritious application medium and time for the attached cells to divide may increase the cell packing density on the desired areas.

The colonization enhancement of wild-type *S. oneidensis* and the enrichment against the *ΔmshA-D* knockout strain suggest the possibility of designing a system to enrich *S. oneidensis* versus any other microbe that does not express mannose recognition. Enrichment enhances utilization of strains in mixed populations of microbes, where a desired strain might be excluded or have reduced presence against faster surface colonizers. If a polymannose surface can enrich *S. oneidensis* against other endemic microbes in its native environment, then a more electroactive biofilm may be produced by amplifying the proportion of the key species. The scope of the ability to enrich a desired strain, species, or functionally active population from other types of cells should be explored. To examine the ability of the glycopolymer surfaces to select a species

of interest, *S. oneidensis* colonization should be tested against a fast biofilm-forming species that binds to surfaces by a method that does not use mannose. Selection of a deletable gene with glycopolymers could be expanded with synthetic genetic sequences that express a saccharide receptor alongside useful genes, thus amplifying genes of interest in an area with the corresponding saccharide. The *mshA* gene could act as a reporter if another gene of interest was expressed proximally on the genome or on a plasmid. In general, controlling colonization enables modulation of consortia of microbes to create designer microbiomes for uses such as biosynthesis or medical treatment.

Many biotechnologies and further studies may be designed using saccharides to colonize surfaces selectively with microbial strains of choice. Besides promoting functional or useful genes in the genome of a biofilm, promoting benign microbes could prevent pathogens or otherwise deleterious microbes from attaching to a surface. The process of benign fouling of a surface could be a useful general strategy addressable by glycopolymer functionalization.

4.5 MATERIALS AND METHODS

Materials

D-Glucose (ACROS, ACS grade), D-galactose (Fisher, off white to white powder), D-mannose (Amresco, high purity grade), D-glucosamine hydrochloride (ACROS, 98+%), acetic anhydride (Fisher, ACS grade), boron trifluoride etherate (ACROS, 48%), trimethylsilyl trifluoromethanesulfonate (ACROS, 99%), trifluoromethanesulfonic acid (ACROS, 99%), hydrochloric acid (Fisher, ACS grade), phenylmagnesium bromide in 2-methyltetrahydrofuran (Strem, Chemicals, 2.9M), carbon disulfide (Fisher, ACS grade), sodium acetate trihydrate (Fisher, ACS grade), 4-dimethylaminopyridine (DMAP) (Alfa Aesar, 99%), triethylamine (Alfa

Aesar, 99%), sodium bicarbonate (Fisher, USP/FCC), sodium methoxide in methanol (ACROS, 5.4 M), iodine (ACROS, resublimed), methanol (EMD DriSolv, 99.8%), ethanol (Decon Labs, 200 proof), diethyl ether (Macron Chemicals, ACS grade), tetrahydrofuran (Fisher, HPLC), dichloroethane (ACROS, ACS grade), dimethyl sulfoxide (Fisher, ACS grade), ethyl acetate (Fisher, ACS grade), hexanes (Fisher, ACS grade), DOWEX 50WX8 ion-exchange resin (ACROS, 200-400 mesh) 2-(2-[2-(11-mercaptoundecyloxy)-ethoxy]-ethoxy)-ethoxy-acetic acid (Toronto Research Chemicals), 2-(2-[2-(11-mercaptoundecyloxy)-ethoxy]-ethoxy)-ethanol (Toronto Research Chemicals), 4-aminophenyl-α-D-mannopyranoside (LC scientific, 98%), trifluoroacetic acid (Sigma-Aldrich, 99%), *N*-hydroxysuccinimide (Aldrich, 98%), 1-ethyl-3-(3-dimethylaminopropyl) carbodiimide (Sigma Aldrich, commercial grade), ethanolamine (Sigma, 98%), and phosphate-buffered saline (Fisher) were used as received.

4,4'-Azobis(4-cyanovaleric acid) (ACVA) (Pfaltz & Bauer, 98%) was recrystallized from methanol.

Hydroxyethyl acrylate (HEA) (Sigma-Aldrich, 96%), dichloromethane (Fisher, ACS grade), pyridine (JT Baker, ACS grade), and water (Fisher, HPLC) were distilled for polymer synthesis procedures. Water for surface assembly and bacterial experiments was deionized (18.2 MΩ cm) using a Milli-Q system (Millipore, Billerica, Massachusetts, USA).

Saccharide Acrylate Monomer Syntheses

2-O-(α-D-Mannosyl)hydroxyethyl acrylate

1,2,3,4,6-Pentaacetyl-α,β-D-mannose: Acetic anhydride (50 mL, 0.53 mol) was added to a solution of D-mannose (10 g, 55 mmol) dissolved in pyridine (100 mL) and stirred for 24 h. The solution was concentrated *in vacuo* and added to cold deionized (DI) water. The product was

taken up in dichloromethane (DCM) and washed with a saturated sodium bicarbonate solution (2×), washed with brine, dried with sodium sulfate, and concentrated *in vacuo* (12.7 g, 59%). ^{1}H NMR (300 MHz, $CDCl_3$): δ6.10 (d, H-1α), 5.89 (d, H-1β), 5.10-5.50 (m, H-2,3,4), 3.71- 4.30 (m, H-5α, H2-6), 3.83 (m, H-5β), 2.00-2.19 (s, 15H, 5 CH_3).

2-O-(2,3,4,6-Tetraacetyl-α-D-mannosyl)hydroxyethyl acrylate: Boron trifluoride etherate (2.7 mL, 21 mmol) was added dropwise to a stirring solution of 1,2,3,4,6-pentaacetyl-α,β-D-mannose (2.7 g, 6.9 mmol) and hydroxyethyl acrylate (1.0 mL, 8.7 mmol) dissolved in DCM (25 mL) cooled in an ice bath. The solution was allowed to warm to room temperature after the addition was completed and stirred for 96 h. The reaction was washed with DI water (3×), a saturated solution of sodium bicarbonate, and brine. The organic solution was dried with sodium sulfate, concentrated, and isolated by silica column chromatography using 11:9 ethyl acetate in hexanes as an eluent (1.5 g, 49%). ^{1}H NMR (300 MHz, $CDCl_3$): δ6.43 (d, 1H, CH_2═CH), 6.15 (m, CH_2═CH), 5.87 (d, 1H, CH_2═CH), 5.20-5.40 (m, H-2,3,4), 4.87 (d, H-1), 4.34 (m, 2H, OCH_2CH_2OC═O), 4.03-4.27 (m, 3H, H-5, H2-6), 3.78-3.90 (m, 2H, OCH_2CH_2OC═O), 1.99-2.17 (s, 12H, 4 CH_3).

2-O-(α-D-Mannosyl)hydroxyethyl acrylate: Sodium methoxide (1 mL, 0.2 M) was added to a solution of 2-O-(2,3,4,6-tetraacetylα-D-mannosyl)hydroxyethyl acrylate (1.5 g, 3.4 mmol) dissolved in DCM (5 mL) and methanol (4 mL) and stirred for 3 min before quenching with DOWEX 50WX8 ion-exchange resin for 30 min. The glycomonomer was isolated by silica column chromatography using 2:8 methanol in DCM as an eluent (368 mg, 39%). ^{1}H NMR (300 MHz, MeOD): δ6.40 (d, 1H, C*H*$_2$═CH), 6.19 (m, CH_2═C*H*), 5.90 (d, 1H, C*H*$_2$═CH), 4.80 (d, H-1), 4.34 (m, 2H, OCH_2CH_2OC═O), 3.94 (m, 1H, OCH_2CH_2OC═O), 3.58- 3.81 (m, 7H, H-2,3,4,5, H2-6, OCH_2CH_2OC═O).

2-O-(β-D-Glucosyl)hydroxyethyl acrylate

1,2,3,4,6-Pentaacetyl-β-D-glucose: D-Glucose (6 g, 33 mmol) was added gradually to a solution of sodium acetate trihydrate (3 g, 22 mmol) dissolved in acetic anhydride (42 mL, 0.45 mol) previously heated at 140 °C for 20 min. The reaction was removed from heat after 15 min and allowed to cool to room temperature before gradually pouring into ice water and allowed to precipitate at 4 °C overnight. The solid was collected by vacuum filtration and recrystallized in ethanol (6.9 g, 53%). ^{1}H NMR (300 MHz, $CDCl_3$): δ5.73 (d, H-1), 5.10-5.30 (m, H-2,3,4), 4.10-4.30 (m, 2H, H2-6), 3.85 (m, H-5), 2.01-2.11 (s, 15H, 5 CH_3).

2-O-(2,3,4,6-Tetraacetyl-β-D-glucosyl)hydroxyethyl acrylate: Boron trifluoride etherate (2.7 mL, 21 mmol) was added dropwise to a stirring solution of 1,2,3,4,6-pentaacetyl-β-D-glucose (2.7 g, 7 mmol) and hydroxyethyl acrylate (1.2 mL, 10.4 mmol) dissolved in DCM (25 mL) cooled in an ice bath. The solution was allowed to warm to room temperature after the addition was completed and stirred for 16 h. The reaction was washed with DI water (2×), a saturated solution of sodium bicarbonate (2×), and brine. The organic solution was dried with sodium sulfate, concentrated, and isolated by silica column chromatography using 1:1 ethyl acetate in hexanes as an eluent (1.7 g, 55%). ^{1}H NMR (300 MHz, $CDCl_3$): δ6.42 (d, 1H, CH_2═CH), 6.11 (m, CH_2═CH), 5.85 (d, 1H, CH_2═CH), 5.00-5.20 (m, H-2,3,4), 4.55 (d, H-1), 4.10-4.30 (m, 4H, H2-6, OCH_2CH_2OC═O), 4.01 (m, 1H, OCH_2CH_2OC═O), 3.80 (m, 1H, OCH_2CH_2OC═O), 3.70 (m, H-5), 2.00-2.10 (s, 12H, 4 CH_3).

2-O-(β-D-Glucosyl)hydroxyethyl acrylate: Sodium methoxide (2 mL, 0.2 M) was added to a solution of 2-O-(2,3,4,6-tetraacetyl-β-D-glucosyl)hydroxyethyl acrylate (1.7 g, 4 mmol) dissolved in DCM (8 mL) and methanol (10 mL) and stirred for 7 min before quenching with DOWEX 50WX8 ion-exchange resin for 30 min. The glycomonomer was isolated by silica

column chromatography using 2:8 methanol in DCM as an eluent (207 mg, 20%). ^{1}H NMR (300 MHz, MeOD): δ6.42 (d, 1H, CH_2═CH), 6.19 (m, CH_2═CH), 5.91 (d, 1H, CH_2═CH), 4.35 (m, 3H, H-1, OCH_2CH_2OC═O), 4.12 (m, 1H, OCH_2CH_2OC═O), 3.88 (m, 2H, H2-6, OCH_2CH_2OC═O), 3.69 (dd, 1H, H2-6), 3.31 (m, H-3,4,5), 3.19 (t, H-2).

N-acetylglucosamine acrylate monomer

2-Acetamido-1,3,4,6-tetraacetyl-2-deoxy-α-D-glucose: Acetic anhydride (47 mL, 0.5 mol) was added to a solution of D-glucosamine hydrochloride (10 g, 46 mmol) and 4-dimethylaminopyridine (10 mg) dissolved in pyridine (50 mL) and stirred for 72 h. The reaction was chilled in an ice bath and sodium bicarbonate was gradually added until no gas evolved. The product was extracted with ethyl acetate, washed with brine, concentrated *in vacuo*, and crystallized with ethanol (15 g, 84%). ^{1}H NMR (300 MHz, $CDCl_3$): δ6.18 (d, H-1), 5.61 (d, H-4), 5.24 (m, H-2,3), 4.52 (m, -NH), 4.27 (dd, 1H, H2-6), 4.09 (dd, 1H, H2-6), 4.02 (m, H-5), 1.95-2.21 (s, 15H, 5 CH_3).

2-Methyl-2-(3,4,6-triacetyl-1,2-dideoxy-α-D-glucosyl)-[2,1-d]-2-oxazoline: Trimethylsilyl trifluoromethanesulfonate (1 mL, 5.5 mmol) was added to a solution of 2-acetamido-1,3,4,6-tetraacetyl-2-deoxy-α-D-glucose (2.0 g, 5.1 mmol) dissolved in dichloroethane (9 mL) and heated at 50 °C for 21 h before quenching with triethylamine (1 mL). The reaction was washed with DI water (4×) and dried with sodium sulfate. The product was isolated by silica column chromatography using 9:1 ethyl acetate in hexanes as an eluent (1.5 g, 88%). ^{1}H NMR (300 MHz, $CDCl_3$): δ5.94 (d, H-1), 5.24 (t, H-3), 4.91 (d, H-4), 4.16 (m, H-5, H2-6), 3.60 (m, H-2), 2.07 (s, 12H, 4 CH_3).

2-O-(2-Acetamido-3,4,6-triacetyl-2-deoxy-β-D-glucosyl)hydroxyethyl acrylate: Trifluoromethanesulfonic acid (25 µL, 0.3 mmol) was added to a solution of 2-methyl-2-(3,4,6-triacetyl-1,2-dideoxy-α-D-glucosyl)-[2,1-d]-2-oxazoline (1.0 g, 3 mmol) and hydroxyethyl acrylate (0.54 mL, 4.7 mmol) dissolved in dichloroethane (8.3 mL) and heated at 60 °C for 6 h before quenching with triethylamine and diluting with DCM. The reaction was washed with DI water (2×), washed with brine, dried with sodium sulfate, and crystallized from diethyl ether (1.0 g, 75%). ^{1}H NMR (300 MHz, $CDCl_3$): δ6.44 (d, 1H, CH_2═CH), 6.14 (m, CH_2═CH), 5.87 (d, 1H, CH_2═CH), 5.67 (d, H-4), 5.30 (t, H-2), 5.04 (t, H-3), 4.78 (d, H-1), 4.43 (m, -NH), 4.25 (m, 2H, OCH_2CH_2OC═O), 4.15 (dd, 1H, H2-6), 4.02 (m, 1H, OCH_2CH_2OC═O), 3.86 (m, 2H, H2-6, OCH_2CH_2OC═O), 1.91-2.08 (s, 12H, 4 CH_3).

2-O-(2-Acetamido-2-deoxy-β-D-glucosyl)hydroxyethyl acrylate: Sodium methoxide (1 mL, 0.2 M) was added to a solution of 2-O-(2-acetamido-3,4,6-triacetyl-2-deoxy-β-D-glucosyl)hydroxyethyl acrylate (511 mg, 1.1 mmol) dissolved in DCM (2.5 mL) and methanol (1.5 mL) and stirred for 1 min before quenching with DOWEX 50WX8 ion-exchange resin for 30 min. The glycomonomer was isolated by silica column chromatography using 2:8 methanol in DCM as an eluent (106 mg, 29%). ^{1}H NMR (300 MHz, MeOD): δ6.40 (d, 1H, CH_2═CH), 6.16 (m, CH_2═CH), 5.88 (d, 1H, CH_2═CH), 4.47 (d, H-1), 4.28 (m, 2H, OCH_2CH_2OC═O), 4.04 (m, 1H, OCH_2CH_2OC═O), 3.88(dd, 1H, H2-6), 3.78 (m, 1H, OCH_2CH_2OC═O), 3.65 (m, 3H, H-3,4, H2-6), 3.46 (t, H-2), 3.32 (m, H-5).

2-O-(β-D-Galactosyl)hydroxyethyl acrylate

1,2,3,4,6-Pentaacetyl-β-D-galactose: D-Galactose (20 g, 111 mmol) was added gradually to a solution of sodium acetate trihydrate (10 g, 74.5 mmol) dissolved in acetic anhydride (200 mL, 2.1 mol) previously heated at 120 °C for 30 min. The reaction was removed from heat after an

hour and allowed to cool to room temperature before gradually pouring into a solution of sodium bicarbonate. Additional sodium bicarbonate was added until no gas was produced upon addition. The solid was taken up in DCM and washed with saturated sodium bicarbonate (4×), DI water, and brine. The organic solution was dried with sodium sulfate, concentrated, and covered with diethyl ether at -20 °C. The white crystals were collected by vacuum filtration (24.84 g, 67%). ^{1}H NMR (300 MHz, $CDCl_3$): δ5.71 (d, H-1), 5.43 (d, H-4), 5.34 (dd, H-2), 5.09 (dd, H-3), 4.15 (m, 2H, H2-6), 4.05 (t, H-5), 2.00-2.17 (s, 15H, 5 CH_3).

2-O-(2,3,4,6-Tetraacetyl-β-D-galactosyl)hydroxyethyl acrylate: Boron trifluoride etherate (2.0 mL, 16 mmol) was added dropwise to a stirring solution of 1,2,3,4,6-pentaacetyl-β-D-galactose (2.0 g, 5.1 mmol) and hydroxyethyl acrylate (1.2 mL, 10.4 mmol) dissolved in DCM (25 mL) cooled in an ice bath. The solution was allowed to warm to room temperature after the addition was completed and stirred for 16 h. The reaction was washed with DI water (3×), a saturated solution of sodium bicarbonate, and brine. The organic solution was dried with sodium sulfate, concentrated, and isolated by silica column chromatography using 7:3 ethyl acetate in hexanes as an eluent (2.0 g, 87%). ^{1}H NMR (300 MHz, $CDCl_3$): δ6.44 (d, 1H, CH_2═CH), 6.13 (m, CH_2═CH), 5.87 (d, 1H, CH_2═CH), 5.39 (d, H-4), 5.21 (dd, H-2), 5.03 (dd, H-3), 4.54 (d, H-1), 4.32 (m, 2H, OCH_2CH_2OC═O), 4.15 (m, 3H, H2-6, OCH_2CH_2OC═O), 3.93 (t, H-5), 3.83 (m, 1H, OCH_2CH_2OC═O), 1.99–2.16 (s, 12H, 4 CH_3).

2-O-(β-D-Galactosyl)hydroxyethyl acrylate: Sodium methoxide (300 µL, 0.2 M) was added to a solution of 2-O-(2,3,4,6-tetraacetylβ-D-galactosyl)hydroxyethyl acrylate (2.0 g, 4.5 mmol) dissolved in methanol (20 mL) and stirred for 10 min before quenching with DOWEX 50WX8 ion-exchange resin for 30 min. The glycomonomer was isolated by silica column chromatography using 2:8 methanol in DCM as an eluent (357 mg, 29%). ^{1}H NMR (300 MHz,

MeOD): δ6.39 (d, 1H, CH_2═CH), 6.17 (m, CH_2═CH), 5.87 (d, 1H, CH_2═CH), 4.33 (m, 2H, OCH_2CH_2OC═O), 4.26 (d, H-1), 4.09 (m, 1H, OCH_2CH_2OC═O), 3.60- 3.80 (m, 4H, H-4, H2-6, OCH_2CH_2OC═O), 3.50 (m, H-2,3,5).

4-Cyano-4-(thiobenzoylthio)pentanoic Acid Chain-Transfer Agent Synthesis

Bis(thiobenzyl) disulfide (BTBD)

Carbon disulfide (5.25 mL, 87 mmol) was added dropwise to a phenylmagnesium bromide solution in 2-methyl tetrahydrofuran (30 mL, 2.9M) diluted with tetrahydrofuran (THF) (15 mL) at 0 °C and stirred under argon. The solution was stirred for 45 min and quenched by the addition of water dropwise. The THF was removed *in vacuo* and the solution was filtered. The product was extracted with DCM as hydrochloric acid was added until the aqueous layer was colorless. The organic layer was washed with brine (2×) and reduced to a red oil *in vacuo*. The oil was crystallized with ethanol (10 mL), dimethyl sulfoxide (2 mL), and catalytic amounts of crystalline iodine at 0 °C. The magenta crystals were filtered and washed with water (4.18 g, 31%). ^{1}H NMR (300 MHz, $CDCl_3$): δ7.40-8.10 (m, 10H, ϕ).

4-Cyano-4-(thiobenzoylthio)pentanoic acid

4,4'-azobis(4-cyanovaleric acid) (584 mg, 2.1 mmol) and bis(thiobenzyl) disulfide (425 mg, 1.4 mmol) were dissolved in distilled ethyl acetate (8 mL) and heated to 80 °C for 18 h. The product was isolated as a magenta solid by silica column chromatography using 1:1 ethyl acetate in hexanes as an eluent (470 mg, 60%). ^{1}H NMR (300 MHz, $CDC1_3$): δ7.40-8.00 (m, 5H, ϕ), 2.76 (m, C$H_2$$CH_2$COOH), 2.45-2.63 (m, CH_2CH_2COOH), 1.96 (s, CH_3).

Reversible Addition-Fragmentation Chain Transfer (RAFT) Polymerization

Representative polymerization of glycomonomer attached through a glycosidic bond

Glycomonomer (100 equivalents), 4-cyano-4-(thiobenzoylthio)pentanoic acid (1 equivalent), and 4,4'-azobis(4-cyanovaleric acid) (0.3 equivalents) were dissolved in a solution of water/ethanol (3:1). The solution was degassed by five freeze/pump/thaw cycles and heated at 70 °C for 18 h followed by quenching in liquid nitrogen and exposure to air. The reaction was diluted with water, and a sample was lyophilized to determine conversion by ^{1}H NMR. The remainder of the polymer solution was dialyzed in DI water over 16 h, changing the water every 2 h, and lyophilized. The resultant polymer was analyzed by ^{1}H NMR and GPC.

Poly(2-hydroxyethylacrylamide) synthesis

2-hydroxyethylacrylamide (Sigma-Aldrich, 97%, St. Louis, Missouri, USA) was used in place of the glycomonomer following the same procedure as above.

Synthetic Technique Details

Dialysis was conducted using a Spectra/Por® dialysis membrane (1000 Da) in DI water. Lyophilization was conducted on a Labconco FreeZone 4.5 freeze dryer. Gel permeation chromatography (GPC) was conducted on a Jasco system equipped with a UV detector, a refractive index detector, and four Waters ultrahydrogel columns (100-5K, 1K-80K, 10K-400K, 2K-4M, 500-10M) using 10 mM PBS with 0.3 M NaCl at pH 6.6 as an eluent at 30 °C and a flow rate of 1.0 mL/min calibrated using pullulan standards.

Poly(saccharide acrylate) Self-Assembly

An adhesion layer of 7.5 nm of titanium, followed by 75 nm of gold, were evaporated onto a black polystyrene 96-well microtiter plate or a silicon wafer. Wafer pieces were annealed for 1 min with a hydrogen flame before self-assembly. Well plates were visually inspected and wells that were not fully covered by gold were excluded from the sample. Glycopolymers were dissolved in water at a concentration of 3 mg/mL. 100 µL of ethanolamine added for each 1 mL of water to the glycopolymer solution. The glycopolymers reacted with the ethanolamine for 30 min before aliquoting 250 µL of solution to each appropriate well on the microtiter plate or 1 mL or more, if applying to pieces of gold covered wafers. Self-assembly proceeded for 3 days at room temperature. The solution was removed, and the surfaces rinsed three times with ethanol followed by sterile 137 mM NaCl, 2.7 mM KCl, 10 mM Na_2HPO_4, 1.8 mM KH_2PO_4, (1×) pH 7.2 phosphate-buffered saline (PBS).

11-[(*p*-Phenyl-α-D-mannopyranosyl) aminocarbonyl methoxy hexa(ethoxy)]undec-1-yl-thiol, (Tethered Mannose Monomer), Assembly and Synthesis

Thiol solutions of 0.5 mM 2-(2-[2-(11-mercaptoundecyloxy)-ethoxy]-ethoxy)-ethoxy-acetic acid, 0.5 mM 2-(2-[2-(11-mercaptoundecyloxy)-ethoxy]-ethoxy)- ethanol, and 130 mM trifluoroacetic acid were mixed and added to the gold surfaces for 3 days. Samples removed from solution and rinsed with 10% (v/v) triethylamine in ethanol followed by neat ethanol. 0.05 M *N*-hydroxysuccinimide with 0.2 M 1-ethyl-3-(3-dimethylaminopropyl)carbodiimide in water were added to the surfaces for 30 min. The samples were rinsed with water, nitrogen dried, and added to 2 mg/mL 4-aminophenyl-α-D-mannopyranoside in aqueous 25 mM pH 8.0 sodium phosphate for 2 days. Samples were removed from solution, rinsed with water, ethanol, then either dried by nitrogen stream or rinsed with sterile PBS.

Ellipsometry

Ellipsometry was measured with a Gaertner LSE Stokes Ellipsometer (Gaertner Scientific Corporation, Skokie, Illinois, USA). A 632.8 nm HeNe laser was used at a 70° incidence angle. Each glycopolymer was self-assembled on 100-nm-thick Au substrates produced by electron-beam evaporation.

Electrochemical Desorption

A BASi Epsilon potentiostat (Bioanalytical Systems Inc., West Lafayette, Indiana, USA) was used to measure the current during electrochemical desorption. The voltage was swept from 0 to -1200 mV with a Ag/AgCl reference electrode at a scan rate of 50 mV/s. Pt was used as the counter electrode in a 0.5 M KOH electrolyte solution. A 1/8-inch inner diameter O-ring was used to define the effective surface area of the analyte.

Contact Angle

A FTA1000 Drop Shape Instrument (First Ten Angstroms, Inc., Portsmouth, Virginia, USA) was used to record images of water droplets on the surfaces and calculate contact angles with the associated software. Water was applied the surfaces by a syringe. It was pumped in and out of the syringe repeatedly to determine receding and advancing contact angles, respectively.

Polarization Modulation-Infrared Reflection-Absorption Spectroscopy

A Nicolet 8700 FT-IR spectrometer, with Hinds Instruments PEM-100 photoelastic modulator, and MCTA detector (Thermo Scientific, Wilmington, Delaware, USA) was used for PM-IRRAS measurements. The sample chamber was purged with dry nitrogen gas before recording. Spectra were acquired over the range of 1000-3500 cm^{-1}. The PEM wavelength was set to 3100 cm^{-1}. Measurements were averaged over 2048 scans with a resolution of 2 cm^{-1}.

X-ray Photoelectron Spectroscopy

An AXIS Ultra DLD X-ray photoelectron spectrometer (Kratos Analytical Inc., Chestnut Ridge, New York, USA) was used for elemental surface analysis. This spectrometer uses a monochromatic Al K_α X-ray source, which has an energy of 1486.7 eV, with a 200 µm circular spot size and ultrahigh vacuum (10^{-9} Torr). Spectra were acquired at a pass energy of 160 eV for survey spectra and 20 eV for high-resolution spectra of C 1s, N 1s, O 1s, S 2p, and Au 4f regions using a 250 ms dwell time. The emission current was 10 mA and 20 mA for survey and high-resolution spectra, respectively. The applied electric potential was 15 kV for both scan types. Three scans were performed for survey and Au spectra, 10 scans for N, C, and O spectra, and 15 scans for S spectra.

Bacterial Growth

Lysogeny broth (LB) agar plates containing 50 mg/L kanamycin were used for inoculating liquid cultures. Plates were streaked with *Shewanella oneidensis* MR-1 WT p519nGFP from -80 °C freezer and incubated for 24 h at 32 °C while shaking at 200 rpm. Stored at 4 °C. *S. oneidensis* was precultured by inoculating 20 mL of LB medium in a 125 mL flask and incubating at 32 °C for 24 h shaking at 200 rpm. 1 mL of the preculture solutions were diluted into 20 mL of in LB

with 50 mg/L kanamycin. The cultures were incubated until the optical density at 600 nm reached 0.9 typically after about 2 h. The cells were washed by spinning at 2300*g* in a centrifuge for 5 min then resuspending in PBS. Cells were then spun down and resuspended two more times. The resuspended solutions were diluted 10-fold into PBS and applied to the surface of interest. *S. oneidensis* Δ*msh*A-D was cultured under the same conditions without kanamycin.

Microtiter Plate Fluorescence Measurements

Diluted *S. oneidensis* MR-1 WT p519nGFP culture, 250 µL, was aliquoted into each appropriate sample well and incubated at 32 °C for 18 h. For measurement of adhesion without inhibitors, as presented in **Figure 4-9**, each well was rinsed 3 times with 250 µL of PBS and imaged with a fourth addition of 50 µl of PBS.

A Synergy H1 microplate reader was used for surface fluorescent measurements. The excitation was set for 470 nm and the emission for 507 nm. The gain was set to 100. A xenon flashlamp was used as a light source with a 100-ms delay. Ten measurements were used per data point per sample. The read height was 7 mm.

For the experiments measuring the susceptibility of adhered cells to rinses of methyl α-D-mannopyranoside, as shown in **Figure 4-10**, the cell culture was prepared and incubated on the surfaces as described above. Then, the culture solution was removed and replaced with 250 µL 200 mM methyl α-D-mannopyranoside in PBS. The solution was left in the wells as the fluorescence was measured as described above. This measurement constitutes the baseline rinse. The methyl α-D-mannopyranoside solution was incubated on the adhered cells for 5 h before being removed and replaced with another 250 µL of 200 mM methyl α-D-mannopyranoside in PBS. Fluorescence was measured again and recorded as the final rinse.

For the experiments measuring the influence of concurrent incubation with methyl α-D-mannopyranoside, as shown in **Figure 4-11**, the cell culture was again prepared as described above. Before adding the cells to the surfaces 200 mM methyl α-D-mannopyranoside in PBS was added to the appropriate samples to produce a final concentration of 180 mM. Control samples were prepared alongside the methyl α-D-mannopyranoside incubated samples from the same culture and incubated at the same time in PBS. These samples were incubated in their respective solutions for 18 h, as done for the other experiments. The samples were then rinsed 1 time with 250 µL of PBS for all samples and the fluorescence was recorded as above.

Unpaired t-test used for statistical comparison of the samples.

Co-Culture Competition Experiment

For the mixed strain experiments shown in **Figure 4-12**, cultures of both *S. oneidensis* MR-1 WT p519nGFP and *S. oneidensis* Δ*msh*A-D were grown and resuspended in PBS as described above. Due to differing growth rates the optical density of the initial cell cultures was not grown to 0.9. Instead, both strains were incubated for a fixed time of 2.5 h. The two strains were mixed together and diluted before adding to the surfaces of interest. The volumes of each strain added were adjusted based on optical density to have the same number of cells of each type added to the surfaces. The samples were incubated at 32 °C for 18 h with shaking at 200 rpm. The surfaces were then mounted on a glass coverslip and imaged by optical microscopy.

Unpaired t-test were used for statistical comparison of the samples.

Glycopolymer Patterning

The surface shown in **Figure 4-14** was produced by photolithography. Silicon wafers covered with 100 nm of gold and a titanium adhesion layer were annealed by a hydrogen flame for 1 min. AZ nLOF 2020 negative tone photoresist was used to pattern a series of 2 μm lines with a periodicity of 10 μm on the wafers as follows. Wafers were baked at 150 °C for 10 min to dehydrate. They were then exposed to hexamethyldisilazane vapors for 15 min. Photoresist was spin-coated at 500 rpm for 5 s then 3000 rpm for 30 s. Wafers were then soft baked for 1 min at 110 °C. Total exposure on Karl Suss contact aligner was 60 mJ. Post exposure bake was performed for 1 min at 110 °C. Finally, the surfaces were descummed with oxygen plasma at 100 °C for 3 min.

Glycopolymers were self-assembled on the patterned surface as described above for gold coated wafer pieces. After removing the glycopolymer solution the samples were rinsed with water and dried with nitrogen. The photoresist was removed by placing the sample in Baker PRS-3000 photoresist stripper composed of approximately 50% 1-methyl-2-pyrrolidinone, 40% tetrahydrothiophene 1,1-dioxide, and 1-amino-2-propanol. The samples were left in the photoresist stripper for 1 h with gentle heating then rinsed three times with water and dried with nitrogen. Poly(2-hydroxyethylacrylamide), 8 mg, was dissolved in 750 μL water, 200 μL ethanol and 50 μL ethanolamine and was added to the patterned glycopolymer surfaces for 19 h to backfill the gold areas previously covered by the photoresist before stripping. The samples were then rinsed with water and dried with nitrogen.

Application of Bacteria to Glycopolymer Patterns

The molecularly patterned glycopolymer pieces were rinsed with ethanol to sterilize and dried with nitrogen. 5 mL of diluted *S. oneidensis* MR-1 WT p519nGFP in PBS was added to each sample and incubated for 18 h at 32 °C. Cell culture solutions were removed and replaced with 5 mL of fresh PBS. Just before imaging by optical microscopy, the samples were rinsed with PBS and placed on a glass coverslip.

Optical Microscopy of *Shewanella oneidensis* Samples

An upright ZEISS LSM-800 confocal microscope (Carl Zeiss Microscopy, LLC, White Plains, New York, USA) was used for optical imaging of cells. Green fluorescent protein was excited at 488 nm. Brightfield was imaged with confocal reflection at 640 nm and detected at the same wavelength using a photomultiplier tube.

Patterning Polymannose by Microcontact Printing

The surface shown in **Figure 4-8** was prepared by microcontact printing. Polydimethylsiloxane (PDMS) stamps with formed on silicon masters with 10 μm square features. The stamps were soaked in hexane for 1 hour then removed. A PDMS stamp was submerged in a solution of 15 mg of poly(mannose acrylate), 48 μL of ethanolamine, and 8 mL of water and left overnight. The stamp was removed from solution, rinsed with water and ethanol, dried, and printed on a flame-annealed 100 nm thick gold surface adhered to a silicon substrate by a titanium adhesion layer. A 38 g weight was placed on the stamp and allowed to sit for 2 h. The stamp was removed from the gold sample.

Atomic Force Microscopy

The microcontact printed polymannose sample was scanned with a Dimension Icon atomic force microscope (Bruker, Billerica, Massachusetts, USA) using ScanAsyst-Air probes (Bruker, Billerica, Massachusetts, USA). Peak force tapping mode was used.

Patterning and Optical Microscopy of *Vibrio cholerae* samples

The pattern of *V. cholerae* cells shown in **Figure 4-15** was produced as follows. A gold coated silicon wafer was flame annealed and printed with a PDMS stamp that had been soaking in 1 mM (11-mercaptoundecyl)hexa(ethylene glycol) in ethanol overnight. The stamp was rinsed with ethanol and dried with nitrogen. Printing was established by conformal contact for 10 min. 16 mg of polymannose was dissolved in 8 mL millipore water. 200 μL of ethanolamine was added to the polymannose solution. The sample patterned with (11-mercaptoundecyl)hexa(ethylene glycol) was added to the polymannose solution and removed after 7.5 days. The sample was rinsed three times with water then dried with nitrogen.

V. cholerae O1 El Tor A1552 was grown in LB with a culture tube at 32 °C while shaking at 200 rpm for 18 h. The culture was used to inoculate a new culture in 2 mL of 2% LB in water (final concentration 0.2 g/L tryptone, 0.1 g/L yeast extract, 10 g/L NaCl). The chemically patterned surface was added to the new culture at the start of incubation at 32 °C with 200 rpm shaking. After 21 h the surface was removed from solution. The sample was imaged with a Leica TCS-SP5 AOBS confocal microscope (Leica Microsystems, Wetzlar, Germany). Laser excitation at 405 nm was used and reflection was recorded over the same wavelength using a photomultiplier tube.

4.6 REFERENCES

1. Thomas, W. Catch bonds in adhesion. *Annual Review of Biomedical Engineering* **2008,** *10*, 39–57.

2. Gelimson, A.; Zhao, K.; Lee, C. K.; Kranz, W. T.; Wong, G. C. L.; Golestanian, R. Multicellular self-organization of *P. aeruginosa* due to interactions with secreted trails. *Physical Review Letters* **2016,** *117*, 178102.

3. O'Toole, G. A.; Wong, G. C. L. Sensational biofilms: Surface sensing in bacteria. *Current Opinion in Microbiology* **2016,** *30*, 139–146.

4. Ma, L.; Lu, H.; Sprinkle, A.; Parsek, M. R.; Wozniak, D. J. *Pseudomonas aeruginosa* Psl is a galactose- and mannose-rich exopolysaccharide. *Journal of Bacteriology* **2007,** *189*, 8353–8356.

5. Berne, C.; Ducret, A.; Hardy, G. G.; Brun, Y. V. Adhesins involved in attachment to abiotic surfaces by Gram-negative bacteria. *Microbiology Spectrum* **2015,** *3*, 10.1128/microbiolspec.MB–0018–2015.

6. Firon, N.; Ofek, I.; Sharon, N. Carbohydrate-binding sites of the mannose-specific fimbrial lectins of enterobacteria. *Infection and Immunity* **1984,** *43*, 1088–1090.

7. Busch, A.; Waksman, G. Chaperone-usher pathways: Diversity and pilus assembly mechanism. *Philosophical Transactions of the Royal Society B* **2012,** *367*, 1112–1122.

8. Eshdat, Y.; Ofek, I.; Yashouv-Gan, Y.; Sharon, N.; Mirelman, D. Isolation of a mannose-specific lectin from *Escherichia coli* and its role in the adherence of the bacteria to epithelial cells. *Biochemical and Biophysical Research Communications* **1978,** *85*, 1551–1559.

9. Evans, D. J., Jr.; Evans, D. G.; Young, L. S.; Pitt, J. Hemagglutination typing of *Escherichia coli*: Definition of seven hemagglutination types. *Journal of Clinical Microbiology* **1980,** *12*, 235–242.

10. Qian, X.; Metallo, S. J.; Choi, I. S.; Wu, H.; Liang, M. N.; Whitesides, G. M. Arrays of self-assembled monolayers for studying inhibition of bacterial adhesion. *Analytical Chemistry* **2002,** *74*, 1805–1810.

11. Fasting, C.; Schalley, C. A.; Weber, M.; Seitz, O.; Hecht, S.; Koksch, B.; Dernedde, J.; Graf, C.; Knapp, E.-W.; Haag, R. Multivalency as a chemical organization and action principle. *Angewandte Chemie International Edition* **2012,** *51*, 10472–10498.

12. Lundquist, J. J.; Toone, E. J. The cluster glycoside effect. *Chemical Reviews* **2002,** *102*, 555–578.

13. Sisu, C.; Baron, A. J.; Branderhorst, H. M.; Connell, S. D.; Weijers, C. A. G. M.; de Vries, R.; Hayes, E. D.; Pukin, A. V.; Gilbert, M.; Pieters, R. J.; Zuilhof, H.; Visser, G.

M.; Turnbull, W. B. The influence of ligand valency on aggregation mechanisms for inhibiting bacterial toxins. *ChemBioChem* **2009,** *10*, 329–337.

14. Munoz, E. M.; Correa, J.; Riguera, R.; Fernandez-Megia, E. Real-time evaluation of binding mechanisms in multivalent interactions: A surface plasmon resonance kinetic approach. *Journal of the American Chemical Society* **2013,** *135*, 5966–5969.

15. Barth, K. A.; Coullerez, G.; Nilsson, L. M.; Castelli, R.; Seeberger, P. H.; Vogel, V.; Textor, M. An engineered mannoside presenting platform: *Escherichia coli* adhesion under static and dynamic conditions. *Advanced Functional Materials* **2008,** *18*, 1459–1469.

16. Zhu, X. Y.; Holtz, B.; Wang, Y.; Wang, L.-X.; Orndorff, P. E.; Guo, A. Quantitative glycomics from fluidic glycan microarrays. *Journal of the American Chemical Society* **2009,** *131*, 13646–13650.

17. Song, W.; Xiao, C.; Cui, L.; Tang, Z.; Zhuang, X.; Chen, X. Facile construction of functional biosurface via SI-ATRP and "click glycosylation". *Colloids and Surfaces B: Biointerfaces* **2012,** *93*, 188–194.

18. Yu, L.; Hou, Y.; Cheng, C.; Schlaich, C.; Noeske, P.-L. M.; Wei, Q.; Haag, R. High-antifouling polymer brush coatings on nonpolar surfaces *via* adsorption-cross-linking strategy. *ACS Applied Materials & Interfaces* **2017,** *9*, 44281–44292.

19. Saville, R. M.; Dieckmann, N.; Spormann, A. M. Spatiotemporal activity of the *mshA* gene system in *Shewanella oneidensis* MR-1 biofilms. *FEMS Microbiology Letters* **2010,** *308*, 76–83.

20. Utada, A. S.; Bennett, R. R.; Fong, J. C. N.; Gibiansky, M. L.; Yildiz, F. H.; Golestanian, R.; Wong, G. C. L. *Vibrio cholerae* use pili and flagella synergistically to effect motility switching and conditional surface attachment. *Nature Communications* **2014,** *5*.

21. Marsh, J. W.; Taylor, R. K. Genetic and transcriptional analyses of the *Vibrio cholerae* mannose-sensitive hemagglutinin type 4 pilus gene locus. *Journal of Bacteriology* **1999,** *181*, 1110–1117.

22. Watnick, P. I.; Fullner, K. J.; Kolter, R. A role for the mannose-sensitive hemagglutinin in biofilm formation by *Vibrio cholerae* El Tor. *Journal of Bacteriology* **1999,** *181*, 3606–3609.

23. Dalisay, D. S.; Webb, J. S.; Scheffel, A.; Svenson, C.; James, S.; Holmstrom, C.; Egan, S.; Kjelleberg, S. A mannose-sensitive haemagglutinin (MSHA)-like pilus promotes attachment of *Pseudoalteromonas tunicata* cells to the surface of the green alga *Ulva australis*. *Microbiology* **2006,** *152*, 2875–2883.

24. Boyd, J. M.; Dacanay, A.; Knickle, L. C.; Touhami, A.; Brown, L. L.; Jericho, M. H.; Johnson, S. C.; Reith, M. Contribution of type iv pili to the virulence of *Aeromonas*

salmonicida subsp. *salmonicida* in atlantic salmon (*Salmo salar* L.). *Infection and Immunity* **2008,** *76*, 1445–1455.

25. Jones, C. J.; Utada, A.; Davis, K. R.; Thongsomboon, W.; Zamorano Sanchez, D.; Banakar, V.; Cegelski, L.; Wong, G. C. L.; Yildiz, F. H. C-di-GMP regulates motile to sessile transition by modulating MshA pili biogenesis and near-surface motility Behavior in *Vibrio Cholerae*. *PLoS Pathogens* **2015,** *11*, e1005068.

26. Liau, W. T.; Bonduelle, C.; Brochet, M.; Lecommandoux, S.; Kasko, A. M. Synthesis, characterization, and biological interaction of glyconanoparticles with controlled branching. *Biomacromolecules* **2015,** *16*, 284–294.

27. Fais, M.; Karamanska, R.; Allman, S.; Fairhurst, S. A.; Innocenti, P.; Fairbanks, A. J.; Donohoe, T. J.; Davis, B. G.; Russell, D. A.; Field, R. A. Surface plasmon resonance imaging of glycoarrays identifies novel and unnatural carbohydrate-based ligands for potential ricin sensor development. *Chemical Science* **2011,** *2*, 1952–1959.

28. Lowe, S.; O'Brien-Simpson, N. M.; Connal, L. A. Antibiofouling polymer interfaces: Poly(ethylene glycol) and other promising candidates. *Polymer Chemistry* **2015,** *6*, 198–212.

29. Zheng, X.; Zhang, C.; Bai, L.; Liu, S.; Tan, L.; Wang, Y. Antifouling property of monothiol-terminated bottle-brush poly(methylacrylic acid)-graft-poly(2-methyl-2-oxazoline) copolymer on gold surfaces. *Journal of Materials Chemistry B* **2015,** *3*, 1921–1930.

30. Biggs, C. I.; Walker, M.; Gibson, M. I. "Grafting to" of RAFTed responsive polymers to glass substrates by thiol–ene and critical comparison to thiol–gold coupling. *Biomacromolecules* **2016,** *17*, 2626–2633.

31. Weck, M.; Jackiw, J. J.; Rossi, R. R.; Weiss, P. S.; Grubbs, R. H. Ring-opening metathesis polymerization from surfaces. *Journal of the American Chemical Society* **1999,** *121*, 4088–4089.

32. Coullerez, G.; Gorodyska, G.; Reimhult, E.; Textor, M.; Grandin, H. M. Self-Assembled Multifunctional Polymers for Biointerfaces. In *Functional Polymer Films*; Knoll, W., Advincula, R. C., Eds.; Wiley-VCH Verlag GmbH & Co. KgaA: Weinheim, Germany, 2011; Vol. 2, pp 859–863.

33. Wang, Y.; Narain, R.; Liu, Y. Study of bacterial adhesion on different glycopolymer surfaces by quartz crystal microbalance with dissipation. *Langmuir* **2014,** *30*, 7377–7387.

34. Chiefari, J.; Chong, Y. K.; Ercole, F.; Krstina, J.; Jeffery, J.; Le, T. P. T.; Mayadunne, R. T. A.; Meijs, G. F.; Moad, C. L.; Moad, G.; Rizzardo, E.; Thang, S. H. Living free-radical polymerization by reversible addition−fragmentation chain transfer: The RAFT process. *Macromolecules* **1998,** *31*, 5559–5562.

35. Kane, A. L.; Bond, D. R.; Gralnick, J. A. Electrochemical analysis of *Shewanella oneidensis* engineered to bind gold electrodes. *ACS Synthetic Biology* **2013,** *2*, 93–101.

36. Dumas, C.; Basseguy, R.; Bergel, A. Electrochemical activity of *Geobacter sulfurreducens* biofilms on stainless steel anodes. *Electrochimica Acta* **2008,** *53*, 5235–5241.

37. Zhou, M.; Chi, M.; Luo, J.; He, H.; Jin, T. An overview of electrode materials in microbial fuel cells. *Journal of Power Sources* **2011,** *196*, 4427–4435.

38. He, Y.-R.; Xiao, X.; Li, W.-W.; Sheng, G.-P.; Yan, F.-F.; Yu, H.-Q.; Yuan, H.; Wu, L.-J. Enhanced electricity production from microbial fuel cells with plasma-modified carbon paper anode. *Physical Chemistry Chemical Physics* **2012,** *14*, 9966–9971.

39. Zhang, T.; Nie, H.; Bain, T. S.; Lu, H.; Cui, M.; Snoeyenbos-West, O. L.; Franks, A. E.; Nevin, K. P.; Russell, T. P.; Lovley, D. R. Improved cathode materials for microbial electrosynthesis. *Energy & Environmental Science* **2013,** *6*, 217–224.

40. Baudler, A.; Schmidt, I.; Langner, M.; Greiner, A.; Schroder, U. Does it have to be carbon? Metal anodes in microbial fuel cells and related bioelectrochemical systems. *Energy & Environmental Science* **2015,** *8*, 2048–2055.

41. Aryal, N.; Ammam, F.; Patil, S. A.; Pant, D. An overview of cathode materials for microbial electrosynthesis of chemicals from carbon dioxide. *Green Chemistry* **2017,** *19*, 5748–5760.

42. Shuster, M. J.; Vaish, A.; Szapacs, M. E.; Anderson, M. E.; Weiss, P. S.; Andrews, A. M. Biospecific recognition of tethered small molecules diluted in self-assembled monolayers. *Advanced Materials* **2008,** *20*, 164–167.

43. Shuster, M. J.; Vaish, A.; Gilbert, M. L.; Martinez-Rivera, M.; Nezarati, R. M.; Weiss, P. S.; Andrews, A. M. Comparison of oligo(ethylene glycol)alkanethiols versus *n*-alkanethiols: Self-assembly, insertion, and functionalization. *The Journal of Physical Chemistry C* **2011,** *115*, 24778–24787.

44. Li, X.; Lin, J.; Qiu, Y. Influence of He/O_2 atmospheric pressure plasma jet treatment on subsequent wet desizing of polyacrylate on PET fabrics. *Applied Surface Science* **2012,** *258*, 2332–2338.

45. Yang, D. F.; Wilde, C. P.; Morin, M. Electrochemical desorption and adsorption of nonyl mercaptan at gold single crystal electrode surfaces. *Langmuir* **1996,** *12*, 6570–6577.

46. Levan, S.; De, S.; Olson, R. *Vibrio cholerae* cytolysin recognizes the heptasaccharide core of complex N-glycans with nanomolar affinity. *Journal of Molecular Biology* **2013,** *425*, 944–957.

47. Fong, J. N. C.; Yildiz, F. H. Biofilm matrix proteins. *Microbiology Spectrum* **2015,** *3*, 10.1128/microbiolspec.MB-0004-2014.

48. Teschler, J. K.; Zamorano-Sánchez, D.; Utada, A. S.; Warner, C. J. A.; Wong, G. C. L.; Linington, R. G.; Yildiz, F. H. Living in the matrix: Assembly and control of *Vibrio cholerae* biofilms. *Nature Reviews Microbiology* **2015,** *13*, 255–268.

49. Yu, K.; Creagh, A. L.; Haynes, C. A.; Kizhakkedathu, J. N. Lectin interactions on surface-grafted glycostructures: Influence of the spatial distribution of carbohydrates on the binding kinetics and rupture forces. *Analytical Chemistry* **2013,** *85*, 7786–7793.

50. Koster, D. A.; Mayo, A.; Bren, A.; Alon, U. Surface growth of a motile bacterial population resembles growth in a chemostat. *Journal of Molecular Biology* **2012,** *424*, 180–191.

51. Ellison, C. K.; Kan, J.; Dillard, R. S.; Kysela, D. T.; Ducret, A.; Berne, C.; Hampton, C. M.; Ke, Z.; Wright, E. R.; Biais, N.; Dalia, A. B.; Brun, Y. V. Obstruction of pilus retraction stimulates bacterial surface sensing. *Science* **2017,** *358*, 535–538.

Chapter 5. Conclusions and Future Directions

5.1 Dissertation Summary

This dissertation has described components of bacterial interfaces with solid surfaces, focusing on the attachment of bacterial cells to surfaces and analyses of bacterial cell appendages.

Cell attachment to surfaces was measured with three different methods: removal by sonication and colony counting, measurement of total fluorescence of surfaces with cells producing a fluorescent reporter protein, and counting cells on a surface by microscopy. Microscopy can be highly precise when individual cells are spatially resolvable. However, image analysis can be burdensome and lead to inaccuracies, especially when contrast enhancement, such as fluorescence, is not used. Besides single cell resolution, confocal microscopy is frequently used for mature biofilms to determine their thickness.[1] Sonication and colony counting is an accessible method, but can produce errors with strong adhesion of the cells to the surface. Although microscale surface roughness seems to be one characteristic that inhibits cell removal for colony counting, use of colony counting on three-dimensional samples with varied geometry, such as soil, has been used in standardized assays.[2] Colony counting is readily scalable by adjusting the dilution of the cell solution. The experimental time required has a fixed growth period determined by the microbes doubling time and is otherwise fast compared to microscopy. Due to these scalable features, the sonication and colony counting method has utility for large or numerous samples. Fluorescence measurements of entire surfaces provide a simple, streamlined way to quantify cellular attachment. The ensemble measurement of the surface will miss visually obstructed cells, and have reduced accuracy for colonies of multiple cell layers. Microbial populations with inconstant fluorophore expression could also produce

erroneous readings. However, entire surface fluorescence measurements do not have uncertainty from the removal of cells and are faster than microscopy, which make it a useful tool for studying initial attachment and early biofilm formation. Each of the methods investigated here can be practical for particular uses and can be combined with one another for thorough analyses of cell adhesion.

The colony counting method described here for quantifying surface-attached bacteria could be improved through the removal technique. Chemical treatments, including dispersal signals, that facilitate detachment could be used combined with, or instead of, sonication. Altering physical parameters, such as temperature and sonication frequency, may also improve cell removal for colony counting. Problems with entire surface fluorescence resulting from cell occlusion could be improved by lysing cells. We attempted this strategy, but noisier data were produced with the system tested.

Hydrophobic and mannosylated surfaces were found to increase attachment of *S. oneidensis*. Multivalency was found to increase the adhesiveness of mannosylated surfaces to *S. oneidensis* further, and was found to produce more persistent attachment. Interestingly, the multivalent attachment persistence was determined to be a kinetic effect, rather than a thermodynamic one. Multivalency may be an effective design parameter for systems where long-term bacterial surface attachment, or attachment in areas of much hydrodynamic disturbance, is desired. Similarly, the results of colony counting and microscopic imaging of *S. oneidensis* applied to steel surfaces indicate that surface topography may influence resistance to applied sheer force and hydrodynamic stress. Decreased detachment rate due to surface topography is a possible mechanism for the increased net attachment of cells on rough surfaces reported previously.[3]

The multivalent mannose glycopolymer surfaces have promising opportunities for improvement and future use. The saccharide units can be customized for specific microbial targets and expanded to include oligosaccharide motifs for greater adhesion and specificity. For use on electrodes, conductive polymers could be glycosylated to improve electrical conductivity of the interface as well as adhesiveness.

Greater surface adhesion and cellular attachment are useful in several ways. Technologically, useful microbes can be positioned so as to empower devices. The most prominent examples are electrodes of bioelectrical systems. With the right kinds and proportions of microbes on electrode surfaces, useful redox reactions can be facilitated. Promoting cellular attachment not only ensures proximity between the microbes and the electrodes, it enables the selection of particular microbial strains from a mixture—as demonstrated in this dissertation. Much work likely remains to be done to realize practical selection of desired strains from many different species of microbes in the sort of environment common in natural systems. The selection enhancement should be improved and the specificity for desired strains should be tested against various other kinds of microbes. Another approach for replicating the biochemical capabilities of natural consortia of microbes, besides reproducing the ratio of microbial species, is to engineer the metabolic pathways to operate all within a single strain. Such an engineered micro-organism, manipulated by gene editing and chemical metabolic regulators, could function effectively in a pure culture. The engineered microbe could then be designed to express MSH, the suspected agent of the mannose interaction shown in this dissertation, to prevent dispersal from device surfaces.

Controlling cellular surface attachment has utility through spatial organization as well. Spatially organized microbes, such as those shown in chapter 4, can be implemented in studies of

cell-cell interactions and nanoscopic analytical techniques, such as our investigation of bacterial appendages by atomic force microscopy. The fidelity over spatial control of microbe surface attachment can be augmented by improving either the adhesiveness of the attractive parts of the surface or the inertness and proclivity for detachment of the repulsive parts of the surface.

Several scanning probe microscopy modalities were used to analyze bacterial appendages considered to be electrically conductive. Peak force tapping mode was used to measure mechanical properties along with topographic features, which were then correlated with electrical conductance measurements at fixed points. The mechanical property of adhesion was found to be a potentially useful property for characterizing bacterial appendages that serve as nanowires, since the adhesion of the appendages was distinct from the cell bodies and other matter from the cell culture. The characteristic of adhesion is advantageous for conclusive identification of bacterial nanowires, because it can be easily analyzed alongside electrical measurements, which define whether an appendage is a nanowire, and it can be measured independently with less sample restrictions than conductive AFM. Electrostatic force microscopy was used to analyze isolated *G. sulfurreducens* pili, which revealed electronic mobility in the fiber. Electrostatic force microscopy is useful for delicate biological samples as it is a non-contact imaging mode. The *G. sulfurreducens* pili were preserved over many scans.

Atomic force microscopy and force spectroscopy are promising techniques to apply to cellular appendages. The nanoscale resolution is necessary for the small size of cellular appendages, and the ability to probe electrical and mechanical properties can also be applied with nanometer precision. In addition to correlating mechanical properties, methods for correlating electrical measurements by AFM and fluorescence microscopy were considered here. Fluorescent probes can provide specific chemical information through physical interactions but

complicate experimental set-ups. Overall, correlated measurements of fluorescence microscopy and AFM should be able to provide copious information on sub-cellular features, and warrant future methodological developments. Another promising technique for investigating bacterial nanowires is SICM-SECM, which can map topography with nanometer precision by ion conductance and probe electrochemical potentials.

The interactions of microbes with surfaces are an important area to understand due to the relevance of microbial biofilms in natural ecosystems and the ability to engineer biofilms that can produce power, biodegrade pollutants, and access the wealth of products created by living things.

5.2 REFERENCES

1. Reichhardt, C.; Parsek, M. R., Confocal laser scanning microscopy for analysis of *Pseudomonas aeruginosa* biofilm architecture and matrix localization. *Frontiers in Microbiology* **2019,** *10*, 677.

2. Egdell, J. W.; Cuthbert, W. A.; Scarlett, C. A.; Thomas, S. B.; Westmacott, M. H.; Bird, E. R.; Harrison, J., Some studies of the colony count technique for soil bacteria. *Journal of Applied Bacteriology* **1960,** *23* (1), 69–86.

3. Cheng, Y.; Feng, G.; Moraru, C. I., Micro- and nanotopography sensitive bacterial attachment mechanisms: A review. *Frontiers in Microbiology* **2019,** *10*, 191.